Chapter 4

ISOTOPIC FRACTIONATIONS ASSOCIATED WITH DEGASSING OF CO_2 FROM AQUEOUS SOLUTIONS AND IMPLICATIONS FOR CARBONATE CLUMPED ISOTOPE THERMOMETRY

Weifu Guo [1], Mathieu Daëron [1,2], Paul Niles [3] , William A. Goddard [4], John M. Eiler [1]

a. Division of Geological and Planetary Sciences, California Institute of Technology, Pasadena, CA, 91125, USA
b. Laboratoire des Sciences du Climat et de l'Environnement, CNRS - CEA - Univ. Versailles St-Quentin, Paris, France
c. NASA Johnson Space Center, Houston, TX, USA
d. Materials and Process Simulation Center, California Institute of Technology, Pasadena, CA, 91125, USA

ABSTRACT

Degassing of CO_2 from aqueous solutions occurs through bicarbonate dehydration ($H^+ + HCO_3^-(aq) \rightarrow H_2CO_3 \rightarrow CO_2 + H_2O$) and bicarbonate dehydroxylation ($HCO_3^-(aq) \rightarrow CO_2 + OH^-$). Kinetic isotope fractionations occur during this process, influencing the isotopic compositions not only of the degassed CO_2, but also of the carbonate minerals that precipitate from partially degassed solutions. We present here models of isotopic fractionations associated with HCO_3^- dehydration and dehydroxylation in aqueous solution, calculated using techniques from ab initio transition state theory, and tests of these models based on measurements of synthetic cryogenic carbonates and natural modern speleothems and laboratory synthesized speleothem-like carbonates, all of which grow from solutions that actively degas CO_2.

Our model predicts the kinetic isotopic fractionations associated with bicarbonate dehydration and dehydroxylation for $^{13}C/^{12}C$, $^{18}O/^{16}O$ ratios, as well as abundance anomalies (i.e., relative to a stochastic distribution) of ^{13}C-^{18}O and ^{18}O-^{17}O multiply-substituted species; these fractionations are, respectively, -29.7‰, -9.0‰, -0.05‰, –0.0002‰ and –0.004‰ for HCO_3^- dehydration; and -22.5‰, -16.7‰, 0.10‰ and –0.06‰ for HCO_3^- dehydroxylation, both at 25°C. These fractionations increase the $\delta^{13}C$ and $\delta^{18}O$ but decrease the relative proportion of ^{13}C-^{18}O bonds in the residual HCO_3^-, and thus potentially in the carbonate minerals that precipitate from that HCO_3^-. We combine the estimated isotope fractionations that accompany CO_2 degassing with models of isotopic fractionations accompanying carbonate precipitation to predict that at 25°C the $^{13}C/^{12}C$ ratio of carbonate increases by 1.1-3.2‰ and its Δ_{47} value decrease by 0.017-0.026‰ for every 1‰ kinetic enrichment in its $^{18}O/^{16}O$, with the exact values depending

on the pathway for CO_2 degassing (i.e., HCO_3^- dehydration vs. HCO_3^- dehydroxylation) and on the amount of carbonate formation accompanying the degassing. If one does not account for the kinetically controlled reductions of Δ_{47} values of carbonate minerals that grow from partially degassed solutions, one would overestimate the carbonate growth temperature (i.e., using carbonate clumped isotope thermometry) by 3~6°C for every 1‰ kinetic enrichment in carbonate $^{18}O/^{16}O$. These predictions compare favorably with the experimental constraints from our lab synthesized cryogenic carbonates and with the available isotopic data of both natural modern speleothems and speleothem-like carbonates synthesized in the laboratory, though some discrepancies between model and data are observed. These discrepancies could arise from the kinetic isotope fractionations associated with rapid precipitation of the carbonate minerals, or might reflect errors in our models.

CO_2 produced from HCO_3^- dehydration and HCO_3^- dehydroxylation reactions are predicted to be depleted in ^{13}C-^{18}O clumped isotope anomalies relative to CO_2 in thermodynamic equilibrium, by ~0.40‰ for HCO_3^- dehydration and by ~0.12‰ for HCO_3^- dehydroxylation at 25°C. This effect might explain why CO_2 produced by respiration appears to be depleted in ^{13}C-^{18}O bonds relative to thermodynamic equilibrium (Affek et al., 2007).

1. INTRODUCTION

Isotopic compositions of carbon dioxide and carbonate minerals are among the most important proxies in geochemistry research, with applications to the global carbon cycle and paleoclimate reconstruction (among many others). However, the isotopic

compositions of these materials can be interpreted only in light of a detailed understanding of the various equilibrium and kinetic isotopic fractionation processes that have influenced them; this is particularly true of ancient materials preserved in the geological record. While our understanding of the equilibrium isotope fractionation processes involving CO_2 and carbonates are relatively well understood, the understanding of kinetic isotope fractionations is rather limited and semi-quantitative. In this study, we focus on the kinetic isotope fractionations associated with degassing of CO_2 from aqueous solutions.

Degassing of CO_2 from aqueous solutions proceeds through bicarbonate dehydration ($H^+ + HCO_3^-(aq) \rightarrow H_2CO_3 \rightarrow CO_2 + H_2O$) and bicarbonate dehydroxylation ($HCO_3^-(aq) \rightarrow CO_2 + OH^-$). These reactions occur in all aqueous solutions that contain dissolved inorganic carbon, and are involved in a number of important geologic processes, including cryogenic carbonate formation (Clark and Lauriol, 1992), speleothem deposition (Fairchild et al., 2007), air-sea CO_2 exchange (Siegenthaler and Munnich, 1981), and CO_2 degassing from hydrothermal fluids (Gaillardet and Galy, 2008). It has been documented that, significant kinetic isotope fractionations occur during this process (Marlier and O'Leary, 1984; Paneth and O'Leary, 1985; Clark and Lauriol, 1992; O'Leary et al., 1992; Zeebe and Wolf-Gladrow, 2001). These kinetic isotope fractionations influence the isotopic compositions of both the degassed CO_2 and carbonate minerals that might grow from degassing solutions, and often lead to deviations of the isotopic composition of carbonate minerals from their expected equilibrium values. Such kinetic isotopic fractionations complicate the interpretation of isotopic signals in potential

paleoclimate records such as speleothems (Fairchild et al., 2006) and cryogenic carbonates (Lacelle, 2007).

To-date a complete quantitative understanding of the kinetic isotope fractionations that accompany CO_2 degassing from aqueous solutions has not been presented. To the best of our knowledge, Marlier and O'Leary (1984) and Paneth and O'Leary (1985) are the only two studies that attempted to systematically characterize these isotope fractionations. They experimentally determined the carbon isotope fractionations between evolved CO_2 and residual dissolved inorganic carbon ('DIC') to be –21.8‰ and –19.8‰, respectively, for HCO_3^- dehydration and dehydroxylation at 24°C (according to O'Leary et al., 1992 and Zebee and Wolf-Gladrow, 2001). For comparison, kinetic fractionations between evolved CO_2 and residual DIC of -31.2‰ for carbon isotope and -5.5‰ for oxygen isotopes have been inferred for HCO_3^- dehydration based on experiments in which solutions that were saturated in $Ca(HCO_3)_2$ were quickly frozen to synthesize cryogenic carbonates (Clark and Lauriol, 1992). These fractionations presumably apply at 0 ˚C (though the exact temperature of carbonate growth is not well defined in these experiments).

Recent evidence suggests that speleothem growth might be accompanied by a kinetic isotopic fractionation that influences the proportions of ^{13}C-^{18}O bonds in carbonates (the basis of carbonate "clumped isotope" thermometer(Ghosh et al., 2006; Schauble et al., 2006). Two recent studies, one of a modern speleothem from Soreq cave in Israel (Affek et al., 2008), the other of modern speleothems from caves in France, Austria and Patagonia and of speleothem-like carbonates synthesized in the laboratory (Daeron et al., 2008), have found that the relative proportions of ^{13}C-^{18}O bonds in

carbonates are lower than those expected for equilibrium at their respective carbonate growth temperatures. These non-equilibrium effects would, if unaccounted for, lead to overestimations of carbonate formation temperature of 4-22°C if the carbonate clumped isotope thermometer were applied to these materials (Table 4-1). The presence of this kinetic isotope fractionation of ^{13}C-^{18}O bonds during speleothem deposition complicates the application of carbonate clumped isotope thermometry to speleothem samples, adding a new reason why we require a quantitative understanding of isotope fractionations that accompany CO_2 degassing from aqueous solutions.

In this study we apply transition state theory (Eyring, 1935a; Eyring, 1935b) to predict the isotopic fractionations (including fractionations of multiply-substituted isotopologues) associated with HCO_3^- dehydration and dehydroxylation reactions in aqueous solution. We then integrate the results of this model with a model of the isotopic fractionations associated with carbonate precipitation to quantitatively predict the combined effects of kinetic and equilibrium isotopic fractionations on the isotopic composition (including distribution of multiply-substituted isotopologues) of carbonate minerals that grow from a partially degassed solution. Finally, we compare the predictions of these models with isotopic measurements of cryogenic carbonates grown from freezing, degassing solutions, natural modern speleothems, and synthetic carbonates grown in a fashion resembling speleothems formation. Some of these data are newly reported in this study and others are taken from recent studies (Affek et al., 2008; Daeron et al., 2008). We observe a loose agreement between our model predictions and all of these experimental and natural data sets. On this basis, we propose a quantitative framework for understanding the isotopic compositions of speleothem carbonates,

Table 4-1 Isotopic compositions of natural modern speleothem and lab synthesized "speleothem" (IVS series). Data are reproduced from Daeron et al., 2008 and Affek et al. 2008 (sample 12-1-57).

Sample No.	Cave site	Type	T_{cave} (°C)	$\delta^{18}O_{water}$ (‰)	Expected equil. Values		Observed Values				
					$\delta^{18}O_{cc}$ (‰)	Δ_{47} (‰)	$\delta^{13}C_{cc}$ (‰)	$\delta^{18}O_{cc}$ (‰)	$^{\&}\Delta_{47}$ (‰)	1σ (‰)	$^{*}T_{Apparent}$ (°C)
Vil-plq8	Villars, France	Stalag-mite	11.3±0.1	-6.26±0.08	25.24	0.712	-11.33	25.85	0.684 (5)	0.023	16.8
Vil-10B	Villars, France	Stalag-mite	12.3±0.2	-6.2±0.08	25.07	0.706	-10.07	25.38	0.688 (3)	0.006	15.9
Vil-Gal	Villars, France	Pebble	11.5±0.1	-6.42±0.06	25.03	0.711	-10.94	25.70	0.671 (8)	0.012	19.6
Vil-1A	Villars, France	Stalag-mite	11.3±0.1	-6.3±0.1	25.20	0.712	-10.91	26.00	0.643 (4)	0.011	23.5
Fau-stm6	La Faurie, France	Stalag-mite	12.9±0.1	-6.10±0.02	25.04	0.703	-9.76	26.27	0.673 (5)	0.015	19.2
K-RZ6	Katerloch, Austria	Glass plate	5.7±0.3	-8.6±0.2	24.13	0.741	-11.36	24.69	0.688 (1)	0.010	16.1
K-Top3	Katerloch, Austria	Stalag-mite	3.7±0.3	-8.8±0.2	24.40	0.752	-8.16	25.24	0.692 (1)	0.009	15.3
Bar-A	Le Baron, Patagonia	Soda straw	9.2	-5.98±0.05	26.01	0.722	0.39	28.52	0.621 (3)	0.026	30.9
Cas-B	Cassis, Patogonia	Cave coral	7.3	-5.6±0.05	26.85	0.733	14.89	31.76	0.635 (2)	0.003	27.5

Table 4-1 (Continued)

Sample No.	Cave site	Type	T_{cave} (°C)	$\delta^{18}O_{water}$ (‰)	Expected equil. Values		Observed. Values				
					$\delta^{18}O_{cc}$ (‰)	Δ_{47} (‰)	$\delta^{13}C_{cc}$ (‰)	$\delta^{18}O_{cc}$ (‰)	$^{\&}\Delta_{47}$ (‰)	1σ (‰)	$^{*}T_{Apparent}$ (°C)
Mor-A	La Moraine, Patogonia	Soda straw	9.1	-6.12±0.05	25.89	0.723	7.62	30.71	0.621 (2)	0.001	30.7
IVS-1	Paris Lab, France	Synth. Calcite	13.1±0.4	-6.89±0.05	24.18	0.741	-28.54	25.52	0.623 (3)	0.006	30.3
IVS-2	Paris Lab, France	Synth. Calcite.	13.1±0.4	-6.89±0.05	24.18	0.752	-28.13	25.55	0.640 (3)	0.025	26.3
IVS-3	Paris Lab, France	Synth. Calcite.	13.1±0.4	-6.89±0.05	24.18	0.722	-24.53	26.42	0.610 (3)	0.020	33.5
12-1-57	Soreq, Israel	Stalag-mite	18-19	-5.32±0.76	24.60	0.676	-9.53	25.55	0.642 (6)	0.003	25.9

* $T_{Apparent}$ denote the apparent formation temperatures estimated for cryogenic carbonates, based on their observed Δ_{47} (if the cryogenic carbonates were formed in isotopic equilibrium).

$^{\&}$ Number in the bracket indicate the number of replicate isotope analyses for that carbonate sample

including carbon isotope, oxygen isotope and multiply-substituted isotopologues. This scheme may provide a useful basis for quantitative paleotemperature reconstructions from speleothem records. We also use this set of models to predict the isotopic composition of CO_2 degassed from aqueous solution, and discuss the implications of this prediction for understanding the abundances of ^{13}C-^{18}O doubly-substituted isotopologues in atmospheric CO_2.

To the best of our knowledge, this study constitutes the first systematic theoretical study of kinetic isotope fractionations of multiply-substituted isotopologues arising from irreversible chemical reactions in natural systems. Although we focus on the study of dissolved inorganic carbonate (due to its relevance to carbonate clumped isotope thermometry), the principles and methods we employ could be applied to other chemical systems, including nitrates and sulfates.

2. THEORETICAL AND COMPUTATIONAL METHODS

2.1 Kinetics of HCO_3^- dehydration and dehydroxylation reactions

Degassing of CO_2 from aqueous solutions may proceed through two different reaction pathways— HCO_3^- dehydration and HCO_3^- dehydroxylation (Eigen et al. 1961):

$$H^+ + HCO_3^-(aq) \xrightarrow{k_1} CO_2 + H_2O \qquad \text{dehydration}$$

$$HCO_3^-(aq) \xrightarrow{k_2} CO_2 + OH^- \qquad \text{dehydroxylation}$$

where k_1 and k_2 are the rate constants for the respective reactions and vary with the temperature and salinity of the aqueous solutions in which the reactions take place (Schulz et al., 2006 and reference therein):

$$k_1 = \frac{e^{1{,}246.98 - \frac{6.19\times10^4}{T} - 183.0\times\ln(T)}}{K_1^*}$$

$$k_2 = \frac{499{,}002.24\times e^{4.2986\times10^{-4}\,S^2 + 5.75499\times10^{-5}\,S - \frac{90{,}166.83}{RT}}}{K_1^*},$$

where T is the temperature in Kelvin, S is the salinity in practical salinity unit (UNESCO, 1985), R is the universal gas constant, and K_1^* is the first dissociation constant of carbonic acid, which can be evaluate as (Roy et al., 1993):

$$\ln(K_1^*) = 2.83655 - \frac{2307.1266}{T} - 1.5529413\times\ln(T) + (-0.20760841 - \frac{4.0484}{T})\times S^{0.5} + 0.0846834\times S - 0.00654208\times S^{1.5}.$$

The relative importance of the HCO_3^- dehydration and dehydroxylation reactions during CO_2 degassing processes varies with the pH of the aqueous solution, with HCO_3^- dehydration dominating at low pH and HCO_3^- dehydroxylation dominating at high pH (Fig. 4-1a):

$$f_{dehydration} = \frac{k_1\times[HCO_3^-]\times[H^+]}{k_1\times[HCO_3^-]\times[H^+] + k_2\times[HCO_3^-]}$$

$$f_{dehydroxylation} = \frac{k_2\times[HCO_3^-]}{k_1\times[HCO_3^-]\times[H^+] + k_2\times[HCO_3^-]}.$$

$f_{dehydration}$ and $f_{dehydroxylation}$ here denote the relative fractional contribution of HCO_3^- dehydration and dehydroxylation reactions to the degassing of CO_2 respectively; $[HCO_3^-]$ and $[H^+]$ are the concentrations of dissolved HCO_3^- and H^+ in the aqueous solution. Besides pH, the relative rates of HCO_3^- dehydration and dehydroxylation also depend weakly on the solution temperature and salinity, with HCO_3^- dehydration reactions contributing more to the degassing of CO_2 at lower temperature and lower salinity (Fig. 4-1b and 4-1c).

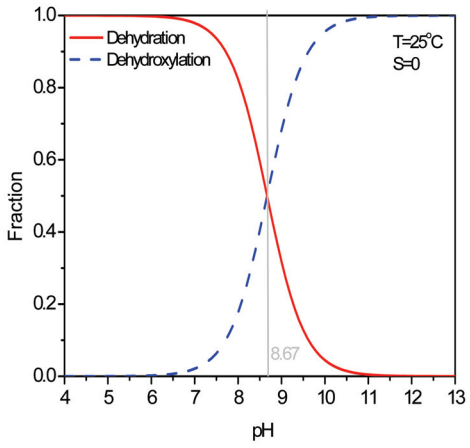

(a)

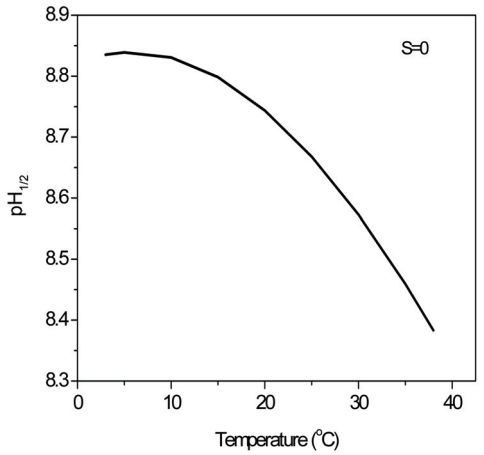

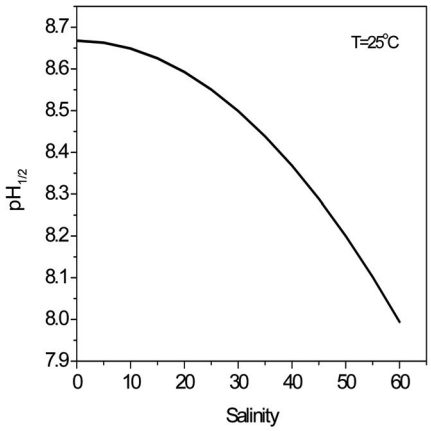

(b) (c)

Figure 4-1: Dependence of relative importance of bicarbonate dehydration and dehydroxylation on the solution (a) pH, (b) temperature and (c) salinity. (a) relative contributions of dehydration and dehydroxylation reactions during degassing of CO_2 aqueous solutions (pure water) of different pH at 25°C; (b) Variation of $pH_{1/2}$ with solution temperature in pure water; (c) Variation of $pH_{1/2}$ with solution salinity at 25°C. $pH_{1/2}$ here denotes the pH value at which HCO_3^- dehydration and HCO_3^- dehydroxylation each contribute 50% of CO_2 degassing. Reaction kinetic data are from Schulz et al. (2006).

At conditions typical for speleothem deposition (solutions with pH<8, T<30°C and S~0), HCO_3^- dehydration is the dominant pathway for degassing of CO_2. For example, HCO_3^- dehydration contributes 97.9% of CO_2 degassing at pH=7, T=25°C and S=0. However, in typical seawater (i.e., pH=8.2, T=25°C, S=35), both HCO_3^- dehydration and dehydroxylation contribute significantly, 63.4% and 36.6% respectively, to the degassing of CO_2 from aqueous solution, e.g. during air-sea CO_2 exchange.

2.2 Transition state theory and the reaction mechanisms of HCO_3^- dehydration and HCO_3^- dehydroxylation

2.2.1 Transition state theory

Transition state theory is long established as a tool for studies of chemical kinetics (Eyring, 1935a; Eyring, 1935b) and has been applied to irreversible reactions in geosciences problems (see Lasaga, 1998 and Felipe et al., 2001 for recent reviews). Based on classical transition state theory, the kinetic isotope effect associated with an irreversible chemical reaction, α, defined as the ratio of the reaction rate constants (k values) for different reactant isotopologues or isotopomers, can be expressed as (Melander and Saunders, 1987):

$$\alpha = \frac{k_{(1)}}{k_{(2)}} = \frac{|\nu_L^\dagger|_{(1)} K_{(1)}}{|\nu_L^\dagger|_{(2)} K_{(2)}}, \qquad (1)$$

where subscripts (1) and (2) denote different isotopic variants of the reactants and transition states; $\nu_L^\dagger$ is the 'decomposition frequency' (defined as the reciprocal of the average life time) of transition state $M^\dagger$; K is the equilibrium constant between reactants

(A, B) and transition state $M^{\dagger}$, and can be evaluated using statistical thermodynamics (Urey, 1947):

$$K = \frac{Q^{\dagger}}{Q_A \times Q_B} = \frac{s_A \times s_B}{s^{\dagger}} \frac{\prod_{i}^{3N^{\dagger}-7} (u_i^{\dagger} \times \frac{1}{e^{\frac{1}{2}u_i^{\dagger}}} \times \frac{1}{1-e^{-u_i^{\dagger}}})}{\prod_{j_A}^{3N_A-6} (u_{j_A} \times \frac{1}{e^{\frac{1}{2}u_{j_A}}} \times \frac{1}{1-e^{-u_{j_A}}}) \times \prod_{j_B}^{3N_B-6} (u_{j_B} \times \frac{1}{e^{\frac{1}{2}u_{j_B}}} \times \frac{1}{1-e^{-u_{j_B}}})} \quad (2)$$

$$u_i^{\dagger} = \frac{hc\varpi_i^{\dagger}}{kT}, u_{j_A} = \frac{hc\varpi_{j_A}}{kT}, u_{j_B} = \frac{hc\varpi_{j_B}}{kT}, \quad (3)$$

where $Q^{\dagger}, Q_A, Q_B$ are the reduced partition functions of transition state $M^{\dagger}$ and reactants A and B, respectively; $\varpi_i^{\dagger}, \varpi_{j_A}, \varpi_{j_B}$ are the vibration frequencies, in wave numbers, for the transition state $M^{\dagger}$ and reactants A and B, respectively (one such term is required for each mode of vibration of each species); $s^{\dagger}, s_A, s_B$ are the symmetry numbers for transition state $M^{\dagger}$ and reactants A and B, respectively; $N^{\dagger}, N_A, N_B$ are the numbers of atoms within transition state $M^{\dagger}$ and reactants A and B, respectively; h is Plank's constant; c is the velocity of light; k is the Boltzmann constant; and T is the reaction temperature in Kelvin.

A more detailed description of transition state theory can be found in our recent study (Guo et al., 2008b), where we have applied it to investigate the kinetic isotope fractionations associated with phosphoric acid digestion of carbonate minerals.

2.2.2 Reaction mechanisms of HCO_3^- dehydration

HCO_3^- dehydration in aqueous solution is commonly thought to proceed through intermediate H_2CO_3 (Kern, 1960), i.e.,

$$H^+ + HCO_3^-(aq) \xrightarrow{k_{11}} H_2CO_3 \xrightarrow{k_{12}} CO_2 + H_2O,$$

where k_{11} and k_{12} refer to the rate constants for the respective reaction steps; $k_{11}[H^+]$ is up to seven orders of magnitude greater than k_{12} (Kern, 1960; Johnson, 1982). Therefore, the second step of the above reaction, the decomposition of carbonic acid, is the rate limiting step during HCO_3^- dehydration, and thus the one controlling the kinetic isotope fractionations associated with HCO_3^- dehydration in aqueous solution. Since the first step of the reaction (and its reverse) proceeds so fast (Kern, 1960; Johnson, 1982), we assume H_2CO_3 is always in isotopic equilibrium with HCO_3^-, i.e.,

$$H^+ + HCO_3^-(aq) \rightleftharpoons H_2CO_3 \longrightarrow CO_2 + H_2O.$$

Thus, any kinetic isotope effects that arise from decomposition of H_2CO_3 will be quantitatively transferred to HCO_3^- (i.e., H_2CO_3 and HCO_3^- will maintain a constant isotopic offset equal to their equilibrium partitioning). Therefore, we focus on the kinetic isotope fractionations associated with decomposition of H_2CO_3 in aqueous solution.

Previous theoretical studies, using also transition state theory, suggest that H_2CO_3 decomposition in aqueous solution involves a transition state structure that is significantly influenced by interactions with adjacent water molecules (Nguyen et al., 1997; Loerting et al., 2000; Tautermann et al., 2002). The participation of water molecules in the reaction stabilizes the transition state structure, lowers the activation energy required for the reaction, and thus facilitates the decomposition of H_2CO_3 in aqueous solution. In particular, Nguyen et al. (1997) examined the possible transition state structures for hydration of CO_2 in aqueous solution (the reverse reaction of H_2CO_3 decomposition) with different numbers of participating water molecules, and suggested that it involves formation of a bridge-complex consisting one CO_2 and three H_2O

molecules. In turn, this suggests H_2CO_3 decomposition in aqueous solution may proceed with the aid of two water molecules. In this study, we adopt this conclusion from Nguyen et al. (1997), and use the corresponding structures of reactant and transition state as our initial guesses for further geometry optimizations (Fig. 4-2a).

(a) Reactant Transition State

(b) Reactant Transition State

Figure 4-2: Optimized reactant and transition state structures for HCO_3^- dehydration and HCO_3^- dehydroxylation reactions in aqueous solution. (a) HCO_3^- dehydration with the aid of two water molecules; (b) HCO_3^- dehydroxylation, both optimized with DFT-B3LYP/ cc-pvtz(-f) method and with a continuum solvation model.

2.2.3 Reaction mechanisms of HCO_3^- dehydroxylation

The reaction mechanism of HCO_3^- dehydroxylation in aqueous solution has received much less attention than that for HCO_3^- dehydration. Previous theoretical studies have

focused on determining the kinetics of its reverse reaction, CO_2 hydroxylation, and tried to simulate and explain the energy barrier for this reaction in aqueous solution (Peng and Merz, 1992; Peng and Merz, 1993; Davidson et al., 1994; Nemukhin et al., 2002; Iida et al., 2007; Leung et al., 2007). In this study, we assume HCO_3^- dehydroxylation in aqueous solution proceeds with the similar transition state structure as determined for CO_2 hydroxylation (Leung et al., 2007), i.e., adopted those transition state structures as the initial guess in our calculation (Fig. 4-2b).

2.3 A model of isotopic fractionations associated with carbonate precipitation induced from CO_2 degassing

A solution containing Ca^{2+} and dissolved inorganic carbon that undergoes degassing of CO_2 will increase in pH, driving precipitation of calcium carbonate. In this section, we outline a model to account for these isotopic effects in carbonate minerals induced by CO_2 degassing. Later sections present theoretical calculations of isotopic fractionations associated with individual steps in this overall process; integration of these steps into the model we present here will lead to quantitative predictions of the isotopic compositions of carbonates produced by degassing of CO_2 from aqueous solutions. Similar isotope models have been proposed previously, but considered only carbon isotope and (in a few cases) oxygen isotope fractionations (Clark and Lauriol, 1992; Mickler et al., 2004; Zak et al., 2004; Mickler et al., 2006; Muehlinghaus et al., 2007; Romanov et al., 2008) . We extend these models to consider fractionations of all isotopologues ($^{13}C/^{12}C$, $^{18}O/^{16}O$, and multiply-substituted isotopologues); our model also makes several assumptions that differ from those adopted by previous studies, as detailed below.

The model on which we primarily focus assumes that kinetic isotope effects occur by HCO_3^- dehydration and dehydroxylation reactions, and that carbonate then precipitates in equilibrium with the fractionated pool of residual HCO_3^-. In section 4.3, we examine alternate models in which this relatively simple process is modified by other fractionations, such as isotopic exchange between HCO_3^- and water, and/or kinetic isotope fractionations between precipitated carbonate and HCO_3^- (section 4.3).

2.3.1 Rayleigh distillation effects

Our model describes kinetic isotope fractionations associated with HCO_3^- dehydration and dehydroxylation in aqueous solution that lead to changes in the isotopic composition of residual HCO_3^-, and thus in the compositions of carbonate minerals that precipitation from that pool of HCO_3^-. If the pool of residual dissolved HCO_3^- does not undergo isotopic re-equilibration with water, its isotopic composition will evolve as a result of dehydration and dehydroxylation, following a Rayleigh distillation relationship:

$$R_{HCO_3^-}(t) = R_{HCO_3^-}(0) \times F^{\alpha-1}, \qquad (4)$$

where R(0) and R(t) are the abundance ratios between any isotopically-substituted isotopologue (including multiply-substituted isotopologues) and the isotopically-non-substituted isotopologue — generally the most abundant isotopologue for the species we consider — (i.e., R=[rare_isotopologue]/[most_abundant_isotopologue]) at time zero and at time t, respectively; $F = \frac{[HCO_3^-]_t}{[HCO_3^-]_0}$ denotes the fraction of HCO_3^- remaining in the aqueous solution at time t; $\alpha = \frac{R_{leaving}}{R_{residual}}$ is the isotope fractionation factor between the consumed HCO_3^- pool and the residual HCO_3^- pool (a different value will apply for each

isotopologue). Note that, the consumed HCO_3^- pool consists not only HCO_3^- that degas to form CO_2 (i.e., through HCO_3^- dehydration and HCO_3^- dehydroxylation), but also those incorporated into the carbonate minerals (if the degassing is accompanied by carbonate precipitation). Accordingly, α here should be the weighted average of the respective isotope fractionation factors associated with each sub-pool of consumed HCO_3^-. We discuss the choice of α under different scenarios in detail section 2.3.2.

If a carbonate mineral precipitates in isotopic equilibrium with the remaining HCO_3^-, its isotopic composition can be expressed as:

$$R_{carbonate}(t) = \alpha^{equil}_{carb\text{-}HCO_3^-} \times R_{HCO_3^-}(t), \qquad (5)$$

where $\alpha^{equil}_{carb\text{-}HCO_3^-}$ is an equilibrium isotope fractionation factor between the precipitated carbonate mineral and dissolved HCO_3^-, and is evaluated with data from previous calibration studies, e.g., for carbon isotope (Deines, 1974) and oxygen isotopes (Kim and O'Neil, 1997; Beck et al., 2005).

Substituting the Rayleigh distillation relationship (equation 4) into the above equation, we obtain

$$\begin{aligned} R_{carbonate}(t) &= \alpha^{equil}_{carb\text{-}HCO_3^-} \times R_{HCO_3^-}(0) \times F^{\alpha-1} \\ &= R^{equil}_{carb}(0) \times F^{\alpha-1}. \end{aligned} \qquad (6)$$

$R^{equil}_{carb}(0) = R_{HCO_3^-}(0) \times \alpha^{equil}_{carb\text{-}HCO_3^-}$ is the expected isotope composition in the carbonate mineral if it formed in isotopic equilibrium with the initial HCO_3^- pool (at time zero). Therefore, the kinetic isotope fractionations for carbon isotope and oxygen isotope (i.e., for ^{13}C singly-substituted isotopologue and ^{18}O singly-substituted isotopologue) in the carbonate minerals can be expressed as:

$$\frac{R_{carb}(t)}{R_{carb}^{equil}(0)} = F^{\alpha-1}, \tag{7}$$

where α, as defined above, is the isotope fractionation factor for the corresponding isotopologue between the consumed HCO_3^- pool and residual HCO_3^- pool.

Note, the equation 7 applies not only ^{13}C singly-substituted isotopologue and ^{18}O singly-substituted isotopologues, but all the isotopologues of HCO_3^-. Thus, for ^{13}C-^{18}O bearing doubly-substituted isotopologue in the carbonate mineral which are most relevant to carbonate clumped isotope thermometry, we have

$$\frac{R_{carb}^{t}(^{13}C^{18}O^{16}O_2)}{R_{carb}^{0,equil}(^{13}C^{18}O^{16}O_2)} = F^{\alpha_{^{13}C^{18}O^{16}O_2}-1}. \tag{8}$$

We combine equation 8 with the similar relationships for ^{13}C singly-substituted isotopologue and ^{18}O singly-substituted isotopologue, i.e.,

$$\frac{R_{carb}^{t}(^{13}C^{16}O_3)}{R_{carb}^{0,equil}(^{13}C^{16}O_3)} = F^{\alpha_{^{13}C^{16}O_3}-1} \tag{9}$$

$$\frac{R_{carb}^{t}(^{12}C^{18}O^{16}O_2)}{R_{carb}^{0,equil}(^{12}C^{18}O^{16}O_2)} = F^{\alpha_{^{12}C^{18}O^{16}O_2}-1} \tag{10}$$

and obtain

$$\frac{\dfrac{R_{carb}^{t}(^{13}C^{18}O^{16}O_2)}{R_{carb}^{t}(^{13}C^{16}O_3)\times R_{carb}^{t}(^{12}C^{18}O^{16}O_2)}}{\dfrac{R_{carb}^{0,equil}(^{13}C^{18}O^{16}O_2)}{R_{carb}^{0,equil}(^{13}C^{16}O_3)\times R_{carb}^{0,equil}(^{12}C^{18}O^{16}O_2)}} = \frac{\dfrac{\Delta_{^{13}C^{18}O^{16}O_2}^{carb}(t)}{1000}+1}{\dfrac{\Delta_{^{13}C^{18}O^{16}O_2}^{carb}(0)}{1000}+1} = \frac{F^{\alpha_{^{13}C^{18}O^{16}O_2}-1}}{F^{\alpha_{^{13}C^{16}O_3}-1}\times F^{\alpha_{^{12}C^{18}O^{16}O_2}-1}}, \tag{11}$$

where $\Delta_{^{13}C^{18}O^{16}O_2}^{carb}$ is the abundance anomaly of the ^{13}C-^{18}O bearing doubly-substituted isotopologue in the carbonate mineral, the basis of carbonate clumped isotope thermometry, and is expressed as $\Delta_{^{13}C^{18}O^{16}O_2}^{carb} = \left(\dfrac{R_{carb}(^{13}C^{18}O^{16}O_2)}{R_{carb}(^{13}C^{16}O_3)\times R_{carb}(^{12}C^{18}O^{16}O_2)}-1\right)\times 1000;$

$\alpha_{^{13}C^{18}O^{16}O_2}$, $\alpha_{^{13}C^{16}O_3}$ and $\alpha_{^{12}C^{18}O^{16}O_2}$ are the isotope fractionation factors for isotopologues

$H^{13}C^{18}O^{16}O_2^-$, $H^{13}C^{16}O_3^-$ and $H^{12}C^{18}O^{16}O_2^-$ respectively, between the consumed HCO_3^- pool and the residual HCO_3^- pool.

Since $\Delta^{carb}_{^{13}C^{18}O^{16}O_2}(t) << 1$, and $\Delta^{carb}_{^{13}C^{18}O^{16}O_2}(0) << 1$, the effect of kinetic fractionations associated with CO_2 degassing on the abundances of ^{13}C-^{18}O bonds in carbonate that precipitates from the residual HCO_3^- pool equals,

$$\Delta^{carb}_{^{13}C^{18}O^{16}O_2}(t) - \Delta^{carb}_{^{13}C^{18}O^{16}O_2}(0) \approx \frac{\frac{\Delta^{carb}_{^{13}C^{18}O^{16}O_2}(t)}{1000}+1}{\frac{\Delta^{carb}_{^{13}C^{18}O^{16}O_2}(0)}{1000}+1} = \frac{F^{\alpha_{^{13}C^{18}O^{16}O_2}-1}}{F^{\alpha_{^{13}C^{16}O_3}-1} \times F^{\alpha_{^{12}C^{18}O^{16}O_2}-1}}. \quad (12)$$

The method outlined above can also be applied to calculate the kinetic isotope fractionations of clumped isotope anomalies of other multiply-substituted isotopologues, e.g.,

$$\Delta^{carb}_{^{12}C^{18}O^{17}O^{16}O}(t) - \Delta^{carb}_{^{12}C^{18}O^{17}O^{16}O}(0) \approx \frac{F^{\alpha_{^{12}C^{18}O^{17}O^{16}O}-1}}{F^{\alpha_{^{12}C^{18}O^{16}O_3}-1} \times F^{\alpha_{^{12}C^{17}O^{16}O_2}-1}} \quad (13)$$

$$\Delta^{carb}_{^{12}C^{18}O^{18}O^{16}O}(t) - \Delta^{carb}_{^{12}C^{18}O^{18}O^{16}O}(0) \approx \frac{F^{\alpha_{^{12}C^{18}O^{18}O^{16}O}-1}}{F^{\alpha_{^{12}C^{18}O^{16}O_3}-1} \times F^{\alpha_{^{12}C^{18}O^{16}O_2}-1}}. \quad (14)$$

2.3.2 Changes in the Rayleigh distillation model arising from significant amounts of carbonate precipitation

Previous studies have inferred that in natural environments in which carbonate precipitation is driven by CO_2 degassing from aqueous solutions (e.g., cave deposits) one mol of carbonate precipitates for every mol of CO_2 degassed from the solution (Fairchild et al., 2007):

$$Ca^{2+} + 2\,HCO_3^-(aq) \longrightarrow CaCO_3 \downarrow + CO_2 \uparrow + H_2O$$

If this is the case, the isotope fractionation factor, α, that describes the change in isotopic composition of the residual HCO_3^- pool in the above equations should reflect the combined effects of isotope fractionation factors resulting from both CO_2 degassing and the carbonate formation:

$$\alpha = \frac{R_{leaving}}{R_{initial}} = \frac{\alpha_{\mathrm{degassing}} + \alpha_{carb-HCO_3^-}^{equil}}{2}, \qquad (15)$$

where $\alpha_{\mathrm{degassing}}$ and $\alpha_{carb-HCO_3^-}^{equil}$ are the isotopic fractionation factors associated with CO_2 degassing, and the equilibrium isotope fractionation factor between carbonate and HCO_3^- respectively, as defined above.

In order to apply the model scheme outlined above to isotope fractionations of multiply substituted isotopologues we must estimate the relevant equilibrium fractionation factors between carbonate minerals and dissolved HCO_3^- (i.e., $\alpha_{carb-HCO_3^-}^{equil}$ in equation 15), which have not been previously studied. We have approached this problem using statistical thermodynamics theory. This theory is applicable to all of the multiply substituted isotopologues of carbonate minerals and DIC species, but we present only the details relevant to isotopologues containing ^{13}C-^{18}O bonds, which are most relevant to carbonate clumped isotope thermometry.

The equilibrium isotope fractionations between two phases (e.g., between carbonate and water) arise from differences among the related isotopologues in the two phases in the vibrational energies of intramolecular bonds. These fractionations can be expressed as functions of the reduced partition functions of the phases of interest (Urey, 1947), e.g.,

$$\alpha_{carb\text{-}HCO_3^-}^{equil}(^{13}C^{16}O_3) = \frac{Q_{Ca^{13}C^{16}O_3}}{Q_{Ca^{12}C^{16}O_3}} \Big/ \frac{Q_{H^{13}C^{16}O_3^-}}{Q_{H^{12}C^{16}O_3^-}} \qquad (16)$$

$$\alpha^{equil}_{carb\text{-}HCO_3^-}({}^{12}C{}^{18}O{}^{16}O_2) = \frac{Q_{Ca^{12}C^{18}O^{16}O_2}}{Q_{Ca^{12}C^{16}O_3}} \Big/ \frac{Q_{H^{12}C^{18}O^{16}O_2^-}}{Q_{H^{12}C^{16}O_3^-}} \quad (17)$$

$$\alpha^{equil}_{carb\text{-}HCO_3^-}({}^{13}C{}^{18}O{}^{16}O_2) = \frac{Q_{Ca^{13}C^{18}O^{16}O_2}}{Q_{Ca^{12}C^{16}O_3}} \Big/ \frac{Q_{H^{13}C^{18}O^{16}O_2^-}}{Q_{H^{12}C^{16}O_3^-}}, \quad (18)$$

where $\alpha^{equil}_{carb\text{-}HCO_3^-}({}^{13}C{}^{16}O_3)$, $\alpha^{equil}_{carb\text{-}HCO_3^-}({}^{12}C{}^{18}O{}^{16}O_2)$ and $\alpha^{equil}_{carb\text{-}HCO_3^-}({}^{13}C{}^{18}O{}^{16}O_2)$ denote the equilibrium isotope fractionation factors of ^{13}C singly-substituted isotopologue (i.e. carbon isotope), ^{18}O singly-substituted isotopologue (i.e., oxygen isotope) and ^{13}C-^{18}O doubly-substituted isotopologue of the carbonate ion between calcium carbonate mineral and dissolved HCO_3^-; Q are the reduced partition functions for the respective isotopologues indicated in the subscript of each Q.

Rearranging equation 16-18, we obtain

$$\frac{\alpha^{equil}_{carb\text{-}HCO_3^-}({}^{13}C{}^{18}O{}^{16}O_2)}{\alpha^{equil}_{carb\text{-}HCO_3^-}({}^{13}C{}^{16}O_3)\times\alpha^{equil}_{carb\text{-}HCO_3^-}({}^{12}C{}^{18}O{}^{16}O_2)} = \frac{\frac{Q_{Ca^{13}C^{18}O^{16}O_2}\times Q_{Ca^{12}C^{16}O_3}}{Q_{Ca^{13}C^{16}O_3}\times Q_{Ca^{12}C^{18}O^{16}O_2}}}{\frac{Q_{H^{13}C^{18}O^{16}O_2^-}\times Q_{H^{12}C^{16}O_3^-}}{Q_{H^{13}C^{16}O_3^-}\times Q_{H^{12}C^{18}O^{16}O_2^-}}} = \frac{K^{equil}_{carb}({}^{13}C-{}^{18}O)}{K^{equil}_{HCO_3^-}({}^{13}C-{}^{18}O)}, \quad (19)$$

where $K^{equil}_{carb}({}^{13}C-{}^{18}O) = \frac{Q_{Ca^{13}C^{18}O^{16}O_2}\times Q_{Ca^{12}C^{16}O_3}}{Q_{Ca^{13}C^{16}O_3}\times Q_{Ca^{12}C^{18}O^{16}O_2}}$ and $K^{equil}_{HCO_3^-}({}^{13}C-{}^{18}O) = \frac{Q_{H^{13}C^{18}O^{16}O_2^-}\times Q_{H^{12}C^{16}O_3^-}}{Q_{H^{13}C^{16}O_3^-}\times Q_{H^{12}C^{18}O^{16}O_2^-}}$ are the equilibrium constants for the ^{13}C-^{18}O isotope 'clumping' reactions in the carbonate mineral and the dissolved HCO_3^- respectively:

$$Ca^{13}C^{16}O_3 + Ca^{12}C^{18}O^{16}O_2 \xleftrightarrow{K^{equil}_{carb}({}^{13}C-{}^{18}O)} Ca^{13}C^{18}O^{16}O_2 + Ca^{12}C^{16}O_3$$

$$H^{13}C^{16}O_3^- + H^{12}C^{18}O^{16}O_2^- \xleftrightarrow{K^{equil}_{carb}({}^{13}C-{}^{18}O)} H^{13}C^{18}O^{16}O_2^- + H^{12}C^{16}O_3^-.$$

Both $K^{equil}_{carb}({}^{13}C-{}^{18}O)$ and $K^{equil}_{HCO_3^-}({}^{13}C-{}^{18}O)$ have been theoretically estimated in

previous studies, using first principle lattice dynamics (Schauble et al., 2006) and quantum mechanics (Guo et al., 2008a) respectively. Based on these theoretical estimations, at any given temperature $K_{carb}^{equil}(^{13}C-^{18}O)$ and $K_{HCO_3^-}^{equil}(^{13}C-^{18}O)$ are very nearly identical to each other, e.g., $K_{carb}^{equil}(^{13}C-^{18}O)=1.000410$ (Schauble et al. 2006) vs. $K_{HCO_3^-}^{equil}(^{13}C-^{18}O)=1.000427$ (Guo et al. 2008a) at 25°C. The difference between the two is within the uncertainties of theoretical estimations (e.g. 1-3×10^{-5}, Schauble et al., 2006). We therefore assume in this study $\frac{K_{carb}^{equil}(^{13}C-^{18}O)}{K_{HCO_3^-}^{equil}(^{13}C-^{18}O)}=1$, and estimate equilibrium isotope fractionation factor of ^{13}C-^{18}O doubly-substituted isotopologue of the carbonate ion between calcium carbonate mineral and dissolved HCO_3^- :

$$\alpha_{carb\text{-}HCO_3^-}^{equil}(^{13}C^{18}O^{16}O_2)=\alpha_{carb\text{-}HCO_3^-}^{equil}(^{13}C^{16}O_3)\times\alpha_{carb\text{-}HCO_3^-}^{equil}(^{12}C^{18}O^{16}O_2). \quad (20)$$

The same method outlined above can also be applied to calculate the equilibrium isotope fractionation factor of other multiply-substituted isotopologues between calcium carbonate mineral and dissolved HCO_3^-, e.g.,

$$\alpha_{carb\text{-}HCO_3^-}^{equil}(^{12}C^{18}O^{17}O^{16}O)=\alpha_{carb\text{-}HCO_3^-}^{equil}(^{12}C^{18}O^{16}O_2)\times\alpha_{carb\text{-}HCO_3^-}^{equil}(^{12}C^{17}O^{16}O_2) \quad (21)$$

$$\alpha_{carb\text{-}HCO_3^-}^{equil}(^{12}C^{18}O^{18}O^{16}O)=\alpha_{carb\text{-}HCO_3^-}^{equil}(^{12}C^{18}O^{16}O_2)\times\alpha_{carb\text{-}HCO_3^-}^{equil}(^{12}C^{18}O^{16}O_2), \quad (22)$$

where $\alpha_{carb\text{-}HCO_3^-}^{equil}(^{12}C^{17}O^{16}O_2)$ is the equilibrium isotope fractionation factor of ^{17}O singly-substituted isotopologues of the carbonate ion between calcium carbonate mineral and dissolved HCO_3^-, and is estimated assuming a mass dependence exponent λ=0.528 between $\alpha_{carb\text{-}HCO_3^-}^{equil}(^{12}C^{17}O^{16}O_2)$ and $\alpha_{carb\text{-}HCO_3^-}^{equil}(^{12}C^{18}O^{16}O_2)$ (Barkan and Luz, 2005), i.e.,

$$\alpha_{carb\text{-}HCO_3^-}^{equil}(^{12}C^{17}O^{16}O_2)=\left\{\alpha_{carb\text{-}HCO_3^-}^{equil}(^{12}C^{18}O^{16}O_2)\right\}^{0.528} \quad (23)$$

It is noted that, the above 1:1 proportionality between CO_2 degassing and carbonate formation holds true only if there are no independent limitations on the rate of carbonate precipitation from the solution. If some kinetic barrier to carbonate precipitation causes it to proceed slower than the rate of CO_2 degassing, of the solution will become supersaturated. Cave waters are generally supersaturated with respect to calcium carbonate (saturation index for calcite up to 0.5-0.6 or more; Fairchild et al., 2007), perhaps suggesting that in cave waters CO_2 degassing outstrips carbonate precipitation (i.e, the proportionality between CO_2 degassing and carbonate formation is bigger than 1:1). This disparity between CO_2 degassing and carbonate precipitation will affect the isotopic compositions of dissolved HCO_3^- and thus the isotopic compositions of the speleothems deposited from this supersaturated solution.

The exact disparity between CO_2 degassing and carbonate precipitation may vary among different cave waters, and might be difficult to evaluate or reconstruct. To account for this disparity, we also model another extreme case, in which CO_2 degassing is the only isotope fractionation process influencing the isotopic composition of HCO_3^- in aqueous solution (i.e., no carbonate precipitation occurs). In this case (CO_2 degassing is associated with negligible carbonate growth), the proportionality between CO_2 degassing and carbonate formation equals infinity, and the fractionation factor between the consumed HCO_3^- pool and the residual HCO_3^- pool will be:

$$\alpha = \frac{R_{leaving}}{R_{initial}} = \alpha_{\deg assing} = f_{dehydration} \times \alpha_{dehydration} + f_{dehydroxylation} \times \alpha_{dehydroxylation}, \quad (24)$$

where $\alpha_{dehydration}$ and $\alpha_{dehydroxylation}$ are the kinetic isotope fractionation factors associated with HCO_3^- dehydration and HCO_3^- dehydroxylation reaction in aqueous solution

respectively; $f_{dehydration}$ and $f_{dehydroxylation}$ are relative contributions of dehydration and dehydroxylation reactions to the degassing of CO_2, as discussed in section 2.1.

2.4 Computational methods

Molecular geometries of reactants and transition states were optimized and bond frequencies were calculated for different isotopologues using the Jaguar program (Version 7.0, release 207; Ringnalda et al., 2007) on a workstation cluster with 79 Dell PowerEdge-2650 server nodes (Xeno, 2.2-2.4GHz, 512K) in the Materials and Process Simulation Center at Caltech. The singlet state electron wave functions of the molecular configurations were built using a density functional theory with hybrid functionals, B3LYP, and extended basis sets cc-pvtz(-f). We also perform an alternate set of these transition state theory calculations for HCO_3^- dehydroxylation reaction using the LMP2/cc-pvtz(-f) method (Ringnalda et al., 2007). We simulated the aqueous environment in which modeled reactions take place using a self consistent reaction field method, using the Poisson-Boltzmann solver imbedded in the Jaguar program (Ringnalda et al., 2007). The dielectric constant for water was assumed to be 80.37.

A universal frequency scaling factor of 0.9614 was employed on the calculated vibration frequencies for both reactants and transition states to correct for the general overestimation of vibration frequencies by ab initio calculations (Scott and Radom, 1996). We discuss the effects of scaling factor on our model results in section 4.2.

3. EXPERIMENTAL METHODS

3.1 Synthesis of cryogenic carbonates

We synthesized six separate samples of cryogenic carbonates at Johnson Space Center (Houston) by rapidly freezing saturated $Ca(HCO_3)_2$ solutions. The typical preparation procedure is described as below, and details unique to each sample are listed in Table 4-2.

0.6 grams of $Ca(OH)_2$ powder were first added into 1500ml of de-ionized water. Then, pure CO_2 gas (99.96%, Air Liquide) was bubbled through this $Ca(OH)_2$ solution at room temperature for 1-2hr. After complete dissolution of $Ca(OH)_2$, the solution (now saturated regarding $Ca(HCO_3)_2$) was sealed in a glass jar and its headspace was flushed with the pure CO_2 gas. The solution was either stored at room temperature (~20°C) or equilibrated at temperatures of 1-7°C for hours to days before being frozen (Table 4-2). Note that samples 0412-07 and 0418-07 were prepared from two aliquots of the same bulk solution, as were samples 0611A-07 and 0611B-07.

At the beginning of each freezing experiment, the solution was transferred from the glass jar into a large, flat tupperware container. We then measured the solution pH using an Accumet 925 pH/Ion Meter and collected an aliquot of solution for later determination of the $\delta^{13}C$ of DIC and the $\delta^{18}O$ of the water. Then, the tupperware container was sealed and placed in a freezer held at a constant temperature of approximately -15°C ± 4°C. The chilled solutions froze thoroughly, during which we inferred that dissolved CO_2 degassed from the solution, increasing the pH of the solution and driving carbonate precipitation. The whole solution typically froze completely within 3 hours. At the end of each experiment, we thawed the frozen solution either at room temperature or at 1-3°C (in a refridgerator), and then filtered the carbonate precipitates from the solution. The collected carbonates were dried at 50°C in a drying oven or freeze-

dried before isotopic analyses. The yields of carbonate solids varied among different experiments, and were estimated to average around 10% of calcium in the solution.

Table 4-2 Preparation conditions of cryogenic carbonates synthesized in this study.

Sample No.		0412-07	0418-07	0504A-07	0611A-07	0611B-07	0920A-07
Solution equilibration	T (°C)	~20	~20	7.6	6	3.1	1-3
	Time (hrs)	2-3	Days	Days	Days	Days	~48
pH		5.7	5.7	5.5	5.5	5.5	5.5
$\delta^{13}C_{DIC}$ (‰)		-31.2	-31.2	-31	-32.8	-32.6	-27.3
$^{\#}\delta^{13}C_{HCO_3^-}$ (‰)		-21.9	-21.9	-21	-21.8	-22.7	-17.3
$\delta^{18}O_{water}$ (‰)		-2.5	-2.5	-2.5	-2.4	-2.2	-1.3
T_{Freeze} (°C)		-15	-15	-15	-15	-15	-15
$T_{Defreeze}$ (°C)		~20	~20	~20	~20	~20	1-3
Drying method		Oven	Oven	Oven	Oven	Oven	Freeze dryer

$^{\#}$ $\delta^{13}C_{HCO_3^-}$ are estimated based on measured carbon isotopic composition of the total DIC, assuming the carbon isotope equilibrium among different DIC species (see section 4.3 for details). All $\delta^{13}C$ and $\delta^{18}O$ are reported vs. VPDB and VSMOW, respectively.

3.2 Mass spectrometric analysis

The $\delta^{18}O$ of the water and $\delta^{13}C$ of DIC in the cryogenic carbonate experiments were determined at Johnson Space Center, by analysis of solution aliquots on a Finnigan MAT-253 gas source mass spectrometer that is equipped with a Gas Bench II apparatus and operating in continuous flow mode. For $\delta^{18}O$ measurements of the water samples, the CO_2–H_2O equilibration method was employed (Epstein and Mayeda, 1953; Horita et al., 1989). 0.7 ml of solution was equilibrated with helium gas—mixed with 0.3% CO_2—overnight, at constant temperature 30°C. The equilibrated gas was then analyzed by flowing it into the MAT-253 mass spectrometer using the Gas Bench II apparatus and a

helium carrier gas. The $\delta^{13}C$ of the DIC was determined in a similar manner (Spotl, 2005). Three drops of 100% phosphoric acid was added to a sealed glass exetainer. After flushing the exetainer with pure helium gas, a 0.1 ml portion of the sample solution was then added into the exetainer. The gas evolved from this mixture was then analyzed using the Gas Bench II and MAT-253 mass spectrometer. Sample solutions were analyzed for $\delta^{18}O$ alongside in-house water standards which have been calibrated through repeat analyses of SMOW, SLAP, and GISP standards. The oxygen isotopic compositions of all of the waters was obtained through plotting the data on a scale normalized to the values of SMOW (0‰ VSMOW) and SLAP (-55.5‰ VSMOW). The $\delta^{13}C$ analyses of the unknowns were also normalized in a similar manner using NBS-19 and NBS-18. The precision (1σ) of the water $\delta^{18}O$ and DIC $\delta^{13}C$ analyses, on the basis of replicate analyses of the laboratory standards, was estimated at ±0.1‰ and ±0.1‰, respectively.

Isotopic analyses of carbonate minerals — $\delta^{13}C$, $\delta^{18}O$ and Δ_{47} value — were performed by reacting the carbonate anhydrous phosphoric acid (ρ=1.92g/cm^3) at 25°C for 18-24 hours and then analyzing the released CO_2 at Caltech on a Finnigan MAT-253 gas source spectrometer that was configured to simultaneously measure masses 44 through 49 AMU, inclusive. Δ_{47} is a measure of the relative proportion of ^{13}C-^{18}O bonds inside carbonate lattice, defined as the deviation of actual mass 47 abundance in the CO_2 derived from phosphoric acid digestion of carbonate minerals relative to its expected mass 47 abundance if all the isotopes were randomly distributed, $\Delta_{47} = \left(\frac{R^{47}_{actual}}{R^{47}_{stochastic}} - 1 \right) \times 1000$ (Eiler and Schauble, 2004; Ghosh et al., 2006). A more detailed description of the mass spectrometer configuration and analysis procedure is given by Ghosh et al (2006). The

external precision of our isotope analyses averages around 0.04‰, 0.01‰, 0.015‰ (1 standard deviation) for $\delta^{13}C$, $\delta^{18}O$ and Δ_{47}, respectively, based on replicate measurements of carbonate standards and sample materials. Values of $\delta^{13}C$ and $\delta^{18}O$ were standardized by comparison with CO_2 generated by phosphoric acid digestion of NBS-19 and are reported vs. VPDB and VSMOW, respectively.

4. RESULTS AND DISCUSSION

4.1 Model results for the kinetic isotope fractionations associated with HCO_3^- dehydration and HCO_3^- dehydroxylation reactions

The calculated vibration frequencies (scaled with a universal scaling factor of 0.9614, section 2.4) for all the isotopologues (and isotopomers) of reactants and transition states during HCO_3^- dehydration and dehydroxylation reactions in aqueous solutions are presented in Appendix (Tables 4-A1 to 4-A4).

Of all the studied species, experimentally determined vibration frequencies exist only for dissolved HCO_3^- (all the other species are either transition state structures or unstable in aqueous solutions). Fig. 4-3 presents the comparison between our model predicted vibration frequencies for dissolved HCO_3^- and the most recent experimentally determined frequencies (Rudolph et al., 2006). For most modes of vibration, our model calculation underestimates the frequencies by about $100cm^{-1}$ relative to the experimentally observed frequencies. The largest discrepancy was observed for the highest mode of vibration (assigned as νCO-H vibration mode), with the model predicted frequency ~$1085cm^{-1}$ higher than the experimentally determined frequency. Similar discrepancies seem to be typical for the ab initio estimations of vibration frequencies for

dissolved HCO_3^-, and have been also reported in several previous theoretical studies (Davidson et al., 1994; Rudolph et al., 2006). They are suspected to arise from the insufficiency of the continuum solvation model to describe the aqueous environment, the inability of the theoretical model (e.g., DFT method and LMP2 method) to fully characterize the hydrogen bonds in aqueous solutions, and the experimental uncertainties associated with determination of vibration frequencies for dissolved ions in aqueous solutions (Rudolph et al., 2006).

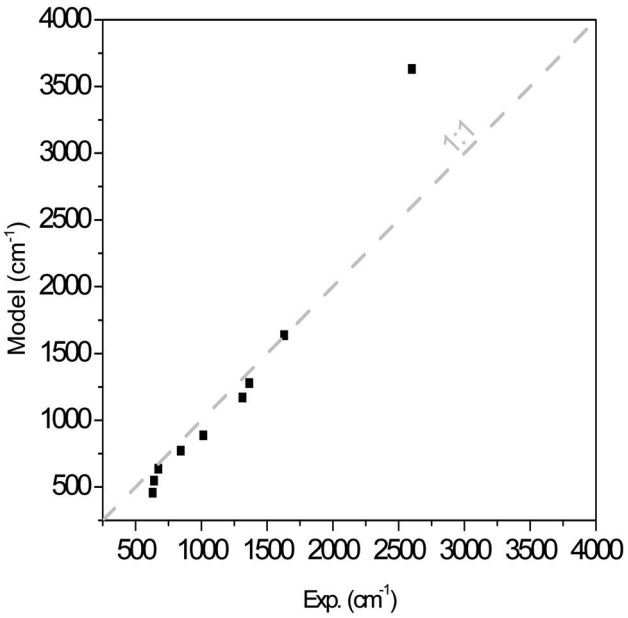

Figure 4-3: Comparison of our calculated vibration frequencies for dissolved HCO_3^- (DFT-B3LYP/ cc-pvtz(-f) with a continuum solvation model, scaled with a universal frequency scaling factor 0.9614; this study) with the experimentally determined vibration frequencies (Rudolph et al., 2006).

A full-scale theoretical investigation (e.g., by improving the theoretical method) to resolve these discrepancies between model predicted frequencies and experimentally observed frequencies are beyond the scope of this study. However, there are several reasons why we think it unlikely that these discrepancies will lead to first-order errors in

calculated isotopic fractionations: 1) when calculating isotope fractionations that arise from statistical thermodynamic effects, the ratios of vibration frequencies among different isotopologues tend to be more important than the absolute values of the frequencies (Urey, 1947); 2) the "νCO-H" vibration mode of dissolved HCO_3^-, the vibration mode showing the largest frequency discrepancy between model prediction and experimental observation, is not among the primary vibration modes involved in the HCO_3^- dehydroxylation reaction, and thus is not expected to introduce any substantial systematic errors in our model predictions on the kinetic isotope fractionation factors; and 3) previous theoretical studies on CO_2 hydroxylation (the reverse reaction of HCO_3^- dehydroxylation) employed similar theoretical methods with similar discrepancies in predicted bicarbonate vibrational frequencies of dissolved bicarbonate ion yet yielded kinetic data agreeing reasonably with experimental values (Davidson et al., 1994; Nemukhin et al., 2002).

We proceed by using our estimated frequencies to theoretically evaluate the magnitude of expected kinetic isotope effects associated with HCO_3^- dehydration and dehydroxylation reactions and compare these calculated fractionations to the experimentally determined kinetic isotope fractionation factors associated with CO_2 degassing from aqueous solutions.

Following the procedures outlined in section 2.2.1, we calculate the kinetic isotope fractionation factors for all isotopologues (and isotopomers) associated with HCO_3^- dehydration and dehydroxylation reactions (see Tables 4-A5 and 4-A6 in Appendix). For the sake of simplicity, we present below the model results only for some representative

isotopolouges (Table 4-3 and Fig. 4-4, 4-5), which are defined as (i.e., equation 1 in section 2.2.1):

$$\alpha_{H^{13}C^{16}O_3^-} = \frac{k_{H^{13}C^{16}O_3^-}}{k_{H^{12}C^{16}O_3^-}} \quad \text{i.e., the fractionation of } H^{13}C^{16}O_3^- \text{ isotopologue}$$

$$\alpha_{H^{12}C^{18}O^{16}O_2^-} = \frac{k_{H^{12}C^{18}O^{16}O_2^-}}{k_{H^{12}C^{16}O_3^-}} \quad \text{i.e., the fractionation of } H^{12}C^{18}O^{16}O_2^- \text{ isotopologue}$$

$$\alpha_{H^{12}C^{17}O^{16}O_2^-} = \frac{k_{H^{12}C^{17}O^{16}O_2^-}}{k_{H^{12}C^{16}O_3^-}} \quad \text{i.e., the fractionation of } H^{12}C^{17}O^{16}O_2^- \text{ isotopologue}$$

$$\alpha_{H^{13}C^{18}O^{16}O_2^-} = \frac{k_{H^{13}C^{18}O^{16}O_2^-}}{k_{H^{13}C^{16}O_3^-}} \quad \text{i.e., the fractionation of } H^{13}C^{18}O^{16}O_2^- \text{ isotopologue}$$

$$\alpha_{H^{12}C^{18}O^{17}O^{16}O^-} = \frac{k_{H^{12}C^{18}O^{17}O^{16}O_2^-}}{k_{H^{12}C^{16}O_3^-}} \quad \text{i.e., the fractionation of } H^{12}C^{18}O^{17}O^{16}O^- \text{ isotopologue.}$$

Follow the definitions of clumped isotope anomalies that are used in carbonate clumped isotope thermometry (e.g., $\Delta_{47}=\left(\frac{^{47}R_{actual}}{^{47}R_{stochastic}}-1\right)\times 1000$, Eiler and Schauble, 2004), we further define:

$$A^{13-18}=\left(\frac{\left(\alpha_{H^{13}C^{18}O^{16}O_2^-}\right)_{actual}}{\left(\alpha_{H^{13}C^{18}O^{16}O_2^-}\right)_{stochastic}}-1\right)\times 1000=\left(\frac{\alpha_{H^{13}C^{18}O^{16}O_2^-}}{\alpha_{H^{13}C^{16}O_3^-}\times\alpha_{H^{12}C^{18}O^{16}O_2^-}}-1\right)\times 1000=\left(\frac{k_{H^{13}C^{18}O^{16}O_2^-}}{k_{H^{13}C^{16}O_3^-}\times k_{H^{12}C^{18}O^{16}O_2^-}}-1\right)\times 1000$$

$$A^{18-17}=\left(\frac{\left(\alpha_{^{12}C^{18}O^{17}O^{16}O}\right)_{actual}}{\left(\alpha_{^{12}C^{18}O^{17}O^{16}O}\right)_{stochastic}}-1\right)\times 1000=\left(\frac{\alpha_{^{12}C^{18}O^{17}O^{16}O}}{\alpha_{^{12}C^{18}O^{16}O_2}\times\alpha_{^{12}C^{17}O^{16}O_2}}-1\right)\times 1000=\left(\frac{k_{^{12}C^{18}O^{17}O^{16}O}}{k_{^{12}C^{18}O^{16}O_2}\times k_{^{12}C^{17}O^{16}O_2}}-1\right)\times 1000$$

.

A^{13-18} and A^{18-17} here have a physical meaning similar to the Δ_{47} value, and indicate the clumped isotope anomaly (i.e., departure from the stochastic distribution) associated with the kinetic reaction. That is, we calculate the difference between the composition of the

reacted pool and the composition it would have if it conformed to the 'the rule of geometric mean' (Bigeleisen, 1955).

Over the temperature range of 0-100°C, our calculated isotope fractionation factors associated with HCO_3^- dehydration in aqueous solution can be represented by (through polynomial fitting of fractionation factors computed at a number of different temperatures; Tables 4-A5 and 4-A6)

$$1000\ln\left(\alpha_{H^{13}C^{16}O_3^-}\right) = -\frac{0.1998\times10^6}{T^2} - \frac{7.964\times10^3}{T} - 0.707 \quad (25a)$$

$$1000\ln\left(\alpha_{H^{12}C^{18}O^{16}O_2^-}\right) = -\frac{0.0168\times10^6}{T^2} - \frac{2.49\times10^3}{T} - 0.4863 \quad (25b)$$

$$1000\ln\left(\alpha_{H^{12}C^{17}O^{16}O_2^-}\right) = -\frac{0.007\times10^6}{T^2} - \frac{1.3305\times10^3}{T} - 0.2244 \quad (25c)$$

$$1000\ln\left(\alpha_{H^{13}C^{18}O^{16}O_2^-}\right) = -\frac{0.2234\times10^6}{T^2} - \frac{10.425\times10^3}{T} - 1.2688 \quad (25d)$$

$$1000\ln\left(\alpha_{H^{12}C^{18}O^{17}O^{16}O^-}\right) = -\frac{0.0257\times10^6}{T^2} - \frac{3.8096\times10^3}{T} - 0.7267 \quad (25e)$$

$$\mathrm{A}^{13-18} = -\frac{0.0068\times10^6}{T^2} + \frac{0.0289\times10^3}{T} - 0.0755 \quad (25f)$$

$$\mathrm{A}^{18-17} = -\frac{0.0018\times10^6}{T^2} + \frac{0.0109\times10^3}{T} - 0.016\,. \quad (25g)$$

Similarly, over the temperature range of 0-100°C, our calculated isotope fractionation factors associated with HCO_3^- dehydroxylation in aqueous solution can be represented by:

$$1000\ln\left(\alpha_{H^{13}C^{16}O_3^-}\right) = -\frac{0.7622\times10^6}{T^2} - \frac{4.0314\times10^3}{T} - 0.3008\,. \quad (26a)$$

Table 4-3 Predicted kinetic isotope fractionations associated with HCO_3^- dehydration and HCO_3^- dehydroxylation reactions at 25°C. See text for the definitions of the fractionation factors.

	Method[&]	Frequency Scaling Factor[&]	1000ln $\alpha_{H^{13}C^{16}O_3^-}$	1000ln $\alpha_{H^{12}C^{18}O^{16}O_2^-}$				A^{13-18}				$CO_2 - HCO_3^-$		
				O1*	O2*	O3*	Aver	O1*	O2*	O3*	Aver	1000lnα^{13}	1000lnα^{18}	A^{13-18}
HCO_3^- dehydration	B3LYP cc-pvtz(-f)	0.9614	**-29.7**	**-4.7**	**-9.3**	**-13.1**	**-9.0**	**-0.06**	**0.24**	**-0.35**	**-0.05**	**-29.7**	**-7.0**	**0.09**
	B3LYP cc-pvtz(-f)	N/A	-30.9	-5.0	-9.8	-13.5	-9.4	-0.06	0.26	-0.37	-0.06	-30.9	-7.3	0.10
	B3LYP cc-pvtz(-f)	1.0318	-32.0	-5.2	-10.1	-13.7	-9.7	-0.07	0.27	-0.38	-0.06	-32.0	-7.6	0.10
HCO_3^- dehydroxylation	B3LYP cc-pvtz(-f)	0.9614	**-22.5**	**12.7**	**12.5**	**-75.2**	**-16.7**	**0.39**	**0.35**	**-0.45**	**0.10**	**-22.4**	**12.6**	**0.37**
	B3LYP cc-pvtz(-f)	N/A	-23.7	13.0	12.8	-78.7	-17.6	0.40	0.36	-0.47	0.10	-23.7	12.9	0.38
	B3LYP cc-pvtz(-f)	1.0318	-24.7	13.4	13.1	-81.6	-18.4	0.41	0.37	-0.28	0.10	-24.8	13.2	0.40
	LMP2 cc-pvtz(-f)	0.9614	-24.8	11.8	11.4	-69.4	-15.4	0.27	0.33	-0.27	0.11	-24.8	11.6	0.30

[&] Fractionation factors predicted with different calculation methods and frequency scaling factors are shown to compare with predictions from our standard model method (bolded), and thus to evaluate their influence on our model predictions (see text for details).

[*] Different isotopomers of the same isotopologue differs in their predicted isotope fractionation factors, depending on the positions of isotopic substitution. O1, O2 and O3 here denote isotopomers with ^{18}O substitution at oxygen positions 1, 2 and 3, respectively (as labeled in Fig. 4-2).

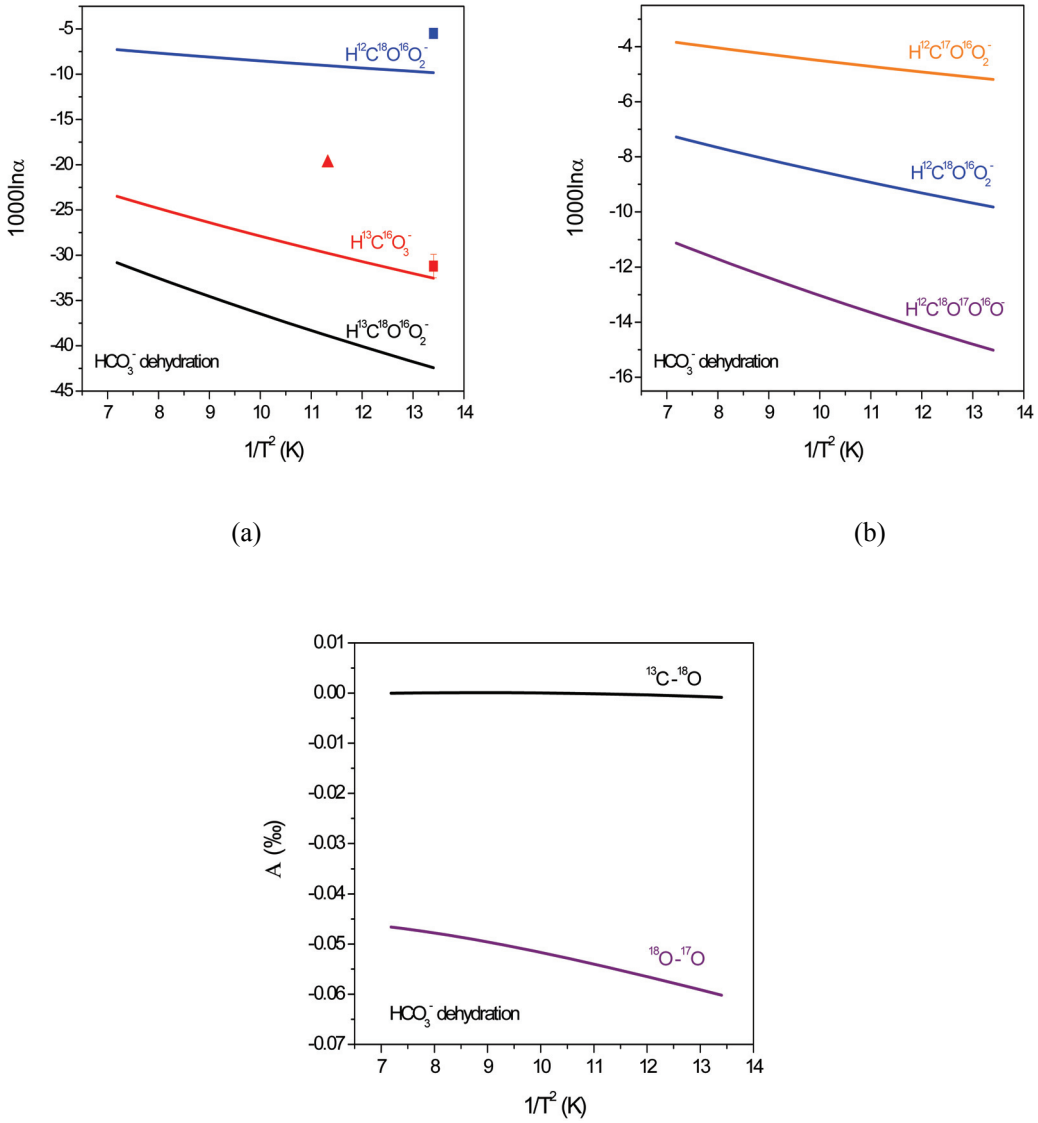

Figure 4-4: Model predicted kinetic isotope fractionation factors associated with HCO_3^- dehydration reaction (0-100°C): (a) fractionation of $H^{13}C^{16}O_3^-$, $H^{12}C^{18}O^{16}O_2^-$ and $H^{13}C^{18}O^{16}O_2^-$ isotopologues; (b) fractionation of $H^{12}C^{18}O^{16}O_2^-$, $H^{12}C^{17}O^{16}O_2^-$, and $H^{12}C^{18}O^{17}O^{16}O^-$ isotopologues; (c) fractionation of ^{13}C-^{18}O and ^{18}O-^{17}O clumped isotopic anomalies. See section 4.1 for the definitions of the plotted fractionation factors. Also shown for comparison are the available experimental estimations on these kinetic isotope fractionations from previous studies (triangle, O'Leary et al. 1992; squares, Clark and Laruriol, 1992).

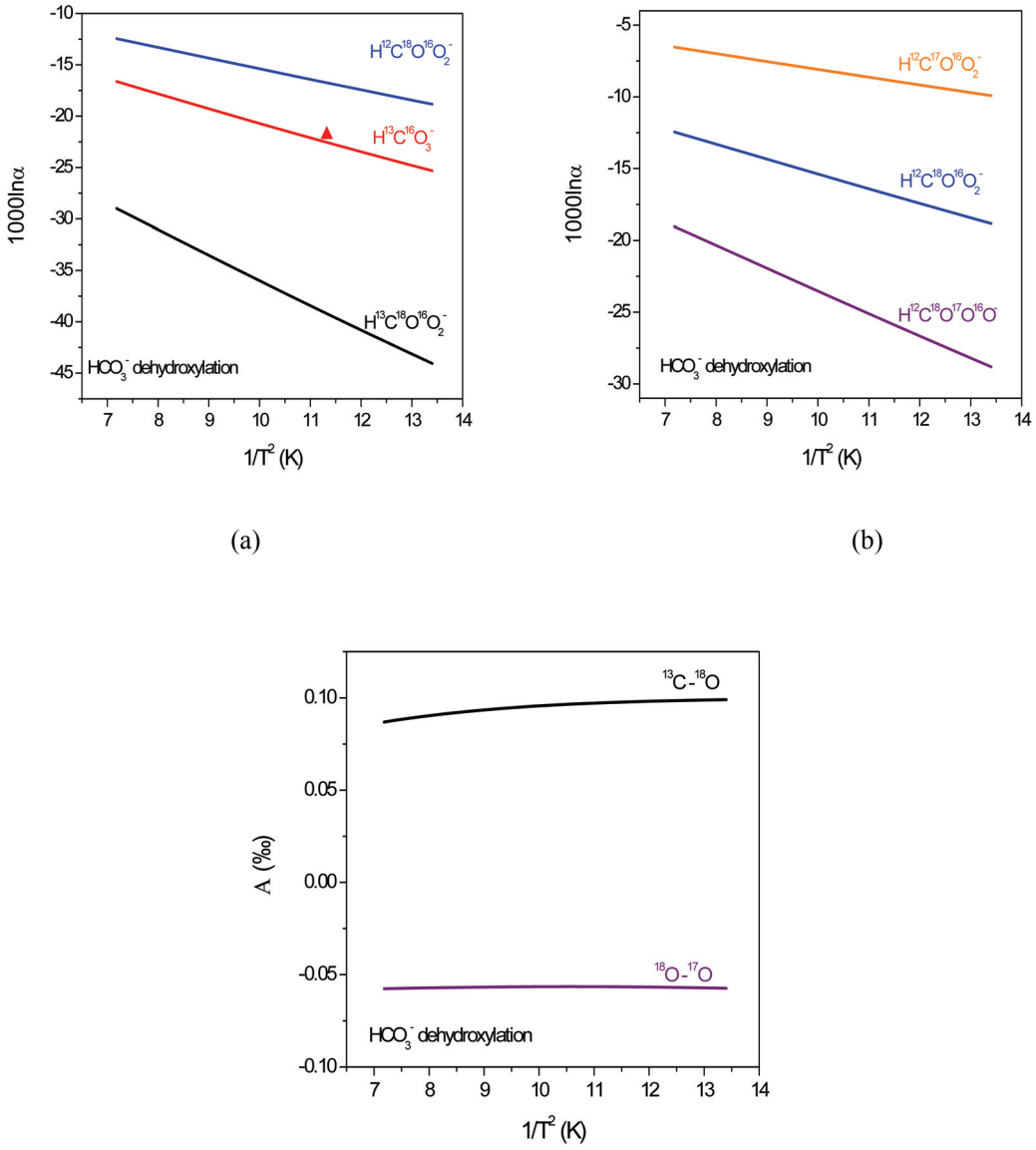

Figure 4-5: Model predicted kinetic isotope fractionation factors associated with HCO_3^- dehydroxylation reaction (0-100°C): (a) fractionation of $H^{13}C^{16}O_3^-$, $H^{12}C^{18}O^{16}O_2^-$ and $H^{13}C^{18}O^{16}O_2^-$ isotopologues; (b) fractionation of $H^{12}C^{18}O^{16}O_2^-$, $H^{12}C^{17}O^{16}O_2^-$, and $H^{12}C^{18}O^{17}O^{16}O^-$ isotopologues; (c) fractionation of ^{13}C-^{18}O and ^{18}O-^{17}O clumped isotopic anomalies. See section 4.1 for the definitions of the plotted fractionation factors. Also shown for comparison are the available experimental estimations on these kinetic isotope fractionations from previous study (triangle, O'Leary et al. 1992).

$$1000\ln\left(\alpha_{H^{12}C^{18}O^{16}O_2^-}\right)=-\frac{0.8666\times10^6}{T^2}-\frac{1.0297\times10^3}{T}-3.4607 \quad (26b)$$

$$1000\ln\left(\alpha_{H^{12}C^{17}O^{16}O_2^-}\right)=-\frac{0.4504\times10^6}{T^2}-\frac{0.6007\times10^3}{T}-1.6845 \quad (26c)$$

$$1000\ln\left(\alpha_{H^{13}C^{18}O^{16}O_2^-}\right)=-\frac{1.6445\times10^6}{T^2}-\frac{4.9746\times10^3}{T}-3.822 \quad (26d)$$

$$1000\ln\left(\alpha_{H^{12}C^{18}O^{17}O^{16}O^-}\right)=-\frac{1.3211\times10^6}{T^2}-\frac{1.6039\times10^3}{T}-5.2443 \quad (26e)$$

$$\mathrm{A}^{13-18}=-\frac{0.0117\times10^6}{T^2}+\frac{0.0865\times10^3}{T}-0.0605 \quad (26f)$$

$$\mathrm{A}^{18-17}=-\frac{0.0041\times10^6}{T^2}+\frac{0.0265\times10^3}{T}-0.0991\,, \quad (26g)$$

where T is the temperature in the unit of Kelvin.

At 25°C, our model predicted carbon isotope and oxygen isotope fractionations (i.e., fractionations of ^{13}C singly-substituted isotopologue $\alpha_{H^{13}C^{16}O_3^-}$ and ^{18}O singly-substituted isotopologue $\alpha_{H^{12}C^{18}O^{16}O_2^-}$) are –29.7‰ and –9.0‰ respectively for HCO_3^- dehydration, and –22.5‰ and –16.7‰ respectively for HCO_3^- dehydroxylation. These predictions agree reasonably well with the available experimental data on the carbon isotope and oxygen fractionation associate with HCO_3^- dehydration and dehydroxylation at 24°C and 0°C (O'Leary et al., 1992 and Clark et al., 1992, Fig. 4-4, 4-5). We also predict the oxygen isotope fractionations associate with HCO_3^- dehydration and HCO_3^- dehydroxylation in aqueous solution follow the mass dependence exponent λ = 0.5279 and λ = 0.5261, respectively, where $\alpha_{H^{12}C^{17}O^{16}O_2^-}=\left(\alpha_{H^{12}C^{17}O^{16}O_2^-}\right)^{\lambda}$. As for kinetic fractionations for ^{13}C-^{18}O, ^{18}O-^{17}O clumped isotopic species ($\alpha_{H^{13}C^{18}O^{16}O_2^-}$ and $\alpha_{H^{12}C^{18}O^{17}O^{16}O^-}$), our model predict –38.8‰, -13.8‰ respectively for HCO_3^- dehydration, and -39.0‰, -25.5‰ respectively for HCO_3^-

dehydroxylation at 25°C. In comparison, the kinetic fractionations for ^{13}C-^{18}O, ^{18}O-^{17}O clumped isotopic anomaly (A^{13-18} and A^{18-17}), are predicted to be 0.05‰, –0.0002‰, respectively for HCO_3^- dehydration, and 0.10‰, –0.06‰, respectively for HCO_3^- dehydroxylation at 25°C. (A^{13-18} and A^{18-17}). Unfortunately, we cannot directly compare these predictions with experimental data.

Note that different isotopomers of the same isotopologue differ significantly in their predicted isotope fractionation factors, depending on the positions of isotopic substitution. For example, at 25°C, our modeled transition state structures (Fig. 4-2) predict that the oxygen isotope fractionations associated with HCO_3^- dehydration and dehydroxylation are –4.7‰, –9.3‰, –13.1‰ and 12.7‰, –75.2‰, 12.5‰ respectively for ^{18}O substitution at positions 1, 2 and 3, (as labeled in Fig. 4-2); Similarly, the fractionation of ^{13}C-^{18}O 'clumped isotope' anomaly associated with HCO_3^- dehydration and dehydroxylation are –0.06‰, 0.24‰, -0.35‰ and 0.39‰, –0.45‰, 0.35‰ respectively for ^{18}O substitution at positions 1, 2 and 3, (Table 3, Fig. 4-6). These position-specific isotope fractionation effects arise from the different bonding environments for different oxygen atoms inside HCO_3^- and their different involvements in the dehydration and dehydroxylation reactions. The isotope fractionation factors presented in the above equations (17a-g and 18a-g) are the average of the fractionation factors of all the isotopomers of the relevant isotopologue (Tables 4-A5 and 4-A6).

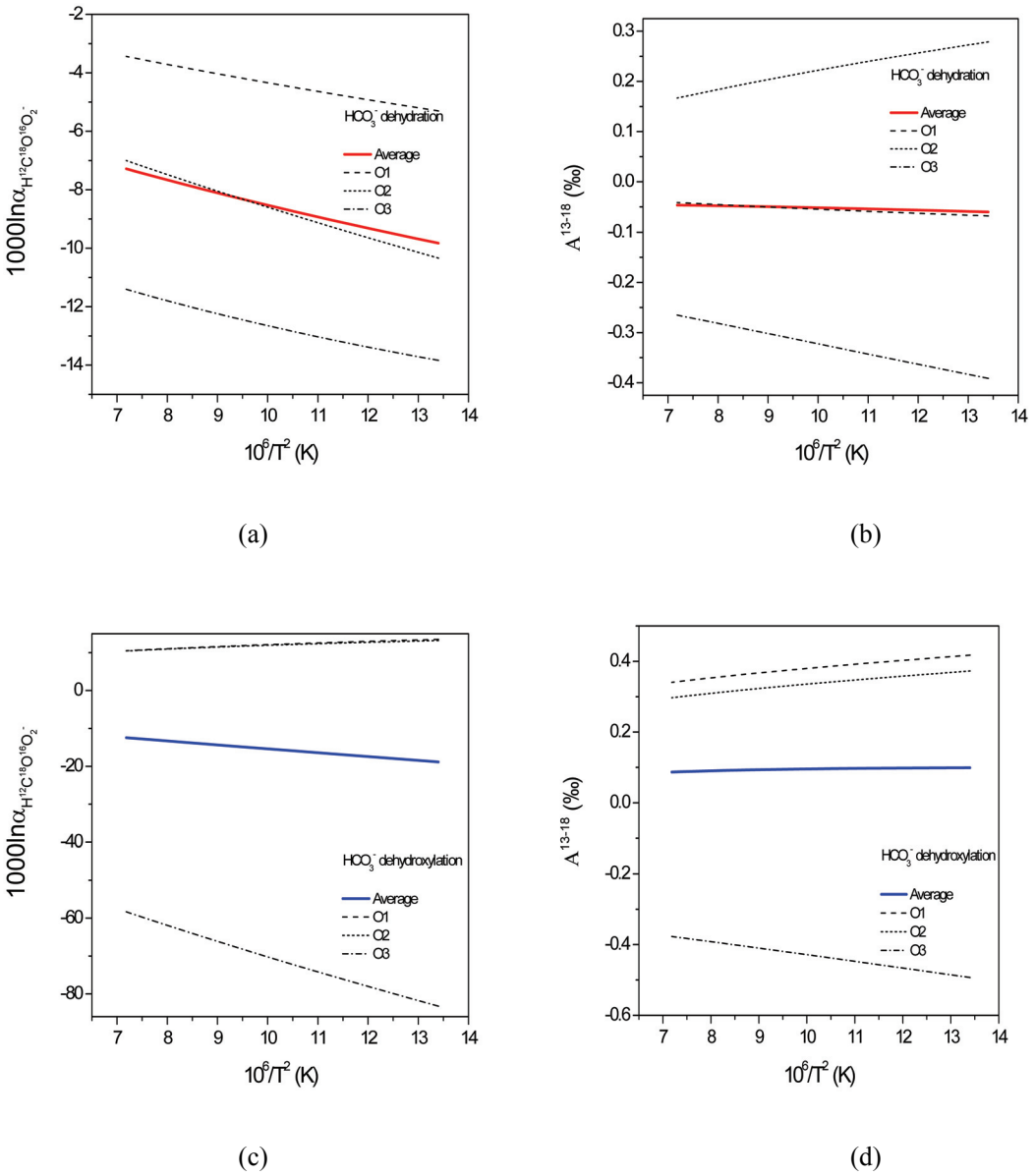

Figure 4-6: Position specificity of kinetic isotope fractionations of (a) oxygen isotope and (b) ^{13}C-^{18}O clumped isotopologues associated with HCO_3^- dehydration; of (c) oxygen isotope and (d) ^{13}C-^{18}O clumped isotopologues associated with HCO_3^- dehydroxylation. O1, O2 and O3 here denote isotopomers with ^{18}O substitution at oxygen position 1, 2 and 3 respectively (as labeled in Figure2).

Our model also makes predictions about the isotopic compositions of the CO_2 produced by dehydration or dehydroxylation of DIC (Table 4-3 and Fig. 4-7, 4-8); this should correspond to the isotopic composition of CO_2 degassed from super-saturated solutions unless some other isotopically fractionating process modifies its composition:

for HCO_3^- dehydration

$$1000\ln\alpha^{13}\left(CO_2\text{-}HCO_3^-\right)=1000\ln\left(\alpha_{H^{13}C^{16}O_3^-}\right)=-\frac{0.1998\times10^6}{T^2}-\frac{7.964\times10^3}{T}-0.707 \quad (28a)$$

$$1000\ln\alpha^{18}\left(CO_2\text{-}HCO_3^-\right)=-\frac{0.1282\times10^6}{T^2}-\frac{1.8414\times10^3}{T}+0.6373 \quad (28b)$$

$$1000\ln\alpha^{17}\left(CO_2\text{-}HCO_3^-\right)=-\frac{0.0663\times10^6}{T^2}-\frac{0.989\times10^3}{T}+0.3555 \quad (28c)$$

$$1000\ln\alpha^{13-18}\left(CO_2\text{-}HCO_3^-\right)=-\frac{0.3282\times10^6}{T^2}-\frac{9.7602\times10^3}{T}-0.1264 \quad (28d)$$

$$1000\ln\alpha^{18-17}\left(CO_2\text{-}HCO_3^-\right)=-\frac{0.1901\times10^6}{T^2}-\frac{2.8317\times10^3}{T}+0.9788 \quad (28e)$$

$$1000\ln A^{13-18}\left(CO_2\text{-}HCO_3^-\right)=-\frac{0.0003\times10^6}{T^2}+\frac{0.0452\times10^3}{T}-0.0567 \quad (28f)$$

$$1000\ln A^{18-17}\left(CO_2\text{-}HCO_3^-\right)=-\frac{0.0045\times10^6}{T^2}-\frac{0.0012\times10^3}{T}-0.014\,, \quad (28g)$$

for HCO_3^- dehydroxylation

$$1000\ln\alpha^{13}\left(CO_2\text{-}HCO_3^-\right)=1000\ln\left(\alpha_{H^{13}C^{16}O_3^-}\right)=-\frac{0.7622\times10^6}{T^2}-\frac{4.0314\times10^3}{T}-0.3008 \quad (29a)$$

$$1000\ln\alpha^{18}\left(CO_2\text{-}HCO_3^-\right)=-\frac{0.5705\times10^6}{T^2}+\frac{6.5416\times10^3}{T}-2.9418 \quad (29b)$$

$$1000\ln\alpha^{17}\left(CO_2\text{-}HCO_3^-\right)=-\frac{0.2968\times10^6}{T^2}+\frac{3.4066\times10^3}{T}-1.4776 \quad (29c)$$

$$1000\ln\alpha^{13-18}\left(CO_2\text{-}HCO_3^-\right)=-\frac{1.3428\times10^6}{T^2}+\frac{2.6262\times10^3}{T}-3.1905 \quad (29d)$$

$$1000\ln\alpha^{18-17}\left(CO_2\text{-}HCO_3^-\right)=-\frac{0.8587\times10^6}{T^2}+\frac{9.9606\times10^3}{T}-4.4739 \quad (29e)$$

$$A^{13-18}\left(CO_2\text{-}HCO_3^-\right)=-\frac{0.0061\times10^6}{T^2}+\frac{0.116\times10^3}{T}+0.0521 \quad (29f)$$

$$A^{18-17}\left(CO_2\text{-}HCO_3^-\right)=-\frac{0.0087\times10^6}{T^2}+\frac{0.0124\times10^3}{T}-0.0545\,, \quad (29g)$$

where $\alpha^{13}\left(CO_2\text{-}HCO_3^-\right)$, $\alpha^{18}\left(CO_2\text{-}HCO_3^-\right)$, $\alpha^{17}\left(CO_2\text{-}HCO_3^-\right)$, $\alpha^{13-18}\left(CO_2\text{-}HCO_3^-\right)$, $\alpha^{18-17}\left(CO_2\text{-}HCO_3^-\right)$, $A^{13-18}\left(CO_2\text{-}HCO_3^-\right)$ and $A^{18-17}\left(CO_2\text{-}HCO_3^-\right)$ refer to the kinetic fractionation factor for ^{13}C singly substituted isotopologue (i.e., carbon isotope), ^{18}O singly substituted isotopologue (i.e., oxygen isotope), ^{17}O singly substituted isotopologue, ^{13}C-^{18}O clumped isotopologue, ^{18}O-^{17}O clumped isotopologue, ^{13}C-^{18}O clumped isotope anomaly and ^{18}O-^{17}O clumped isotope anomaly between product CO_2 and reactant HCO_3^-, respectively, and are defined as above for $\alpha_{H^{13}C^{16}O_3^-}$, $\alpha_{H^{12}C^{18}O^{16}O_2^-}$, $\alpha_{H^{12}C^{17}O^{16}O_2^-}$, $\alpha_{H^{13}C^{18}O^{16}O_2^-}$, $\alpha_{H^{12}C^{18}O^{17}O^{16}O^-}$, A^{13-18} and A^{13-18}. However, instead of averaging the fractionation factors of all the relevant isotopomers of each isotopologue (e.g., as we do for $\alpha_{H^{12}C^{18}O^{16}O_2^-}$ and $\alpha_{H^{13}C^{18}O^{16}O_2^-}$; see above), $\alpha^{18}\left(CO_2\text{-}HCO_3^-\right)$ and $\alpha^{13-18}\left(CO_2\text{-}HCO_3^-\right)$ are calculated by averaging only the kinetic isotope fractionation factors from the isotopomers that are capable of producing ^{18}O-substituted and ^{13}C-^{18}O doubly substituted CO_2 (i.e., isotopomers with ^{18}O substitution at oxygen atom position 1 or 2; Fig. 4-2). At 25°C, the kinetic oxygen isotope and ^{13}C-^{18}O clumped isotope anomaly fractionations between product CO_2 and reactant HCO_3^- are predicted to be –7.0‰, 0.09‰ and +12.6‰, 0.37‰, for HCO_3^- dehydration and dehydroxylation reaction, respectively.

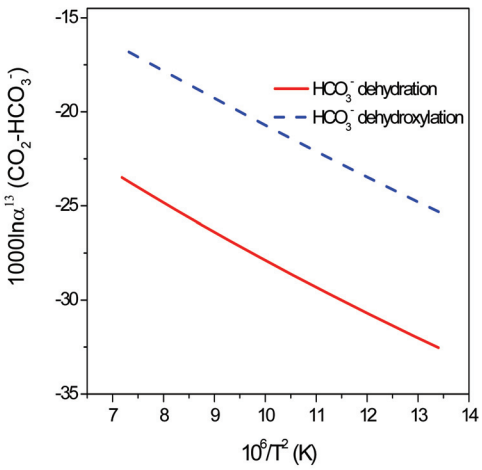

Fig. 7(a)

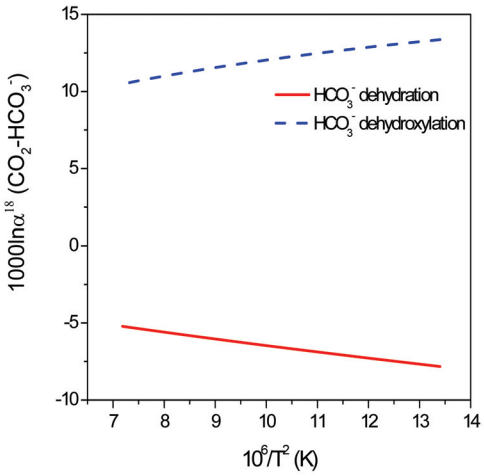

Fig. 7(b)

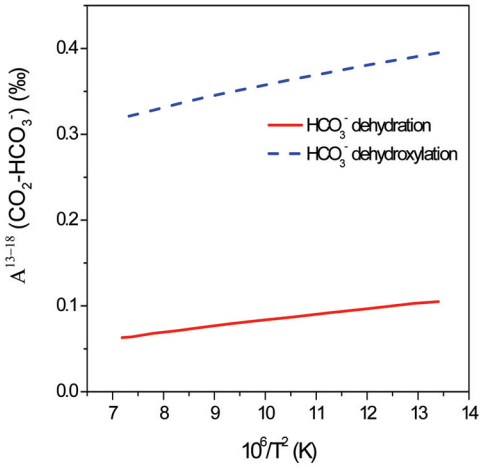

Fig. 7(c)

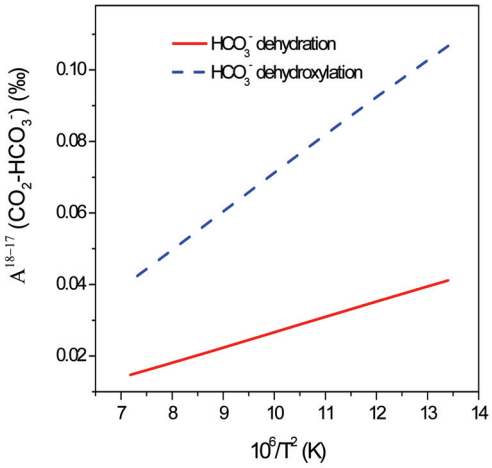

Fig. 7(d)

Figure 4-7: Model predicted fractionations of (a) carbon isotope; (b) oxygen isotope; (c) ^{13}C-^{18}O clumped isotopic anomaly and (d) ^{18}C-^{17}O clumped isotopic anomaly between degassed CO_2 and reactant HCO_3^- during HCO_3^- dehydration and HCO_3^- dehydroxylation.

We investigated the influence of our choice of frequency scaling factor (i.e., the proportionality between modeled vibrational frequencies and those measured for aqueous HCO_3^-) on our model results, by using 1) no scaling factor and 2) a scaling factor of

1.0318 (determined by the comparison between our model predicted and the experimentally determined vibration frequencies for dissolved HCO_3^-, excluding the νCO-H vibration mode). In both cases, our model predicted kinetic isotope fractionations are sufficiently close to our model results that were calculated using the preferred scaling factor of 0.9614 (e.g., differ by less than 2.5‰, 2.0‰ and 0.01‰, respectively for carbon isotope, oxygen isotope and ^{13}C-^{18}O clumped isotope fractionations at 25°C; Table 4-3). We conclude that uncertainties regarding the frequency scaling factor contribute to the absolute accuracy of our models, but are not a first-order systematic error; i.e., the general features of our modeled fractionations are insensitive to this constant.

Similarly, our calculation of isotopic fractionations for HCO_3^- dehydration reaction made with the transition-state structure based on the LMP2 method (with the same frequency scaling factor of 0.9614) also predicts kinetic isotope fractionations close to our standard model results based on the B3LYP method (e.g., –24.8‰, –15.4‰ and 0.11‰ for carbon isotope, oxygen isotope and ^{13}C-^{18}O clumped isotope fractionations respectively at 25°C; LMP2 method; Table 4-3). Therefore our choice of the B3LYP calculation method does not seem to have dictated the general characteristics of our model result.

4.2 Predicted influence of kinetic isotope fractionations on carbonate minerals grown from degassing aqueous solutions

Our models of the kinetic isotope fractionation factors associated with HCO_3^- dehydration and dehydroxylation reaction make predictions regarding the evolution of abundances of different HCO_3^- isotopologues in aqueous solution that is undergoing CO_2

degassing. In order to relate these model predictions to the expected isotopic compositions of carbonates, we must consider isotopic fractionations between DIC and solid carbonates and the relative rates of CO_2 degassing and carbonate growth (following the procedures outlined in section 2.3). Fig. 4-8 illustrates predicted carbon isotope, oxygen isotope, $\Delta_{^{13}C^{18}O^{16}O_2}$ and $\Delta_{^{12}C^{18}O^{17}O^{16}O}$ compositions in carbonate minerals that grow as CO_2 degassing progresses (where the extent of degassing is expressed as the fraction of dissolved HCO_3^- remaining in aqueous solution).

Four different scenarios are considered (as discussed in section 2.3.2):

1) HCO_3^- dehydration is the only isotope fractionation process that influences the isotopic composition of HCO_3^- in aqueous solution; 2) HCO_3^- dehydroxylation is the only isotope fractionation process that influences the isotopic composition of HCO_3^- in aqueous solution. These two cases would describe a system in which a negligible amount of carbonate grows despite extensive degassing; 3) The HCO_3^- dehydration reaction is coupled with carbonate precipitation, at a molar ratio of 1:1; and 4) the HCO_3^- dehydroxylation reaction is coupled with carbonate precipitation, at a molar ratio of 1:1. In all cases, we assume that solid carbonate grows in equilibrium with co-existing DIC.

The predicted kinetic fractionations of various isotopologues are correlated with each other (Table 4-4); i.e., the kinetic mechanism we consider has a distinctive isotopic 'fingerprint', distinct from that for equilibrium fractionations and possibly other processes, that might be used to identify carbonates grown from degassing aqueous solutuions. For example, at 25°C,

1) If CO_2 degassing reactions (i.e., HCO_3^- dehydration and HCO_3^- dehydroxylation) are the only isotope fractionation processes that influence the isotopic composition of

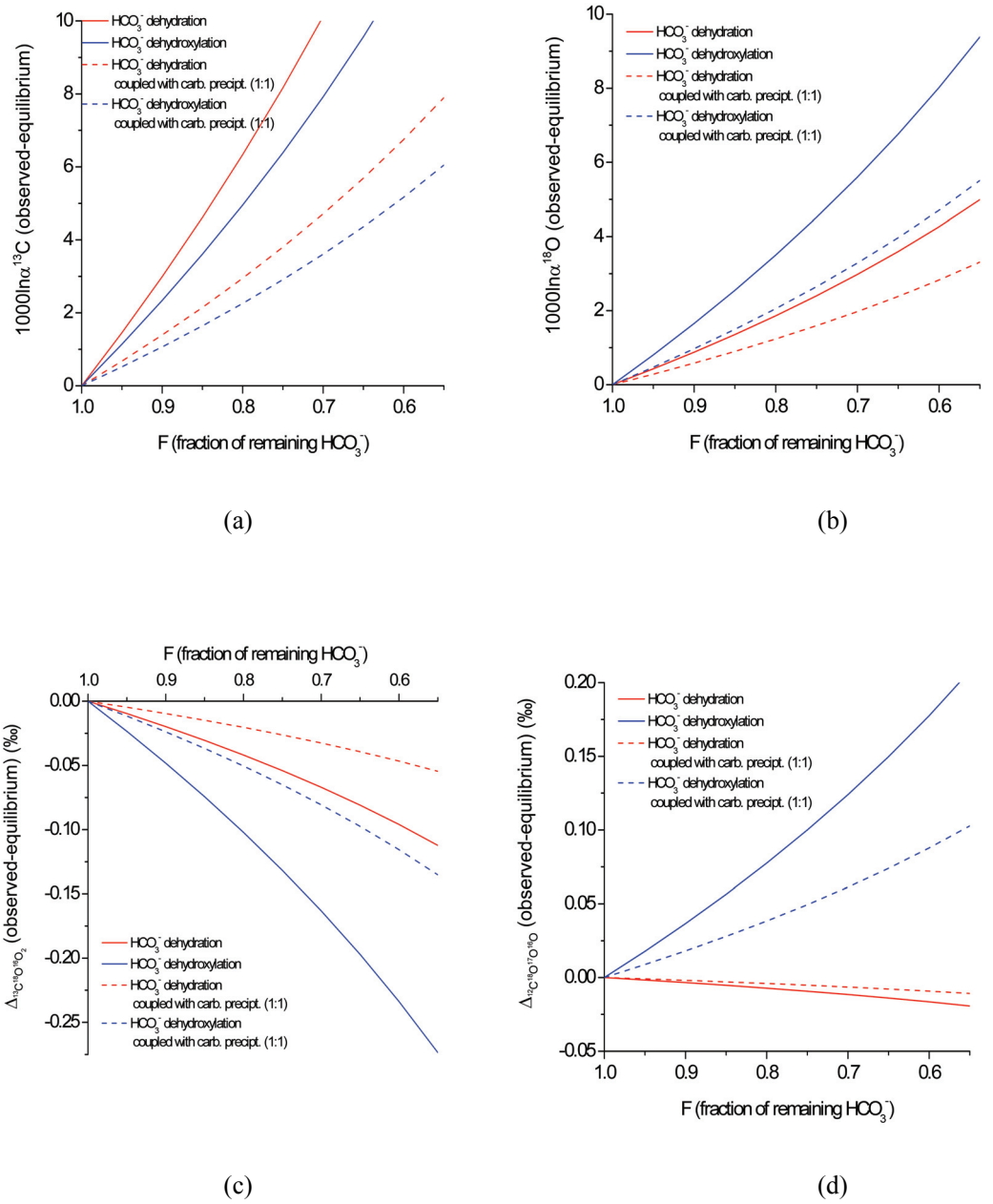

Figure 4-8: The kinetic fractionations of (a) carbon isotope, (b) oxygen isotope, (c) $\Delta_{^{13}C^{18}O^{16}O_2}$ and (d) $\Delta_{^{12}C^{18}O^{17}O^{16}O}$ in the carbonate mineral as a function of the fraction of remaining HCO_3^- (F), predicted by our model. Four different cases are considered, as labeled in the legend (see text for details).

Table 4-4 The co-variations of carbon isotope, $\Delta_{^{13}C^{18}O^{16}O_2}$, $\Delta_{^{12}C^{18}O^{17}O^{16}O}$ and Δ_{63} fractionations in carbonate mineral, relative to 1‰ kinetic increase in its $^{18}O/^{16}O$, predicted from our model.

	Temperature (°C)	CO_2 degassing Only				CO_2 degassing coupled with carbonate formation (molar ratio 1:1)			
		$^{13}C/^{12}C$	$\Delta_{^{13}C^{18}O^{16}O_2}$	$\Delta_{^{12}C^{18}O^{17}O^{16}O}$	Δ_{63}	$^{13}C/^{12}C$	$\Delta_{^{13}C^{18}O^{16}O_2}$	$\Delta_{^{12}C^{18}O^{17}O^{16}O}$	Δ_{63}
HCO_3^- dehydration	0	3.276	-0.0261	-0.0048	-0.0247	2.378	-0.0199	-0.0040	-0.0189
	5	3.271	-0.0256	-0.0047	-0.0242	2.376	-0.0194	-0.0040	-0.0184
	10	3.267	-0.0250	-0.0046	-0.0237	2.370	-0.0190	-0.0039	-0.0180
	15	3.263	-0.0245	-0.0045	-0.0232	2.359	-0.0185	-0.0038	-0.0175
	20	3.259	-0.0239	-0.0045	-0.0226	2.345	-0.0180	-0.0038	-0.0171
	25	3.255	-0.0234	-0.0044	-0.0222	2.328	-0.0175	-0.0037	-0.0166
	30	3.251	-0.0229	-0.0043	-0.0217	2.308	-0.0170	-0.0036	-0.0152
HCO_3^- dehydroxylation	0	1.416	-0.0314	0.0226	-0.0280	1.117	-0.0268	0.0194	-0.0239
	5	1.416	-0.0309	0.0225	-0.0275	1.116	-0.0264	0.0193	-0.0235
	10	1.416	-0.0304	0.0224	-0.0271	1.113	-0.0260	0.0191	-0.0231
	15	1.416	-0.0300	0.0223	-0.0267	1.109	-0.0255	0.0190	-0.0227
	20	1.415	-0.0296	0.0222	-0.0263	1.104	-0.0250	0.0188	-0.0222
	25	1.414	-0.0292	0.0221	-0.0259	1.098	-0.0245	0.0186	-0.0218
	30	1.414	-0.0288	0.0220	-0.0255	1.090	-0.0241	0.0184	-0.0214

HCO_3^- in aqueous solution, we predict for HCO_3^- dehydration that every 1‰ kinetic increase in carbonate $^{18}O/^{16}O$ will be accompanied by an increase in carbonate $^{13}C/^{12}C$ of 3.26‰, a decrease in $\Delta_{^{13}C^{18}O^{16}O_2}$ of 0.0222‰, and a $\Delta_{^{12}C^{18}O^{17}O^{16}O}$ decrease of 0.004‰. Similarly, for every 1 ‰ increase in carbonate d18O produced by HCO_3^- dehydroxylation, carbonate $^{13}C/^{12}C$ will increase by 1.41‰, $\Delta_{^{13}C^{18}O^{16}O_2}$ will decrease by 0.0292‰, and $\Delta_{^{12}C^{18}O^{17}O^{16}O}$ will increase by 0.0221‰.

2) If the progress of CO_2 degassing reactions are coupled to carbonate growth at a molar ratio of 1:1 (i.e., for every one CO_2 molecule degassed from the solution, one formula unit of carbonate precipitates), then our model predicts for HCO_3^- dehydration that for every 1‰ kinetic increase in carbonate $^{18}O/^{16}O$, carbonate $^{13}C/^{12}C$ will increase by 2.34‰, $\Delta_{^{13}C^{18}O^{16}O_2}$ will decrease by 0.0175‰, $\Delta_{^{12}C^{18}O^{17}O^{16}O}$ will decrease by 0.004‰ and $\Delta_{^{12}C^{18}O^{18}O^{16}O}$ will decrease by 0.006‰. And for HCO_3^- will increase by 2.38‰, $\Delta_{^{13}C^{18}O^{16}O_2}$ will decrease by 0.0165‰, $\Delta_{^{12}C^{18}O^{17}O^{16}O}$ will increase by 2.38‰, $\Delta_{^{13}C^{18}O^{16}O_2}$ will decrease by 0.0165‰, $\Delta_{^{12}C^{18}O^{17}O^{16}O}$ will decrease by 0.003‰ and $\Delta_{^{12}C^{18}O^{18}O^{16}O}$ will decrease by 0.006‰. And for HCO_3^- dehydroxylation, for every 1‰ kinetic increase in carbonate $^{18}O/^{16}O$, carbonate $^{13}C/^{12}C$ will increase by 1.10‰, $\Delta_{^{13}C^{18}O^{16}O_2}$ will decrease by 0.0245‰, $\Delta_{^{12}C^{18}O^{17}O^{16}O}$ will increase by 0.0186‰ and $\Delta_{^{12}C^{18}O^{18}O^{16}O}$ will increase by 0.0352‰.

These co-variations of different kinetic isotope fractionations vary little with temperature (Table 4-4).

The predicted effects of kinetic isotope fractionations on clumped isotope anomalies in precipitated carbonate minerals are relatively large, despite the fact that fractionations of multiply substituted isotopologues of the HCO_3^- are relatively modest. For example,

we predict that the HCO_3^- dehydration reaction will lead to a 0.0234‰ decrease in $\Delta_{^{13}C^{18}O^{16}O_2}$ in the carbonate mineral for every 1‰ kinetic enrichment in its $^{18}O/^{16}O$, even though the increase in $\Delta_{^{13}C^{18}O^{16}O_2}$ directly caused by kinetic fractionations of ^{13}C-^{18}O substituted isotopologues is only 0.005‰ for every 1‰ kinetic enrichment in its $^{18}O/^{16}O$ (Table 4-3, section 4.1). This somewhat counter-intuitive amplification of the change in $\Delta^{13}C^{18}O^{16}O_2$ arises from the fact that $\Delta_{^{13}C^{18}O^{16}O_2}$ (and all other clumped isotope anomalies), is not a conservative compositional parameter (Eiler and Schauble, 2004); in this respect, it is unlike $\delta^{13}C$ and $\delta^{18}O$ values. That is, in any system undergoing irreversible fractionations such as those we model, carbon and oxygen isotope changes must conform to the mass balance relations:

$$n_{\text{initial}} \times R^{13}_{initial} = n_{\text{consumed}} \times R^{13}_{consumed} + n_{\text{residual}} \times R^{13}_{residual}$$

$$n_{\text{initial}} \times R^{18}_{initial} = n_{\text{consumed}} \times R^{18}_{consumed} + n_{\text{residual}} \times R^{18}_{residual},$$

where $n_{initial}$, $n_{consumed}$ and $n_{residual}$ represent the moles of HCO_3^- in the initial, consumed and residual pools respectively. But for clumped isotope anomalies like $\Delta_{^{13}C^{18}O^{16}O_2}$ this does not hold true:

$$n_{\text{initial}} \times \Delta^{\text{initial}}_{^{13}C^{18}O^{16}O_2} \neq n_{\text{consumed}} \times \Delta^{\text{consumedl}}_{^{13}C^{18}O^{16}O_2} + n_{\text{residual}} \times \Delta^{\text{residual}}_{^{13}C^{18}O^{16}O_2}.$$

This characteristic of clumped isotope anomalies was first demonstrated by Eiler and Schauble (2004) for the case of mixing two pools of CO_2. If the two end members differ significantly in $\delta^{18}O$ and/or $\delta^{13}C$, their mixture may take on a Δ_{47} value that differs from the weighted average of the Δ_{47} values of the end members. This 'nonlinearity' of mixing ultimately reflects the fact that the abundances of multiply-substituted isotoplogues expected for a stochastic distribution (the '0' point on the Δ_i scale) is a non-

linear function of bulk isotopic composition. Similarly, mixing of two pools of HCO_3^- with the *same* $\Delta_{^{13}C^{18}O^{16}O_2}$ but with different bulk isotopic compositions (i.e., $^{13}C/^{12}C$, $^{18}O/^{16}O$) will produce a mixed pool having a $\Delta_{^{13}C^{18}O^{16}O_2}$ different from that of the end members. The same principle also applies to separation, the reverse of mixing; i.e., if one separates a portion of a HCO_3^- pool that differs in bulk isotopic composition from its initial pool but is identical to that pool in $\Delta_{^{13}C^{18}O^{16}O_2}$, the $\Delta_{^{13}C^{18}O^{16}O_2}$ value of the residual HCO_3^- pool can change. The exact amount of this $\Delta_{^{13}C^{18}O^{16}O_2}$ change depends on the difference in bulk isotopic composition between the separated pool and the initial pool; in case the case we consider in our CO_2 degassing models, this difference corresponds to the carbon and oxygen isotope fractionations between the consumed HCO_3^- pool and residual HCO_3^- pool (i.e., α in equation 4).

We combine our model predicted kinetic fractionations for $\Delta_{^{13}C^{18}O^{16}O_2}$ and $\Delta_{^{12}C^{18}O^{17}O^{16}O}$ to estimate the kinetic fractionation for Δ_{63} (the abundance anomaly of mass 63 of carbonate ion, defined as $\Delta_{63} = \frac{[63]_{actual}/[60]_{actual}}{[63]_{stochastic}/[60]_{stochastic}}$; Guo et al., 2008b) in the carbonate mineral:

$$\Delta_{63} \approx f_{^{13}C^{18}O^{16}O_2} \times \Delta_{^{13}C^{18}O^{16}O_2} + f_{^{12}C^{18}O^{17}O^{16}O} \times \Delta_{^{12}C^{18}O^{17}O^{16}O},$$

where $f_{^{13}C^{18}O^{16}O_2}$ and $f_{^{12}C^{18}O^{17}O^{16}O}$ are the relative abundance fractions of isotopologues $^{13}C^{18}O^{16}O_2^{2-}$ and $^{12}C^{18}O^{17}O^{16}O^{2-}$ in all the mass 63 isotopologues of CO_3^{2-} in the carbonate mineral (Table 4). For typical isotopic compositions of terrestrial carbonates (e.g., $\delta^{13}C_{VPDB}$=-5‰ and $\delta^{18}O_{VSMOW}$=30‰), $f_{^{13}C^{18}O^{16}O_2}$ ≈93.5% and $f_{^{12}C^{18}O^{17}O^{16}O}$ ≈6.5%. We predict, at 25°C, for every 1‰ kinetic increase in carbonate $^{18}O/^{16}O$, carbonate Δ_{63} decreases by 0.0222‰ and 0.0259‰ respectively for HCO_3^- dehydration and

dehydroxylation when these CO_2 degassing reactions are the only processes influencing the isotopic composition of the dissolved HCO_3^-. If the HCO_3^- dehydration and dehydroxylation reactions are coupled with carbonate precipitation, the predicted Δ_{63} decreases are 0.0166‰ and 0.0218‰ respectively for every 1‰ kinetic increase in carbonate $^{18}O/^{16}O$ (Table 4-4; assuming 1 mole of carbonate precipitates for every mole of CO_2 evolved). The Δ_{47} value in the CO_2 derived from acid digestion of carbonate minerals (the basis of carbonate clumped isotope thermometry) is proportional to the Δ_{63} in that carbonate mineral (Guo et al., 2008b). Therefore, we will expect that the effects of kinetic fractionations on the Δ_{47} in the CO_2 derived from acid digestion of carbonate minerals will equal the calculated changes in Δ_{63} for those carbonates (Fig. 4-9).

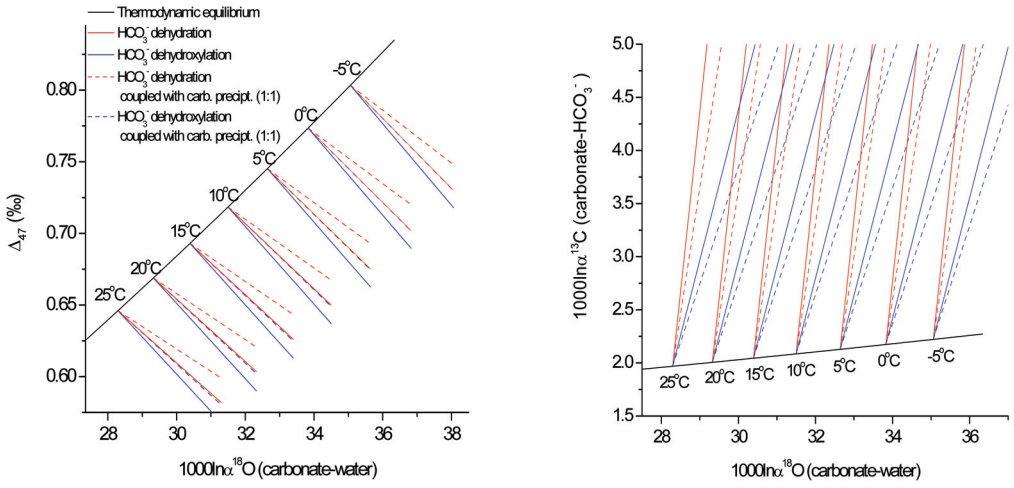

(a) (b)

Figure 4-9: Correlations between kinetic carbon isotope, oxygen isotope and Δ_{47} clumped isotope fractionations expected in the carbonate mineral, based on our predictions of the kinetic isotope fractionation associated with HCO_3^- dehydration and dehydroxylation reactions and our carbonate precipitation model: (a) correlations between kinetic Δ_{47} clumped isotope and oxygen isotope fractionations; (b) correlations between kinetic carbon isotope and oxygen isotope fractionations. Four different scenarios are considered, as labeled in the legend (see text for details).

4.3 Isotopic compositions of cryogenic carbonates

All of the synthetic cryogenic carbonates examined in this study are enriched in $\delta^{13}C$ and in $\delta^{18}O$ relative to the expected compositions for calcite in equilibrium with their parent waters (except 0611B-07). These carbonates are also all lower in Δ_{47} than expected values if they grew at equilibrium at 0°C (Table 4-5). The magnitudes of departures from expected, equilibrium isotopic compositions vary among the different samples, from 1.1‰ to 6.4‰ for $\delta^{13}C$, from 0.4‰ to 2.0‰ for $\delta^{18}O$, and from 0.043‰ to 0.086‰ for Δ_{47}. The size of the departure from isotopic equilibrium does not exhibit any obvious correlations with the sample preparation conditions (Tables 4-2 and 4-5).

Table 4-5 Isotopic compositions of cryogenic carbonates synthesized in this study.

	Sample No.	0412-07	0418-07	0504A-07	0611A-07	0611B-07	0920A-07
Expected equil. values	$\delta^{13}C_{cc}$ (‰)	-19.8	-19.8	-18.9	-19.7	-20.6	-15.2
	$\delta^{18}O_{cc}$ (‰)	31.8	31.8	31.8	31.9	32.1	33.1
	Δ_{47} (‰)	0.773	0.773	0.773	0.773	0.773	0.773
Observed values	$\delta^{13}C_{cc}$ (‰)	-13.42	-15.83	-17.73	-15.1	-15.12	-12.91
	$\delta^{18}O_{cc}$ (‰)	33.71	32.19	32.84	33.38	31.43	34.66
	[&]Δ_{47} (‰)	0.692(4)	0.730(3)	0.715(2)	0.724(3)	0.687(3)	0.716(4)
	1σ (‰)	0.014	0.002	0.006	0.003	0.007	0.014
	[*]$T_{Apparent}$ (°C)	15.2	7.8	10.6	8.9	16.1	16.5

[*] $T_{Apparent}$ denote the apparent formation temperatures estimated for cryogenic carbonates, based on their observed Δ_{47} (if the cryogenic carbonates were formed in isotopic equilibrium).

[&] Number in the bracket indicates the number of replicate isotope analyses for that carbonate sample.

The expected equilibrium isotope compositions of the cryogenic carbonates were estimated based on the $\delta^{13}C$ of the dissolved HCO_3^-, $\delta^{18}O$ of the solution water and the known equilibrium isotope fractionation factors between carbonate and dissolved HCO_3^- and water (carbon isotope, Deines et al., 1974; oxygen isotope, Kim and O'Neil, 1997, Beck et al., 2005; Δ_{47}, Ghosh et al., 2006). Note that, only $\delta^{13}C$ of the total dissolved inorganic carbon (DIC) were determined in the cryogenic experiments. To derive the initial $\delta^{13}C$ of the dissolved HCO_3^-, we first determine the speciation of the dissolved inorganic carbon in the solution based on the determined solution pH and known dissociation constants of carbonic acid (Roy et al., 1993), and then combine this speciation information with the experimentally determined $\delta^{13}C$ of the total DIC and with the known equilibrium carbon isotope fractionation among different DIC species (Zhang et al., 1995).

Both the solution pH and $\delta^{13}C$ of the total DIC used in the above computation were determined at the starting of the freezing experiments (i.e., at either room temperature or 3-7°C; section 3.1), and do not necessarily represent the actual $\delta^{13}C$ of the DIC at the beginning of CO_2 degassing (i.e., at 0°C, the temperature of cryogenic carbonate formation). Although the temperature change itself is not expected to significantly affect $\delta^{13}C$ of the total DIC or solution pH, the possibility of further dissolution of headspace CO_2 in the container during the cooling might change both $\delta^{13}C_{DIC}$ and solution pH. Similarly, the $\delta^{18}O$ values of water used in the above estimation of expected equilibrium carbonate isotopic composition were also determined at the starting of freezing experiments and were assumed to remain unchanged as the solution froze. However, previous studies on cryogenic carbonates indicate the $\delta^{18}O$ of water

might decrease significantly during ice formation due to the preferential incorporation of ^{18}O into water ice (Zak et al., 2004). The errors introduced by these effects on our estimation of expected equilibrium isotopic composition for carbonates are difficult to quantified, but might partially explain the depletion (as opposed to enrichment) of the oxygen isotopic compositions of sample 0611B-07 relative to its expected equilibrium oxygen isotope value (i.e., because we failed to consider the effect of ice formation on the $\delta^{18}O$ of water and thus overestimated the expected equilibrium oxygen isotopic composition of the carbonate). Future cryogenic experiments should be performed under more controlled settings and conditions (e.g., like settings in Killawee et al., 1999), so that the $\delta^{13}C$ of the total DIC and solution pH can be determined at 0°C and the $\delta^{18}O$ of water can be monitored as the solution freezes.

Our observed enrichments of $\delta^{13}C$ and $\delta^{18}O$ and depletion of Δ_{47} in cryogenic carbonates, relative to their expected equilibrium values at 0°C, are consistent with previous carbon and oxygen isotope studies of cryogenic carbonates (Clark and Lauriol, 1992), and with our model predictions on the isotopic compositions of carbonates that form from the degassing solution (section 4.2). Note that, both cryogenic carbonates synthesized in this study and natural speleothems form from the same physiochemical mechanism, i.e., degassing of CO_2 from aqueous solution. Therefore our observed deviations of their isotopic compositions from expected equilibrium values are very similar to those observed for speleothem carbonates (carbon and oxygen isotope, Mickler et al., 2004 and 2006; clumped isotope, Affek et al., 2008, Daeron et al., 2008). In particular, the depletions of Δ_{47} in our cryogenic carbonates, if unaccounted for, will lead to apparent overestimation of their formation temperatures by 8-16°C as determined by

carbonate clumped isotope thermometer (Table 4-5). This compares with the 8-22°C overestimation of carbonate formation temperature when applying carbonate clumped isotope thermometer to natural speleothem and speleothem-like carbonates synthesized in the laboratory (Table 4-1; Affek et al., 2008 and Daeron et al., 2008).

4.4 Comparison between model predictions and isotopic compositions of natural and synthetic carbonates

We compare our model predicted co-variations of kinetic fractionations in carbonate $^{13}C/^{12}C$, $^{18}O/^{16}O$ and Δ_{47} with the available experimental data on cryogenic carbonates (this study) and on speleothem carbonates (both natural modern speleothems and carbonates grown in the laboratory under conditions resembling natural speleothem growth; Affek et al., 2008; Daeron et al., 2008). Fig. 4-10 and 4-11 plot the deviations of isotopic compositions of these carbonates from their expected equilibrium isotopic compositions. Note that we are unable to determine the expected equilibrium carbon isotopic composition of any of the speleothem samples because we do not know the $\delta^{13}C_{HCO_3^-}$ values of the solutions from which they grew. Therefore, for these samples we assume the lowest $\delta^{13}C$ and $\delta^{18}O$ value in a speleothem is the equilibrium value (Fig. 4-11b).

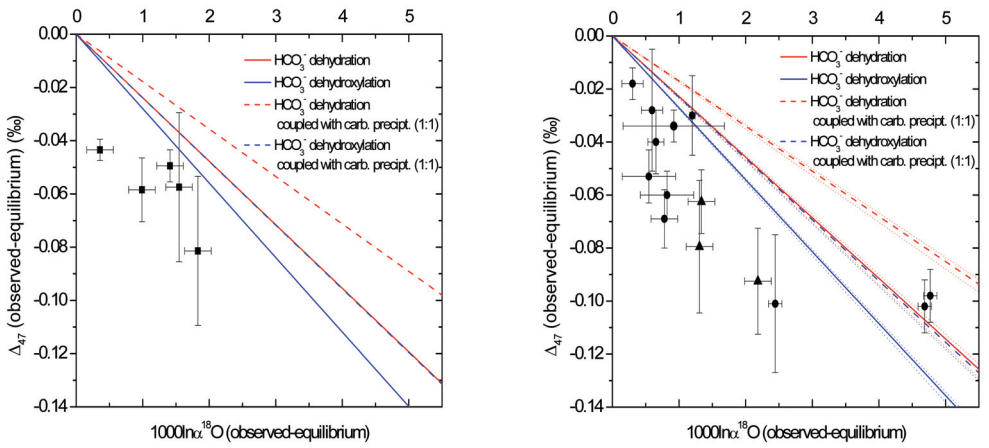

(a) (b)

Figure 4-10: Comparison of our model predicted correlation between kinetic Δ_{47} clumped isotope fractionation and kinetic oxygen isotope fractionation, with the observed isotopic compositions of (a) cryogenic carbonates (formed at ~0°C, this study), and (b) natural modern speleothems (circles) and speleothem-like carbonates synthesized in the laboratory (triangles) (Affek et al. 2008; Daeron et al., 2008). Dotted lines in (b) indicate the variations of predicted correlations over the range of observed cave temperatures (3.7-12.9°C); Plotted error bars represent 2 standard error (2σ).

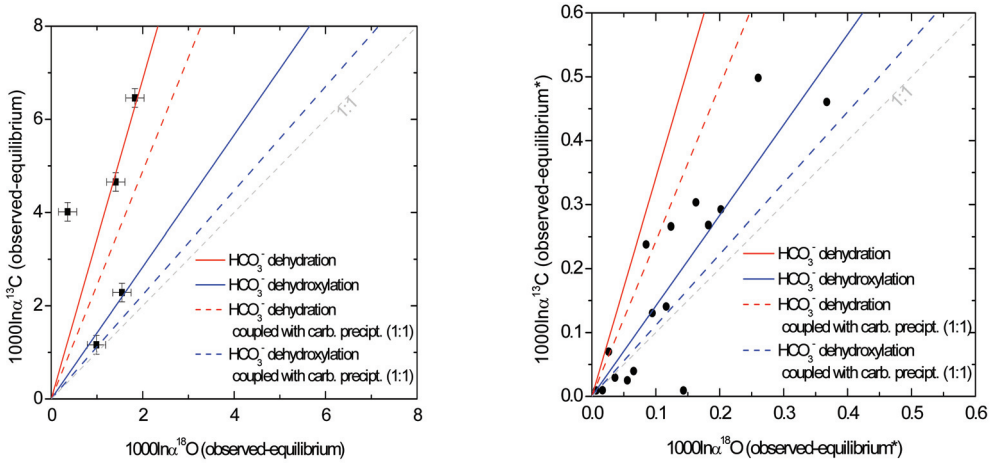

(a) (b)

Figure 4-11: Comparison of our model predicted correlation between kinetic carbon isotope fractionation and kinetic oxygen isotope fractionation, with the observed isotopic compositions of (a) cryogenic carbonates (formed at ~0°C, this study), and (b) the observed isotopic variations among different pieces of speleothem Vil-Gal (Daeron et al., 2008); see text for details. Plotted error bars represent 2 standard error (2σ).

If HCO_3^- dehydration and HCO_3^- dehydroxylation reactions, with or without carbonate accompanying carbonate precipitation, are the only isotopically fractionating processes (as we assumed in our standard model), we would expect the measured isotopic compositions of natural and synthetic carbonate minerals considered by this study to lie within the area confined by our model predictions for the four scenarios outlined above (section 4.2; Fig. 4-9). Based on the known or estimated pH's of the solutions from which these carbonates grew (pH<8 for natural and lab synthesized speleothem, Daeron et al., 2008; pH=5.5~5.7 for synthesized cryogenic carbonate, Table 4-2), HCO_3^- dehydration should be the dominant pathway for CO_2 degassing during both cryogenic carbonate growth and speleothem deposition (section 2.1). Therefore, the observed isotopic compositions of the carbonate minerals are expected to lie closer to the area confined by the model predictions for the two scenarios where HCO_3^- dehydration reactions are the dominant fractionating step, i.e., the two red lines (HCO_3^- dehydration only and HCO_3^- dehydration coupled with carbonate formation, respectively) in Fig. 4-10 and Fig. 4-11.

The correlations between kinetic fractionations of Δ_{47} and oxygen isotopes observed for all cryogenic carbonates and most of the speleothems define a trend parallel to our model predictions, and lie below the model predictions for all four scenarios (Fig. 4-10). The observed correlations between carbon isotope and oxygen isotopes defined by most the cryogenic carbonates and most of the speleothems lie within our range of model predictions for the four scenarios, but differ noticeably from the HCO_3^- dehydration dominated scenarios, which we expected would best describe the data (Fig. 4-11).

The discrepancies between our model predictions and experimental data could arise from kinetic isotope fractionations between the carbonate mineral and dissolved

HCO_3^- during carbonate growth (i.e., because we assumed that carbonates grow in equilibrium with co-existing DIC). Most speleothems form from supersaturated solutions and can grow quickly (Fairchild et al., 2007). The same could be true for growth cryogenic carbonates because rapid degassing during freezing could result in high supersaturation in the solution, driving rapid growth (though these experiments are not sufficiently well controlled to tell definitively if this is the case). It is known that rapid precipitation of carbonate from solution leads to kinetic isotope fractionations between DIC and precipitating carbonate. These effects generally lead to depletions of both $\delta^{13}C$ and $\delta^{18}O$ in the carbonate minerals relative to their values expected from equilibrium with dissolved HCO_3^- (e.g., ~2.3‰ depletion in $\delta^{13}C$ at 25°C, Turner, 1982; and ~0.5‰ depletion in $\delta^{18}O$ at 25°C, Kim et al., 2006). There are so far no systematic studies on the kinetic fractionations of clumped isotope anomalies associated with fast precipitation of carbonate minerals. However, in our preliminary experiments where we precipitated aragonite by pumping and mixing concentrated seawater and sodium carbonate solution together, we observed the depletion of Δ_{47} and $\delta^{18}O$ in the aragonite precipitates as the pumping rate (and thus precipitation rate) increases (Fig. 4-12; Eiler et al., 2008 and Gabitov et al., 2006). These observations suggest that rapid precipitation of carbonate minerals leads to depletion in carbon isotope, oxygen isotopes and Δ_{47} values of carbonates relative to equilibrium with co-existing DIC. The directions of these kinetic depletions are consistent with the discrepancies observed between the predictions of our CO_2 degassing models and the experimental data.

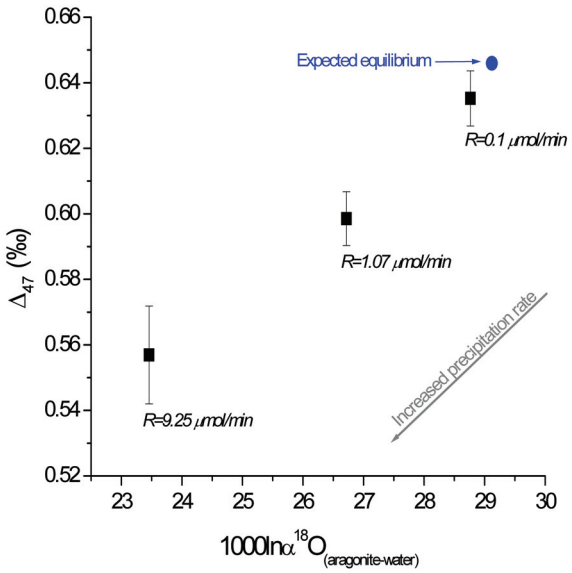

Figure 4-12: Depletion of Δ_{47} and $^{18}O/^{18}O$ in aragonite during its fast precipitation (samples from Gabitov et al. 2006). R is the rate at which concentrated seawater and Na_2CO_3 solution were pumped and mixed together, expressed as μmol of pumped CO_3^{2-} per minute. Circle represents the expected isotopic composition of the aragonite if it formed in isotopic equilibrium with the solution at experimental temperature (25°C).

Even if the non-equilibrium fractionations that occur during growth of some carbonates are well described by the CO_2 degassing model we present, it is not obvious what controls the extent of that dis-equibrium for a given sample; i.e., even if samples are displaced from equilibrium along composition space vectors parallel to our model trends in Fig. 4-9 and 4-10, we still must establish how far they are displaced along such a trend. This question is particularly important for the interpretation of the stable isotope compositions of speleothems. The following paragraphs review some of the factors that likely control the extent of isotopic disequilibrium shown up in speleothem samples.

1) The proportion of HCO_3^- degassed and precipitated from the solution (relative to the initial HCO_3^- present in the solution), '1-F' (where F is the fraction of HCO_3^-

remaining in the aqueous solution; see equation 2), must control the extent of isotopic disequilibrium and sets an upper-limit of isotopic disequilibrium that can be exhibited in the speleothem carbonates.

2) The pathway of CO_2 degassing — dehydration vs. dehydroxylation — and the ratio between the progress of degassing reactions and carbonate precipitation (i.e., the four different scenarios we discussed above) influence the kinetic isotope fractionation factors (α values in equation 2) and thus also affect the upper-limit of isotopic disequilibrium that could be exhibited in the speleothem carbonates. Even with the same fractions of HCO_3^- removed from the solution (i.e., the same F values, above), different reaction pathways cause different extents of kinetic disequilibrium in the residual HCO_3^- and thus in any carbonate minerals that grow from that residual DIC (Fig. 4-7).

3) The kinetic isotope fractionation processes described by our model must compete with isotope re-equilibration reactions — including isotope re-equilibration among the DIC species and between the dissolved HCO_3 and water. These re-equilibration reactions will tend to reduce or completely remove the effects of kinetic isotope fractionation, by an amount that is proportional to the relative rates of CO_2 degassing reactions vs. re-equilibration reactions. Carbon isotope isotopic compositions of dissolved inorganic carbonate species re-equilibrate with one another quickly (e.g., 17.5s at 25°C, for a solution with a salinity of 35 and at pH 8.2; Zeebe et al., 1999). In contrast, re-equilibration of their oxygen isotope compositions through exchange with water requires that C-O bonds break and re-form and is much slower (e.g., half-times for oxygen isotope exchange between HCO_3^- and H_2O is ~1.4 hrs at 25°C, Beck et al., 2004). There are so far no data available on the time required for the re-equilibration of the Δ_{47}

clumped isotope anomaly in the DIC system. However, these values reflect isotopic ordering among C-O bonds, so we suspect it should be of the same order of magnitude as the time for oxygen isotope re-equilibration.

Isotope re-equilibration processes should most strongly influence the isotopic compositions of speleothem carbonates that form under a relatively thick layer of water (e.g., pool carbonates and some flowstones) because in such cases the rate of CO_2 degassing is limited by diffusion (Buhmann and Dreybrodt, 1985). Therefore, we expect that carbonate growth from sufficiently thick water layers will be accompanied by isotope re-equilibrations reactions that out-compete kinetic isotope fractionation processes (i.e., CO_2 degassing). And, slower CO_2 degassing from thick water layers will also lead to lower degrees of supersaturation in the solution, lower carbonate precipitation rates, and thus diminished opportunity for any additional kinetic isotopic fractionations associated with fast precipitation of carbonate minerals. As a result, we expect those carbonate mineral formed under a sufficient thick water body/film will show oxygen isotope and clumped isotope compositions (i.e., Δ_{47} values) that are in equilibrium with the isotopic compositions of the cave water and cave temperatures. Evidence supporting this hypothesis can be found in studies of carbon isotope compositions of DIC in cave water (Bar-Matthews et al., 1996) and of the oxygen isotopic compositions of carbonates synthesized in the lab through CO_2 degassing (Wiedner et al., 2008).

It will be helpful for paleo-climate reconstructions to find speleothem samples that exhibit equilibrium isotope compositions, including clumped isotope compositions, so that we can circumvent the complications resulted from kinetic isotope fractionation processes. Based on the evidence presented above, we propose that pool carbonates are

promising candidates.

4.5 Implications for the isotopic studies in other natural systems

Besides cryogenic carbonates and speleothems, the model we present can also be applied to other systems in which the degassing of CO_2 from aqueous solution is an important process.

4.5.1 Other natural carbonate formations induced by the degassing of CO_2

Soil carbonates, evaporative carbonate (e.g., caliches), tufas and travertine deposits are carbonate formations that are often influenced by CO_2 degassing from aqueous solutions. Despite the importance of their isotopic compositions as proxies for paleoclimate and paleoelevation reconstruction, our quantitative understanding of the mechanisms by which these types of carbonates form remains limited (Andrews, 2006; Quade et al., 2007). One often observes that co-genetic suites of these classes of carbonates exhibit co-variations of $\delta^{13}O$ and $\delta^{18}O$ that resemble those observed in some speleothem carbonates (Cerling and Quade, 1993; Knauth et al., 2003; Andrews, 2006). This co-incidence is consistent with the notion that kinetic isotope effects associated with CO_2 degassing contribute to isotopic diversity in diverse carbonate types. However, it is important to note that these other carbonate types grown in complex, dynamic systems and almost certainly also exhibit isotopic diversity due to evaporation of water (perhaps combined with degassing; i.e., in the case of tufas; Andrew, 2006), the combined effects from evaporation and microbial activity (i.e., in caliches; Knauth, 2003), or the combined effects from precipitation and carbon cycling by plants (i.e., in soil carbonates, Cerling

and Quade, 1993). A detailed discussion of isotope fractionations accompanying formation of these diverse and complex carbonate types is beyond the scope of this study. However, if the kinetic isotope fractionations associated with CO_2 degassing are among the causes of $\delta^{13}O$ and $\delta^{18}O$ variations observed in these carbonate, we would expect an accompanying depletion of their Δ_{47} relative to the expected equilibrium values, i.e., an overestimation of their formation temperature as determined by carbonate clumped isotope thermometry. A recent clumped isotope study of soil carbonates from Tibet yielded apparent temperatures greater than plausible growth temperatures, consistent with our expectation (M. Daeron, personal communications). Though this does not constitute proof of a role of CO_2 degassing in soil carbonates, we conclude that the kinetic isotope fractionations associated with CO_2 degassing should be considered in future stable isotope studies (including clumped isotope studies) of carbonates formed in environments that might contain aqueous solutions that are super-saturated in CO_2.

4.5.2 Air-sea CO_2 exchange and isotopic composition of respiration CO_2

Our model of kinetic isotope effects associated with degassing of aqueous solutions predicts that the isotope composition of the outgassed CO_2 differs significantly from that of the dissolved HCO_3^- and from the expected values if the CO_2 was in isotopic equilibrium with the solution water. Particularly, the ^{13}C-^{18}O clumped isotope anomalies in the degassed CO_2 are predicted to be ~0.09‰ and ~0.37‰ (for CO_2 produced by HCO_3^- dehydration or HCO_3^- dehydroxylation, respectively) higher than that of the dissolved HCO_3^- at 25°C, and therefore are ~0.40‰ and ~0.12‰ lower than their expected equilibrium values (assuming equilibrium ^{13}C-^{18}O clumped isotope anomaly in

dissolved HCO_3^- and in gaseous CO_2 are 0.43‰ [Guo et al., 2008a] and 0.92‰ [Wang et al., 2004] respectively at 25°C). These isotope effects, if fully expressed, could greatly influence the isotopic budget of atmospheric CO_2, by way of both the air-sea exchange flux and the respiration flux (if the respiration CO_2 first dissolves in aqueous solutions, i.e., forms dissolved HCO_3^-, before its emissions into atmosphere).

A recent study of the clumped isotope composition of atmospheric CO_2 (Affek et al., 2007) found that, Δ_{47} values of most air samples differ significantly from (mostly lower than) that expected from based on thermodynamic equilibrium and exhibit considerable seasonal and diurnal variations (as much as 0.25‰ and 0.14‰ respectively; Affek et al., 2007). Both depletion in Δ_{47} relative to thermodynamic equilibrium and the seasonal and diurnal variations have been largely attributed to the terrestrial respiration flux, which is estimated to have Δ_{47} values of 0.77 ± 0.28‰ (Affek et al., 2007). Similarly, study of Δ_{47} in human breath revealed a similar Δ_{47} value, 0.76 ± 0.03‰ (Affek and Eiler, 2006). Both of these estimations of Δ_{47} in respiration CO_2 lie close to our predicted Δ_{47} values for CO_2 degassed from HCO_3^- dehydration and dehydroxylation (0.52‰ and 0.80‰, respectively, at 25°C; see above), suggesting kinetic isotope fractionations associated with HCO_3^- dehydration and HCO_3^- dehydroxylation reactions as a possible explanation for the depletion of ^{13}C-^{18}O bonds (relative to thermodynamic equilibrium) in respiration CO_2.

It is however noted that, air samples collected from Cape Grim, Tasmania and Barrow, Alaska (considered to likely reflect hemispheric background air and to be affected by air-sea exchange) have Δ_{47} values close to those expected for thermodynamic equilibrium at ambient temperatures (Affek et al., 2007). This result is consistent with

previous studies of the carbon isotope budget of air-sea CO_2 exchange (Siegenthaler and Munnich, 1981; Inoue and Sugimura, 1985), which show that the carbon isotope fractionation during air-sea CO_2 exchange is dominated by diffusion (-1.8 to -2.3‰ for atmosphere-to-ocean transfer, and -9.7 to -10.2‰ for ocean-to-atmosphere transfer) rather than a kinetic isotope effect associated with dehydration or dehydroxilation. The relative unimportance of dehydration and dehydroxylation reactions (and their reverse) presumably reflects the slow kinetics of hydration/dehydration and hydroxylation/dehydroxylation reactions compared to the rapid renewal of CO_2 in the surface layer through turbulence. For example, at 20°C, the CO_2 lifetime for hydration is ~50s (Kern, 1960) and is 25 times longer than for the typical time constant for surface CO_2 renewal through turbulence (Siegenthaler and Munnich, 1981). Accordingly, the kinetic isotope fractionations associated with these reactions will be diminished by a factor by 25 during air-sea CO_2 exchange (Siegenthaler and Munnich, 1981). If our model predicted kinetic fractionations associated with HCO_3^- dehydration and dehydroxylation reactions are diminished by this factor, the total expected impact on the isotopic composition of CO_2 exchanged with the ocean is ~1‰, ~0.4‰ and ~0.02‰ for $\delta^{13}O$, $\delta^{18}O$ and Δ_{47} respectively. It would be challenging to detect such small effects in natural samples; in any event, it is consistent with findings from previous isotope studies (Siegenthaler and Munnich, 1981; Inoue and Sugimura, 1985; Affek et al., 2007).

5. SUMMARY

Based on ab initio models of molecular structures and transition state theory models of irreversible reactions, we calculate the isotope fractionations (including $^{13}C/^{12}C$, $^{18}O/^{16}O$, and multiply-substituted isotopologues) associated with degassing of CO_2 aqueous solutions, considering both CO_2 produced by HCO_3^- dehydration and HCO_3^- dehydroxylation. When coupled with a model for the isotope fractionations associated with carbonate precipitation, we predict that the isotope fractionations during CO_2 degassing from aqueous solutions increase the $\delta^{13}O$, $\delta^{18}O$ and deplete the distribution of ^{13}C-^{18}O clumped isotopologues of the residual DIC species and in carbonate minerals that precipitate from the DIC pool. For example, our model predicts that at 25°C $\delta^{13}C$ and Δ_{47} in carbonate will increase by 1.1-3.3‰ and decrease by 0.017-0.026‰ respectively, for every 1‰ kinetic enrichment in its $\delta^{18}O$, depending on the exact pathway for CO_2 degassing and carbonate formation. The reduction in Δ_{47} in the carbonate minerals accompanying these kinetic fractionations mostly arise from the non-linear relationship between bulk isotope composition (i.e., $\delta^{18}O$ and $\delta^{13}C$) and abundances of clumped isotopic species, combined with a large difference in $\delta^{18}O$ and $\delta^{13}C$ between the consumed and residual HCO_3^- pools. These predictions approximately agree with the isotopic compositions (including carbon isotope, oxygen isotope and Δ_{47} clumped isotope) of cryogenic carbonates observed in this study and modern natural speleothem and lab synthesized speleothem-like carbonate samples from previous studies. This agreement suggests that kinetic isotope fractionations associated with CO_2 degassing are among the primary causes for the disequilibrium isotopic compositions observed in cryogenic carbonates and speleothem samples. The discrepancies between Δ_{47} values observed in

carbonate minerals and our model predictions might result from the additional kinetic isotope fractionations associated with the fast precipitation of carbonate mineral from supersaturated solutions.

The extents of isotopic disequilibrium found in natural carbonates are controlled not only by the kinetic isotope fractionations described by our model, but also by isotope re-equilibration reactions that tend to remove the isotopic disequilibrium effects. We propose that speleothem samples formed under water films/bodies of sufficient thickness (e.g., pool carbonates, flowstones, etc) are most likely to exhibit equilibrium oxygen isotope and Δ_{47} compositions due to the suppression of CO_2 degassing processes relative to isotope re-equilibration reactions. Such materials should be targeted in future applied studies of the clumped isotope geochemistry of cave deposits.

This study constitutes the first systematic theoretical and experimental study of kinetic isotope fractionations associated with HCO_3^- dehydration and dehydroxylation reactions (especially for multiply-substituted isotopologues). The method and principles employed in this study can be applied to studies of other chemical reactions, e.g., CO_2 hydration and hydroxylation reactions, which are also important in natural systems (e.g., in biogenic carbonates, plant photosynthesis and respiration, air-sea exchange, etc.).

ACKNOWLEDGEMENTS

We would like to thank Rinat Gabitov for providing the synthesized aragonite samples for analyses, Haigt Affek and Anna Meckler for helpful discussions.

REFERENCES

Affek H. P., Bar-Matthews M., Ayalon A., Matthews A. and Eiler J. M. (2008). Glacial/interglacial temperature variations in Soreq cave speleothems as recorded by 'clumped isotope' thermometry. *Geochim. Cosmochim. Acta* **in press**.

Affek H. P. and Eiler J. M. (2006). Abundance of mass 47 CO_2 in urban air, car exhaust, and human breath. *Geochim. Cosmochim. Acta*. **70:** 1-12.

Affek H. P., Xu X. and Eiler J. M. (2007). Seasonal and diurnal variations of $^{13}C^{18}O^{16}O$ in air: Initial observations from Pasadena, CA. *Geochim. Cosmochim. Acta*. **71:** 5033-5043.

Andrews J. E. (2006). Palaeoclimatic records from stable isotopes in riverine tufas: synthesis and review. *Earth Sci. Rev.* **75:** 85-104.

Bar-Matthews M., Ayalon A., Matthews A., Sass E. and Halicz L. (1996). Carbon and oxygen isotope study of the active water-carbonate system in a karstic Mediterranean cave: Implications for paleoclimate research in semiarid regions. *Geochim. Cosmochim. Acta*. **60:** 337-347.

Barkan E. and Luz B. (2005). High precision measurements of $^{17}O/^{16}O$ and $^{18}O/^{16}O$ ratios in H_2O. *Rapid Commun. Mass Spectrom.* **19**: 3737-3742.

Beck W. C., Grossman E. L. and Morse J. W. (2005). Experimental studies of oxygen isotope fractionation in the carbonic acid system at 15°, 25°, and 40°C. *Geochim. Cosmochim. Acta*. **69:** 3493-3503.

Bigeleisen J. (1955). Statistical mechanics of isotopic systems with small quantum corrections .1. General considerations and the rule of the geometric mean. *J. Phys. Chem.* **23**: 2264-2267.

Buhmann D. and Dreybrodt W. (1985). The kinetics of calcite dissolution and precipitation in geologically relevant situations of karst areas. 1. Open system. *Chem. Geol.* **48:** 189-211.

Cerling T. E. and Quade J. (1993). Stable carbon and oxygen isotopes in soil carbonates.In *Climate Change in Continental Isotopic Records*. American Geophysical Union Geophysical Monograph. 217-231.

Clark I. D. and Lauriol B. (1992). Kinetic enrichment of stable isotopes in cryogenic calcites. *Chem. Geol.* **102:** 217-28.

Daeron M., Guo W., Genty D. and Eiler J. M. (2008).^{13}C-^{18}O clumped isotope compositions of modern speleothems. **in prep**

Davidson M. M., Hillier I. H., Hall R. J. and Burton N. A. (1994). Modeling the reaction $OH^- + CO_2 ^- > HCO_3^-$ in the gas phase and in aqueous solution: a combined density functional continuum approach. *Mol. Phys.* **83:** 327-333.

Deines P., Langmuir D. and Harmon, R.S. (1974). Stable carbon isotope ratios and the existence of a gas phase in the evolution of carbonate ground waters. *Geochim. Cosmochim. Acta* **38**: 1147-1164.

Eiler J. M. and Schauble E. (2004). $^{18}O^{13}C^{16}O$ in Earth's atmosphere. *Geochim. Cosmochim. Acta*. **68:** 4767-4777.

Eiler J., Affek H., Daeron M., Ferry J., Guo W., Huntington K., Thiagarajan N. and Tripati A. (2008). Carbonate 'clumped isotope' thermometry: a status report, *Geochim. Cosmochim. Acta*. **72**: A239-A239.

Epstein S. and Mayeda T. (1953) Variation of O^{18} content of waters from natural sources. *Geochim. Cosmochim. Acta*. **4**: 213-224.

Eyring H. (1935a). Activated complex in chemical reactions. *J. Chem. Phys.* **3**: 107-15.

Eyring H. (1935b). The activated complex and the absolute rate of chemical reactions. *Chem. Rev.* **17**: 65-77.

Fairchild I. J., Frisia S., Borsato A. and Tooth A. F. (2007). Speleothems.In *Geochemical Sediments and Landscapes*, Blackwells, Oxford.

Fairchild I. J., Smith C. L., Baker A., Fuller L., Spoetl C., Mattey D. and McDermott F. (2006). Modification and preservation of environmental signals in speleothems. *Earth Sci. Rev.* **75:** 105-153.

Gabitov, R. I., Cohen, A. L., Gaetani, G. A., Holcomb, M. and Watson, E. B. (2006). Growth rate dependence of Mg, Sr, and U incorporation into aragonite: experimental constraints on the origin of vital effects. *Eos Trans. AGU, 87*(52), Fall Meet. Suppl., Abstract B13B-1076.

Gaillardet J. and Galy A. (2008). Himalaya-Carbon Sink or Source? *Science*. **320:** 1727-1728.

Ghosh P., Adkins J., Affek H., Balta B., Guo W., Schauble E. A., Schrag D. and Eiler J. M. (2006). ^{13}C-^{18}O bonds in carbonate minerals: A new kind of paleothermometer. *Geochim. Cosmochim. Acta* **70**: 1439-1456.

Guo W., Daeron M., Niles P. B., Genty D., Kim S.-T., Vonhof H. B., Affek H. P., Blamart D., Wainer K. and Eiler J. M. (2008a). ^{13}C-^{18}O bonds in dissolved inorganic carbon: implications for carbonate clumped Isotope thermometry. *Geochim. Cosmochim. Acta* **72**: A336-A336.

Guo W., Mosenfelder J. L., Goddard W. A. and Eiler J. M. (2008b). Isotopic fractionations associated with phosphoric acid digestion of carbonate minerals. *Geochim. Cosmochim. Acta* **in review**.

Horita J., Ueda A., Mizukami K., and Takatori I. (1989) Automatic δD and $\delta^{18}O$ analyses of multi-water samples using H_2-water and CO_2-water equilibration methods with a common equilibration set-up. *Appl. Rad. Isot.* **40**: 801-805.

Iida K., Yokogawa D., Sato H. and Sakaki S. (2007). The barrier origin on the reaction of $CO_2 + OH^-$ in aqueous solution. *Chem. Phys. Lett.* **443:** 264-268.

Inoue H. and Sugimura Y. (1985). Carbon isotopic fractionation during the CO_2 exchange process between air and sea-water under equilibrium and kinetic conditions. *Geochim. Cosmochim. Acta* **49**: 2453-2460.

Johnson K. S. (1982). Carbon dioxide hydration and dehydration kinetics in seawater. *Limno. Oceano.* **27:** 849-855.

Kern D. M. H. (1960). The hydration of carbon dioxide. *J. Chem. Educ.* **37:** 14-23.

Kim S.-T. and O'Neil J. R. (1997). Equilibrium and nonequilibrium oxygen isotope effects in synthetic carbonates. *Geochim. Cosmochim. Acta*. **61:** 3461-3475.

Knauth L. P., Brilli M. and Klonowski S. (2003). Isotope geochemistry of caliche developed on basalt. *Geochim. Cosmochim. Acta*. **67:** 185-195.

Lacelle D. (2007). Environmental setting, (micro)morphologies and stable C–O isotope composition of cold climate carbonate precipitates—a review and evaluation of their potential as paleoclimatic proxies. *Quat. Sci. Rev.* **26**: 1670-1689.

Leung K., Nielsen I. M. B. and Kurtz I. (2007). Ab initio molecular dynamics study of carbon dioxide and bicarbonate hydration and the nucleophilic attack of hydroxide on CO_2. *J. Phys. Chem. B*. **111:** 4453-4459.

Loerting T., Tautermann C., Kroemer R. T., Kohl I., Hallbrucker A., Mayer E. and Liedl K. R. (2000). On the surprising kinetic stability of carbonic acid (H_2CO_3). *Angew. Chem. Int. Ed.* **39:** 892-894.

Marlier J. F. and O'Leary M. H. (1984). Carbon kinetic isotope effects on the hydration of carbon dioxide and the dehydration of bicarbonate ion. *J. Am. Chem. Soc.* **106:** 5054-5057.

Mickler P. J., Banner J. L., Stern L., Asmerom Y., Edwards R. L. and Ito E. (2004). Stable isotope variations in modern tropical speleothems: Evaluating equilibrium vs. kinetic isotope effects. *Geochim. Cosmochim. Acta* **68**: 4381-4393.

Mickler P. J., Stern L. A. and Banner J. L. (2006). Large kinetic isotope effects in modern speleothems. *Geol. Soc. Amer. Bull.* **118:** 65-81.

Muehlinghaus C., Scholz D. and Mangini A. (2007). Modelling stalagmite growth and $\delta^{13}C$ as a function of drip interval and temperature. *Geochim. Cosmochim. Acta*. **71:** 2780-2790.

Nemukhin A. V., Topol I. A., Grigorenko B. L. and Burt S. K. (2002). On the origin of potential barrier for the reaction OH^-+CO_2 -> HCO_3^- in water: Studies by using continuum and cluster solvation methods. *J. Phys. Chem. B* **106**: 1734-1740.

Nguyen M. T., Raspoet G., Vanquickenborne L. G. and Van Duijnen P. T. (1997). How many water molecules are actively involved in the neutral hydration of carbon dioxide? *J. Phys. Chem. A* **101**: 7379-7388.

O'Leary M. H., Madhavan S. and Paneth P. (1992). Physical and chemical basis of carbon isotope fractionation in plants. *Plant, Cell and Environment*. **15:** 1099-104.

Paneth P. and O'Leary M. H. (1985). Mechanism of the spontaneous dehydration of bicarbonate ion. *J. Amer. Chem. Soc.* **107:** 7381-7384.

Peng Z. and Merz K. M. (1992). The gas-phase and solution-phase free energy surfaces for carbon dioxide reaction with hydroxide ($CO_2 + OH^-$ -> HCO_3^-). *J. Amer. Chem. Soc.* **114:** 2733-2734.

Peng Z. and Merz K. M., Jr. (1993). Theoretical investigation of the $CO_2 + OH^-$ -> HCO_3^- reaction in the gas and aqueous phases. *J. Am. Chem. Soc.* **115:** 9640-7.

Quade J., Garzione C. and Eiler J. M. (2007). Paleoelevation reconstruction using pedogenic carbonates. *Rev. Miner. Geochem.* **66**: 53-87.

Ringnalda M. N., Langlois J.-M., Greeley B. H., Russo T. V., Muller R. P., Marten B., Won Y., Donnelly R. E., Pollard J., W. Thomas, Miller G. H., Goddard W. A. I. and Friesner R. A. (2007). Jaguar, version 7.0, release 207, Schrodinger, LLC, New York, NY.

Romanov D., Kaufmann G. and Dreybrodt W. (2008). $\delta^{13}C$ profiles along growth layers of stalagmites: Comparing theoretical and experimental results. *Geochim. Cosmochim. Acta*. **72:** 438-448.

Roy R. N., Roy L. N., Vogel K. M., Porter-Moore C., Pearson T., Good C. E., Millero F. J. and Campbell D. M. (1993). The dissociation constants of carbonic acid in seawater at salinities 5 to 45 and temperatures 0 to 45^{o}C. *Mar. Chem.* **44:** 249-67.

Rudolph W. W., Fischer D. and Irmer G. (2006). Vibrational spectroscopic studies and density functional theory calculations of speciation in the CO_2-water system. *Appl. Spectrosc.* **60**: 130-144.

Schauble E. A., Ghosh P. and Eiler J. M. (2006). Preferential formation of ^{13}C-^{18}O bonds in carbonate minerals, estimated using first-principles lattice dynamics. *Geochim. Cosmochim. Acta*. **70:** 2510-2529.

Scott A. P. and Radom L. (1996). Harmonic vibrational frequencies: an evaluation of Hartree-Fock, Moeller-Plesset, Quadratic Configuration Interaction, Density Functional Theory, and semiempirical scale factors. *J. Phys. Chem.* **100**: 16502-16513.

Siegenthaler U. and Munnich K. O. (1981). $^{13}C/^{12}C$ fractionation during CO_2 transfer from air to sea.In *Carbon Cycle Modelling*. **Scope 16**. 249-258.

Spotl C. (2005) A robust and fast method of sampling and analysis of $\delta^{13}C$ of dissolved inorganic carbon in ground waters. *Isot. Environ. Health Stud.* **41**: 217-221.

Tautermann C. S., Voegele A. F., Loerting T., Kohl I., Hallbrucker A., Mayer E. and Liedl K. R. (2002). Towards the experimental decomposition rate of carbonic acid (H_2CO_3) in aqueous solution. *Chem.--Eur. J.* **8:** 66-73.

UNESCO (1985). The International System of Units (SI) in Oceanography. *UNESCO Tech. Pap. Mar. Sci., no. 45.***:** pp124.

Urey H. C. (1947). Thermodynamic properties of isotopic substances. *J. Chem. Soc.*: 562-581.

Urey H. C. (1947). The thermodynamic properties of isotopic substances. *J. Chem. Soc.*: 562-581.

Wiedner E., Scholz D., Mangini A., Polag D., Mühlinghaus C. and Segl M. (2008). Investigation of the stable isotope fractionation in speleothems with laboratory experiments. *Quat. Intl.* **in press**.

Zak K., Urban J., Cilek V. and Hercman H. (2004). Cryogenic cave calcite from several Central European caves: age, carbon and oxygen isotopes and a genetic model. *Chem. Geol.* **206:** 119-136.

Zeebe R. E. and Wolf-Gladrow D. A. (2001). CO_2 in seawater: Equilibrium, kinetics, isotope. Elsevier.

Zhang J., Quay P. D. and Wilbur D. O. (1995). Carbon isotope fractionation during gas-water exchange and dissolution of CO_2. *Geochim. Cosmochim. Acta*. **59:** 107-14.

APPENDIX

Table 4-A1 Scaled vibration frequencies (unit: cm^{-1}) for all 54 isotopologues of our modeled reactant during HCO_3^- dehydration reaction in aqueous solution (Fig. 4-2a; DFT-B3LYP/cc-pvtz(-f) with a frequency scaling factor of 0.9614; see sections 2.2 and 2.4 for details). The frequency set contains 30 modes of vibration frequencies for each isotopologue. Due to space limitation, they are presented as here two sub-tables (a) ϖ_1 to ϖ_{15}; (b) ϖ_{16} to ϖ_{30}.

Sub-table (a)

Isotopologue[&]	ϖ_1	ϖ_2	ϖ_3	ϖ_4	ϖ_5	ϖ_6	ϖ_7	ϖ_8	ϖ_9	ϖ_{10}	ϖ_{11}	ϖ_{12}	ϖ_{13}	ϖ_{14}	ϖ_{15}
$H_2{}^{12}C^{16}O^{16}O^{16}O$	13.80	51.77	82.34	98.66	158.25	188.72	236.08	253.89	325.06	346.39	375.97	533.56	550.78	607.12	658.46
$H_2{}^{13}C^{16}O^{16}O^{16}O$	13.84	51.77	82.20	98.54	158.25	188.71	235.92	253.63	325.04	346.35	375.97	533.23	549.18	605.44	658.08
$H_2{}^{12}C^{18}O^{16}O^{16}O$	12.20	51.51	82.14	98.55	158.23	188.68	235.64	253.08	325.04	346.32	375.94	531.99	544.83	597.11	657.36
$H_2{}^{12}C^{16}O^{18}O^{16}O$	15.71	51.58	81.64	97.12	158.25	188.71	235.72	253.76	324.69	346.08	375.85	530.79	542.93	599.19	657.36
$H_2{}^{12}C^{16}O^{16}O^{18}O$	14.34	51.14	82.10	96.72	158.24	188.64	235.12	253.02	324.91	346.32	375.56	531.74	544.72	599.15	655.53
$H_2{}^{13}C^{18}O^{16}O^{16}O$	12.28	51.51	82.01	98.42	158.23	188.66	235.47	252.86	325.01	346.27	375.93	531.38	543.61	595.34	657.03
$H_2{}^{13}C^{16}O^{18}O^{16}O$	15.72	51.57	81.51	97.01	158.25	188.69	235.55	253.51	324.67	346.03	375.84	530.24	541.53	597.80	657.07
$H_2{}^{13}C^{16}O^{16}O^{18}O$	14.36	51.13	81.97	96.61	158.24	188.63	234.95	252.80	324.88	346.27	375.56	531.15	543.50	597.41	655.18
$H_2{}^{12}C^{17}O^{16}O^{16}O$	13.01	51.64	82.24	98.60	158.24	188.70	235.86	253.47	325.05	346.36	375.95	532.90	547.62	601.82	657.84
$H_2{}^{12}C^{16}O^{17}O^{16}O$	14.85	51.68	81.99	97.85	158.25	188.71	235.90	253.82	324.87	346.23	375.91	532.17	546.60	603.13	657.86
$H_2{}^{12}C^{16}O^{16}O^{17}O$	14.08	51.45	82.22	97.66	158.25	188.68	235.60	253.43	324.98	346.35	375.76	532.75	547.56	603.03	656.82
$H_2{}^{12}C^{17}O^{18}O^{18}O$	15.57	50.84	81.35	95.14	158.23	188.61	234.55	252.58	324.53	345.97	375.42	525.31	536.62	585.24	654.52
$H_2{}^{12}C^{18}O^{17}O^{18}O$	14.03	50.79	81.58	95.82	158.22	188.59	234.48	252.30	324.69	346.09	375.46	525.90	537.84	583.96	654.51
$H_2{}^{12}C^{18}O^{18}O^{17}O$	14.74	51.01	81.35	96.03	158.23	188.63	234.78	252.59	324.59	345.97	375.59	525.46	536.81	584.32	655.31
$H_2{}^{12}C^{16}O^{18}O^{18}O$	16.15	50.98	81.44	95.19	158.24	188.63	234.78	252.93	324.55	346.01	375.43	527.52	537.90	591.20	654.82
$H_2{}^{12}C^{18}O^{16}O^{18}O$	12.86	50.87	81.90	96.61	158.22	188.60	234.66	252.34	324.88	346.25	375.53	528.89	540.62	588.02	654.78
$H_2{}^{12}C^{18}O^{18}O^{16}O$	14.46	51.32	81.45	97.02	158.24	188.67	235.25	252.96	324.67	346.01	375.81	527.85	538.33	589.02	656.58
$H_2{}^{12}C^{18}O^{17}O^{17}O$	13.75	51.09	81.68	96.75	158.23	188.63	234.96	252.64	324.77	346.12	375.65	528.16	539.26	588.33	655.60
$H_2{}^{12}C^{17}O^{18}O^{17}O$	15.34	51.13	81.44	96.07	158.24	188.65	235.01	252.94	324.61	346.00	375.61	527.70	538.14	589.35	655.59
$H_2{}^{12}C^{17}O^{17}O^{18}O$	14.68	50.92	81.67	95.87	158.23	188.61	234.71	252.62	324.71	346.12	375.48	528.05	539.12	589.21	654.79
$H_2{}^{12}C^{16}O^{17}O^{17}O$	15.10	51.36	81.88	96.86	158.25	188.67	235.42	253.37	324.79	346.19	375.69	531.14	543.49	599.01	656.35
$H_2{}^{12}C^{17}O^{16}O^{17}O$	13.33	51.31	82.12	97.60	158.24	188.66	235.37	253.05	324.97	346.32	375.74	531.86	544.79	597.41	656.32
$H_2{}^{12}C^{17}O^{17}O^{16}O$	14.15	51.54	81.89	97.80	158.24	188.69	235.67	253.41	324.86	346.19	375.89	531.29	543.66	597.78	657.35
$H_2{}^{12}C^{16}O^{17}O^{18}O$	15.33	51.06	81.77	95.92	158.24	188.63	234.95	252.97	324.72	346.16	375.50	529.76	540.92	595.14	655.15
$H_2{}^{12}C^{16}O^{18}O^{17}O$	15.94	51.27	81.54	96.12	158.25	188.67	235.25	253.32	324.62	346.04	375.63	529.41	540.06	595.06	655.95

Sub-table (a) Continued

Isotopologue[&]	ϖ_1	ϖ_2	ϖ_3	ϖ_4	ϖ_5	ϖ_6	ϖ_7	ϖ_8	ϖ_9	ϖ_{10}	ϖ_{11}	ϖ_{12}	ϖ_{13}	ϖ_{14}	ϖ_{15}
$H_2{}^{12}C^{17}O^{16}O^{18}\underline{O}$	13.61	51.00	82.00	96.66	158.23	188.62	234.89	252.67	324.90	346.28	375.54	530.52	542.42	593.26	655.10
$H_2{}^{12}C^{17}O^{18}O^{16}\underline{O}$	15.09	51.45	81.54	97.07	158.24	188.69	235.49	253.34	324.68	346.04	375.83	529.59	540.32	593.78	656.92
$H_2{}^{12}C^{18}O^{16}O^{17}\underline{O}$	12.55	51.18	82.02	97.54	158.23	188.64	235.15	252.69	324.96	346.28	375.72	530.61	542.48	592.41	655.92
$H_2{}^{12}C^{18}O^{17}O^{16}\underline{O}$	13.44	51.42	81.79	97.75	158.23	188.67	235.44	253.02	324.85	346.16	375.87	530.02	541.22	593.03	656.94
$H_2{}^{12}C^{17}O^{17}O^{17}\underline{O}$	14.43	51.22	81.78	96.80	158.24	188.65	235.19	252.99	324.78	346.16	375.67	529.88	541.09	593.35	655.93
$H_2{}^{12}C^{18}O^{18}O^{18}\underline{O}$	14.99	50.71	81.25	95.10	158.22	188.59	234.31	252.25	324.52	345.94	375.40	522.75	535.77	579.97	654.28
$H_2{}^{13}C^{17}O^{16}O^{16}\underline{O}$	13.07	51.63	82.10	98.48	158.24	188.68	235.69	253.23	325.03	346.31	375.95	532.46	546.19	600.09	657.49
$H_2{}^{13}C^{16}O^{17}O^{16}\underline{O}$	14.87	51.67	81.86	97.74	158.25	188.70	235.73	253.57	324.85	346.19	375.90	531.76	545.08	601.61	657.53
$H_2{}^{13}C^{16}O^{16}O^{17}\underline{O}$	14.11	51.44	82.08	97.54	158.24	188.67	235.43	253.20	324.96	346.31	375.75	532.31	546.13	601.31	656.47
$H_2{}^{13}C^{17}O^{18}O^{18}\underline{O}$	15.59	50.83	81.22	95.04	158.23	188.60	234.38	252.38	324.51	345.93	375.42	524.04	536.13	583.75	654.23
$H_2{}^{13}C^{18}O^{17}O^{18}\underline{O}$	14.08	50.78	81.45	95.71	158.22	188.58	234.31	252.11	324.67	346.04	375.46	524.70	537.35	582.28	654.21
$H_2{}^{13}C^{18}O^{18}O^{17}\underline{O}$	14.77	51.00	81.23	95.92	158.23	188.61	234.60	252.38	324.57	345.93	375.59	524.18	536.31	582.83	655.03
$H_2{}^{13}C^{16}O^{18}O^{18}\underline{O}$	16.15	50.97	81.31	95.10	158.24	188.62	234.62	252.71	324.52	345.96	375.43	526.43	537.15	589.77	654.53
$H_2{}^{13}C^{18}O^{16}O^{18}\underline{O}$	12.93	50.86	81.78	96.49	158.22	188.59	234.49	252.15	324.86	346.20	375.53	527.92	539.90	586.18	654.46
$H_2{}^{13}C^{18}O^{18}O^{16}\underline{O}$	14.50	51.31	81.32	96.91	158.23	188.65	235.08	252.74	324.65	345.96	375.81	526.75	537.57	587.57	656.31
$H_2{}^{13}C^{18}O^{17}O^{17}\underline{O}$	13.81	51.08	81.56	96.64	158.22	188.62	234.79	252.43	324.74	346.08	375.65	527.10	538.55	586.68	655.30
$H_2{}^{13}C^{17}O^{18}O^{17}\underline{O}$	15.36	51.12	81.32	95.97	158.23	188.63	234.84	252.73	324.58	345.96	375.61	526.62	537.39	587.89	655.31
$H_2{}^{13}C^{17}O^{17}O^{18}\underline{O}$	14.71	50.91	81.55	95.76	158.23	188.60	234.55	252.42	324.68	346.08	375.48	527.01	538.40	587.57	654.49
$H_2{}^{13}C^{16}O^{17}O^{17}\underline{O}$	15.11	51.35	81.75	96.75	158.24	188.66	235.25	253.14	324.77	346.15	375.69	530.54	542.21	597.45	656.04
$H_2{}^{13}C^{17}O^{16}O^{17}\underline{O}$	14.19	51.53	81.76	97.69	158.24	188.68	235.50	253.17	324.83	346.15	375.89	530.69	542.37	596.20	657.04
$H_2{}^{13}C^{17}O^{17}O^{16}\underline{O}$	13.38	51.30	81.99	97.48	158.23	188.64	235.21	252.83	324.94	346.27	375.74	531.26	543.58	595.64	655.98
$H_2{}^{13}C^{16}O^{17}O^{18}\underline{O}$	15.34	51.05	81.64	95.82	158.24	188.62	234.78	252.76	324.70	346.11	375.49	528.94	539.92	593.56	654.84
$H_2{}^{13}C^{16}O^{18}O^{17}\underline{O}$	15.95	51.26	81.41	96.02	158.24	188.65	235.08	253.09	324.60	346.00	375.63	528.60	538.99	593.64	655.66
$H_2{}^{13}C^{17}O^{16}O^{18}\underline{O}$	13.66	50.99	81.87	96.55	158.23	188.61	234.72	252.46	324.87	346.24	375.54	529.74	541.45	591.46	654.78
$H_2{}^{13}C^{17}O^{18}O^{16}\underline{O}$	15.12	51.44	81.41	96.96	158.24	188.67	235.32	253.11	324.66	346.00	375.82	528.77	539.23	592.36	656.64
$H_2{}^{13}C^{18}O^{16}O^{17}\underline{O}$	12.63	51.17	81.89	97.42	158.22	188.62	234.98	252.48	324.93	346.24	375.72	529.82	541.52	590.60	655.60
$H_2{}^{13}C^{18}O^{17}O^{16}\underline{O}$	13.50	51.41	81.66	97.64	158.23	188.66	235.27	252.80	324.82	346.11	375.87	529.18	540.22	591.43	656.65
$H_2{}^{13}C^{17}O^{17}O^{17}\underline{O}$	14.47	51.21	81.65	96.69	158.23	188.64	235.02	252.77	324.76	346.11	375.67	529.07	540.10	591.73	655.63
$H_2{}^{13}C^{18}O^{18}O^{18}\underline{O}$	15.02	50.70	81.13	94.99	158.22	188.58	234.14	252.06	324.50	345.89	375.40	521.36	535.44	578.45	653.99

Sub-table (b)

Isotopologue[&]	ϖ_{16}	ϖ_{17}	ϖ_{18}	ϖ_{19}	ϖ_{20}	ϖ_{21}	ϖ_{22}	ϖ_{23}	ϖ_{24}	ϖ_{25}	ϖ_{26}	ϖ_{27}	ϖ_{28}	ϖ_{29}	ϖ_{30}
$H_2{}^{12}C^{16}O^{16}O^{\underline{16}}O$	761.70	955.08	1009.89	1136.78	1270.97	1349.42	1545.64	1550.84	1695.64	2748.56	3394.43	3566.40	3598.23	3657.10	3672.46
$H_2{}^{13}C^{16}O^{16}O^{\underline{16}}O$	738.07	951.37	1009.73	1126.88	1267.26	1328.45	1545.49	1550.83	1653.31	2748.32	3394.43	3566.38	3598.22	3657.10	3672.45
$H_2{}^{12}C^{18}O^{16}O^{\underline{16}}O$	758.02	943.37	1009.74	1136.39	1263.17	1347.78	1545.50	1550.83	1671.09	2748.42	3394.43	3566.39	3598.23	3657.10	3672.46
$H_2{}^{12}C^{16}O^{18}O^{\underline{16}}O$	759.44	937.08	1009.14	1128.93	1268.39	1340.27	1545.61	1550.83	1694.35	2737.40	3394.39	3566.39	3598.23	3657.10	3672.46
$H_2{}^{12}C^{16}O^{16}O^{\underline{18}}O$	759.32	935.81	1009.86	1126.00	1269.83	1346.91	1545.64	1550.83	1694.94	2748.55	3394.43	3555.16	3598.21	3657.10	3672.45
$H_2{}^{13}C^{18}O^{16}O^{\underline{16}}O$	734.27	940.46	1009.59	1126.72	1258.03	1327.43	1545.22	1550.82	1628.09	2748.18	3394.43	3566.38	3598.22	3657.10	3672.45
$H_2{}^{13}C^{16}O^{18}O^{\underline{16}}O$	735.81	933.97	1008.96	1117.21	1265.07	1319.60	1545.47	1550.82	1652.08	2737.14	3394.39	3566.38	3598.22	3657.10	3672.45
$H_2{}^{13}C^{16}O^{16}O^{\underline{18}}O$	735.61	931.14	1009.70	1116.74	1265.60	1326.18	1545.49	1550.83	1652.63	2748.31	3394.43	3555.14	3598.20	3657.10	3672.45
$H_2{}^{12}C^{17}O^{16}O^{\underline{16}}O$	759.75	949.08	1009.81	1136.58	1266.92	1348.54	1545.57	1550.83	1682.45	2748.48	3394.43	3566.39	3598.23	3657.10	3672.46
$H_2{}^{12}C^{16}O^{17}O^{\underline{16}}O$	760.50	945.86	1009.49	1132.54	1269.61	1344.40	1545.63	1550.83	1694.95	2742.63	3394.41	3566.39	3598.23	3657.10	3672.46
$H_2{}^{12}C^{16}O^{16}O^{\underline{17}}O$	760.43	945.01	1009.87	1130.89	1270.37	1348.08	1545.64	1550.84	1695.27	2748.55	3394.43	3560.43	3598.21	3657.10	3672.45
$H_2{}^{12}C^{17}O^{18}O^{\underline{18}}O$	755.10	912.69	1009.02	1116.74	1263.40	1336.54	1545.54	1550.83	1680.26	2737.32	3394.39	3555.15	3598.21	3657.10	3672.45
$H_2{}^{12}C^{18}O^{17}O^{\underline{18}}O$	754.43	914.98	1009.29	1120.84	1260.72	1340.16	1545.48	1550.83	1669.42	2742.48	3394.41	3555.15	3598.20	3657.10	3672.45
$H_2{}^{12}C^{18}O^{18}O^{\underline{17}}O$	754.49	915.71	1008.96	1121.88	1260.23	1337.11	1545.47	1550.83	1669.11	2737.26	3394.39	3560.42	3598.21	3657.10	3672.45
$H_2{}^{12}C^{16}O^{18}O^{\underline{18}}O$	757.05	918.96	1009.10	1116.94	1267.39	1337.37	1545.61	1550.83	1693.65	2737.39	3394.39	3555.16	3598.21	3657.10	3672.45
$H_2{}^{12}C^{18}O^{16}O^{\underline{18}}O$	755.64	923.61	1009.69	1125.81	1261.87	1345.41	1545.49	1550.83	1670.22	2748.41	3394.43	3555.15	3598.20	3657.10	3672.45
$H_2{}^{12}C^{18}O^{18}O^{\underline{16}}O$	755.76	925.47	1008.98	1128.26	1260.84	1338.58	1545.47	1550.83	1669.57	2737.27	3394.39	3566.39	3598.23	3657.10	3672.45
$H_2{}^{12}C^{18}O^{17}O^{\underline{17}}O$	755.55	924.16	1009.31	1125.92	1261.30	1341.36	1545.48	1550.83	1669.82	2742.49	3394.41	3560.43	3598.21	3657.10	3672.45
$H_2{}^{12}C^{17}O^{18}O^{\underline{17}}O$	756.22	921.51	1009.03	1122.13	1263.92	1337.85	1545.54	1550.83	1680.62	2737.32	3394.39	3560.43	3598.21	3657.10	3672.45
$H_2{}^{12}C^{17}O^{17}O^{\underline{18}}O$	756.17	920.92	1009.37	1120.98	1264.49	1340.86	1545.55	1550.83	1680.92	2742.55	3394.41	3555.15	3598.21	3657.10	3672.45
$H_2{}^{12}C^{16}O^{17}O^{\underline{17}}O$	759.23	936.12	1009.47	1126.31	1269.05	1342.94	1545.63	1550.83	1694.58	2742.63	3394.41	3560.43	3598.21	3657.10	3672.45
$H_2{}^{12}C^{17}O^{16}O^{\underline{17}}O$	758.49	938.87	1009.79	1130.75	1266.28	1347.23	1545.57	1550.83	1682.03	2748.48	3394.43	3560.43	3598.21	3657.10	3672.45
$H_2{}^{12}C^{17}O^{17}O^{\underline{16}}O$	758.55	939.88	1009.41	1132.27	1265.64	1343.50	1545.55	1550.83	1681.70	2742.56	3394.41	3566.39	3598.23	3657.10	3672.46
$H_2{}^{12}C^{16}O^{17}O^{\underline{18}}O$	758.12	927.19	1009.46	1121.13	1268.55	1341.68	1545.62	1550.83	1694.25	2742.62	3394.41	3555.16	3598.21	3657.10	3672.45
$H_2{}^{12}C^{16}O^{18}O^{\underline{17}}O$	758.17	927.63	1009.12	1122.39	1267.87	1338.72	1545.61	1550.83	1693.98	2737.40	3394.39	3560.43	3598.21	3657.10	3672.45
$H_2{}^{12}C^{17}O^{16}O^{\underline{18}}O$	757.37	929.55	1009.77	1125.90	1265.71	1346.10	1545.57	1550.83	1681.67	2748.47	3394.43	3555.16	3598.21	3657.10	3672.45
$H_2{}^{12}C^{17}O^{18}O^{\underline{16}}O$	757.49	931.12	1009.06	1128.58	1264.48	1339.36	1545.54	1550.83	1681.05	2737.33	3394.39	3566.39	3598.23	3657.10	3672.46
$H_2{}^{12}C^{18}O^{16}O^{\underline{17}}O$	756.76	933.04	1009.71	1130.62	1262.48	1346.51	1545.49	1550.83	1670.62	2748.41	3394.43	3560.43	3598.21	3657.10	3672.45
$H_2{}^{12}C^{18}O^{17}O^{\underline{16}}O$	756.82	934.19	1009.34	1132.01	1261.94	1342.73	1545.48	1550.83	1670.28	2742.49	3394.41	3566.39	3598.23	3657.10	3672.46

Sub-table (b) Continued

Isotopologue[&]	ϖ_{16}	ϖ_{17}	ϖ_{18}	ϖ_{19}	ϖ_{20}	ϖ_{21}	ϖ_{22}	ϖ_{23}	ϖ_{24}	ϖ_{25}	ϖ_{26}	ϖ_{27}	ϖ_{28}	ϖ_{29}	ϖ_{30}
$H_2{}^{12}C^{17}O^{17}O^{\underline{17}}O$	757.28	929.98	1009.39	1126.11	1265.04	1342.09	1545.55	1550.83	1681.28	2742.55	3394.41	3560.43	3598.21	3657.10	3672.45
$H_2{}^{12}C^{18}O^{18}O^{\underline{18}}O$	753.36	906.75	1008.94	1116.55	1259.68	1335.84	1545.47	1550.83	1668.71	2737.25	3394.39	3555.15	3598.20	3657.10	3672.45
$H_2{}^{13}C^{17}O^{16}O^{\underline{16}}O$	736.06	945.79	1009.65	1126.80	1262.49	1327.89	1545.36	1550.83	1639.73	2748.25	3394.43	3566.38	3598.22	3657.10	3672.45
$H_2{}^{13}C^{16}O^{17}O^{\underline{16}}O$	736.87	942.51	1009.32	1121.65	1266.11	1323.57	1545.48	1550.83	1652.65	2742.38	3394.41	3566.38	3598.22	3657.10	3672.45
$H_2{}^{13}C^{16}O^{16}O^{\underline{17}}O$	736.76	940.80	1009.71	1121.33	1266.39	1327.23	1545.49	1550.83	1652.94	2748.31	3394.43	3560.42	3598.21	3657.10	3672.45
$H_2{}^{13}C^{17}O^{18}O^{\underline{18}}O$	731.30	909.24	1008.84	1105.63	1258.84	1316.45	1545.33	1550.82	1637.62	2737.06	3394.39	3555.14	3598.20	3657.10	3672.45
$H_2{}^{13}C^{18}O^{17}O^{\underline{18}}O$	730.59	911.60	1009.13	1110.71	1255.29	1320.22	1545.20	1550.82	1626.46	2742.24	3394.41	3555.14	3598.20	3657.10	3672.45
$H_2{}^{13}C^{18}O^{18}O^{\underline{17}}O$	730.68	912.99	1008.79	1110.67	1255.22	1317.19	1545.19	1550.82	1626.17	2737.00	3394.39	3560.41	3598.21	3657.10	3672.45
$H_2{}^{13}C^{16}O^{18}O^{\underline{18}}O$	733.32	915.07	1008.93	1105.72	1263.54	1316.93	1545.46	1550.82	1651.40	2737.13	3394.39	3555.14	3598.20	3657.10	3672.45
$H_2{}^{13}C^{18}O^{16}O^{\underline{18}}O$	731.80	919.81	1009.54	1116.70	1256.25	1325.31	1545.21	1550.82	1627.23	2748.17	3394.43	3555.14	3598.20	3657.10	3672.45
$H_2{}^{13}C^{18}O^{18}O^{\underline{16}}O$	732.00	923.11	1008.82	1116.85	1256.10	1318.53	1545.20	1550.82	1626.63	2737.01	3394.39	3566.37	3598.22	3657.10	3672.45
$H_2{}^{13}C^{18}O^{17}O^{\underline{17}}O$	731.75	921.17	1009.15	1115.55	1256.11	1321.29	1545.20	1550.82	1626.85	2742.24	3394.41	3560.41	3598.21	3657.10	3672.45
$H_2{}^{13}C^{17}O^{18}O^{\underline{17}}O$	732.47	918.43	1008.86	1110.79	1259.60	1317.63	1545.34	1550.82	1637.97	2737.07	3394.39	3560.41	3598.21	3657.10	3672.45
$H_2{}^{13}C^{17}O^{17}O^{\underline{18}}O$	732.38	917.14	1009.20	1110.76	1259.75	1320.62	1545.34	1550.82	1638.24	2742.30	3394.41	3555.14	3598.20	3657.10	3672.45
$H_2{}^{13}C^{16}O^{17}O^{\underline{17}}O$	735.55	932.32	1009.30	1115.71	1265.27	1322.24	1545.47	1550.83	1652.29	2742.38	3394.41	3560.42	3598.21	3657.10	3672.45
$H_2{}^{13}C^{17}O^{16}O^{\underline{17}}O$	734.86	936.93	1009.25	1121.52	1261.41	1323.00	1545.35	1550.82	1639.01	2742.31	3394.41	3566.38	3598.22	3657.10	3672.45
$H_2{}^{13}C^{17}O^{17}O^{\underline{16}}O$	734.74	935.11	1009.63	1121.28	1261.59	1326.72	1545.36	1550.83	1639.32	2748.24	3394.43	3560.42	3598.21	3657.10	3672.45
$H_2{}^{13}C^{16}O^{17}O^{\underline{18}}O$	734.39	922.97	1009.29	1110.81	1264.51	1321.09	1545.47	1550.83	1651.97	2742.37	3394.41	3555.14	3598.20	3657.10	3672.45
$H_2{}^{13}C^{16}O^{18}O^{\underline{17}}O$	734.49	924.14	1008.94	1110.92	1264.27	1318.16	1545.46	1550.82	1651.72	2737.14	3394.39	3560.42	3598.21	3657.10	3672.45
$H_2{}^{13}C^{17}O^{16}O^{\underline{18}}O$	733.59	925.34	1009.61	1116.72	1260.77	1325.71	1545.36	1550.83	1638.96	2748.23	3394.43	3555.14	3598.20	3657.10	3672.45
$H_2{}^{13}C^{17}O^{18}O^{\underline{16}}O$	733.79	928.42	1008.89	1117.03	1260.44	1319.01	1545.34	1550.82	1638.39	2737.07	3394.39	3566.38	3598.22	3657.10	3672.45
$H_2{}^{13}C^{18}O^{16}O^{\underline{17}}O$	732.96	929.67	1009.56	1121.24	1257.09	1326.29	1545.22	1550.82	1627.63	2748.18	3394.43	3560.41	3598.21	3657.10	3672.45
$H_2{}^{13}C^{18}O^{17}O^{\underline{16}}O$	733.07	931.61	1009.18	1121.40	1257.01	1322.53	1545.21	1550.82	1627.31	2742.25	3394.41	3566.37	3598.22	3657.10	3672.45
$H_2{}^{13}C^{17}O^{17}O^{\underline{17}}O$	733.54	926.62	1009.22	1115.63	1260.54	1321.72	1545.35	1550.82	1638.60	2742.30	3394.41	3560.41	3598.21	3657.10	3672.45
$H_2{}^{13}C^{18}O^{18}O^{\underline{18}}O$	729.51	903.68	1008.77	1105.55	1254.43	1316.05	1545.19	1550.82	1625.78	2737.00	3394.39	3555.13	3598.20	3657.10	3672.45

[&] Oxygen atoms here are expressed in the order of atoms 1, 2, 3 as denoted in Fig. 4-2(a). The underlined oxygen atoms (atom 3) are the ones to be abstracted during HCO_3^- dehydration reaction.

Table 4-A2 Scaled vibration frequencies (unit: cm^{-1}) for all 54 isotopologues of our modeled transition state during HCO_3^- dehydration reaction in aqueous solution (Fig. 4-2b; DFT-B3LYP/cc-pvtz(-f) with a frequency scaling factor of 0.9614; see sections 2.2 and 2.4 for details). The frequency set contains 30 modes of vibration frequencies for each isotopologue. Due to space limitation, they are presented as here two sub-tables (a) ϖ_1 to ϖ_{15}; (b) ϖ_{16} to ϖ_{30}.

Sub-table (a)

Isotopologue[&]	ϖ_1	ϖ_2	ϖ_3	ϖ_4	ϖ_5	ϖ_6	ϖ_7	ϖ_8	ϖ_9	ϖ_{10}	ϖ_{11}	ϖ_{12}	ϖ_{13}	ϖ_{14}	ϖ_{15}
$H_2{}^{12}C^{16}O^{16}O^{16}O$	-553.91	49.61	64.27	117.31	175.76	224.62	271.11	332.42	418.22	503.84	519.20	544.32	567.01	621.84	646.26
$H_2{}^{13}C^{16}O^{16}O^{16}O$	-548.72	49.65	64.26	117.03	175.43	224.56	270.99	332.40	416.77	503.82	519.11	544.14	566.83	618.07	645.42
$H_2{}^{12}C^{18}O^{16}O^{16}O$	-553.82	47.58	64.35	117.39	173.84	224.43	271.02	332.41	410.19	503.66	515.52	543.74	566.45	621.11	644.88
$H_2{}^{12}C^{16}O^{18}O^{16}O$	-553.88	51.11	63.19	114.58	172.74	224.39	270.93	332.42	414.68	503.47	517.47	543.80	565.89	620.85	638.99
$H_2{}^{12}C^{16}O^{16}O^{18}O$	-550.15	49.00	64.16	116.32	175.23	224.42	270.95	332.18	416.62	503.46	508.36	540.48	563.73	612.86	641.07
$H_2{}^{13}C^{18}O^{16}O^{16}O$	-548.63	47.65	64.35	117.11	173.53	224.37	270.90	332.40	408.80	503.64	515.44	543.56	566.28	617.20	644.05
$H_2{}^{13}C^{16}O^{18}O^{16}O$	-548.69	51.13	63.19	114.33	172.45	224.34	270.81	332.40	413.31	503.45	517.37	543.64	565.70	616.81	638.15
$H_2{}^{13}C^{16}O^{16}O^{18}O$	-544.91	49.03	64.14	116.06	174.90	224.36	270.82	332.15	415.15	503.45	508.26	540.23	563.58	609.36	640.49
$H_2{}^{12}C^{17}O^{16}O^{16}O$	-553.86	48.56	64.31	117.35	174.77	224.52	271.06	332.42	414.11	503.75	517.23	544.00	566.70	621.47	645.55
$H_2{}^{12}C^{16}O^{17}O^{16}O$	-553.89	50.40	63.72	115.90	174.20	224.50	271.02	332.42	416.41	503.66	518.32	544.05	566.43	621.35	642.34
$H_2{}^{12}C^{16}O^{16}O^{17}O$	-551.95	49.29	64.20	116.81	175.49	224.52	271.03	332.30	417.41	503.69	513.88	542.16	565.17	617.21	643.41
$H_2{}^{12}C^{17}O^{18}O^{18}O$	-550.08	49.47	63.19	113.67	171.37	224.10	270.72	332.17	408.91	501.23	505.32	540.04	562.84	610.41	634.30
$H_2{}^{12}C^{18}O^{17}O^{18}O$	-550.05	47.77	63.73	115.01	171.86	224.11	270.76	332.17	406.90	500.81	504.86	540.07	563.06	610.86	636.69
$H_2{}^{12}C^{18}O^{18}O^{17}O$	-551.84	48.86	63.24	114.18	170.73	224.11	270.76	332.29	405.98	502.36	508.12	541.38	563.90	614.69	635.61
$H_2{}^{12}C^{16}O^{18}O^{18}O$	-550.12	50.48	63.14	113.62	172.28	224.19	270.77	332.17	412.83	502.52	506.74	540.16	562.99	611.03	634.73
$H_2{}^{12}C^{18}O^{16}O^{18}O$	-550.07	46.93	64.25	116.41	173.30	224.23	270.85	332.17	408.73	502.06	505.10	540.23	563.42	611.88	640.07
$H_2{}^{12}C^{18}O^{18}O^{16}O$	-553.79	49.21	63.28	114.66	170.97	224.22	270.84	332.41	406.84	503.11	513.57	543.21	565.39	619.90	637.74
$H_2{}^{12}C^{18}O^{17}O^{17}O$	-551.85	48.09	63.75	115.49	172.10	224.21	270.84	332.29	407.67	502.92	508.93	541.57	564.32	615.54	638.63
$H_2{}^{12}C^{17}O^{18}O^{17}O$	-551.88	49.79	63.20	114.14	171.59	224.20	270.80	332.29	409.77	502.86	509.81	541.55	564.07	615.24	636.10
$H_2{}^{12}C^{17}O^{17}O^{18}O$	-550.09	48.74	63.68	114.97	172.76	224.20	270.81	332.17	410.72	502.22	505.69	540.19	563.19	611.41	637.14
$H_2{}^{12}C^{16}O^{17}O^{17}O$	-551.94	50.08	63.66	115.40	173.95	224.40	270.93	332.30	415.54	503.46	512.91	541.95	564.70	616.53	639.73
$H_2{}^{12}C^{17}O^{16}O^{17}O$	-551.91	48.24	64.24	116.85	174.50	224.42	270.98	332.29	413.33	503.55	511.71	541.95	564.94	616.77	642.82
$H_2{}^{12}C^{17}O^{17}O^{16}O$	-553.85	49.38	63.76	115.94	173.26	224.41	270.97	332.42	412.35	503.54	516.28	543.74	566.14	620.94	641.66
$H_2{}^{12}C^{16}O^{17}O^{18}O$	-550.14	49.78	63.64	114.93	173.71	224.30	270.86	332.18	414.69	503.06	507.46	540.31	563.35	611.96	637.61
$H_2{}^{12}C^{16}O^{18}O^{17}O$	-551.92	50.78	63.15	114.09	172.50	224.29	270.85	332.29	413.74	503.20	511.99	541.75	564.27	615.81	636.62

Sub-table (a) Continued

Isotopologue[&]	ϖ_1	ϖ_2	ϖ_3	ϖ_4	ϖ_5	ϖ_6	ϖ_7	ϖ_8	ϖ_9	ϖ_{10}	ϖ_{11}	ϖ_{12}	ϖ_{13}	ϖ_{14}	ϖ_{15}
$H_2{}^{12}C^{17}O^{16}O^{18}\underline{O}$	-550.11	47.93	64.20	116.37	174.24	224.32	270.90	332.17	412.59	503.02	506.30	540.35	563.56	612.36	640.56
$H_2{}^{12}C^{17}O^{18}O^{16}\underline{O}$	-553.83	50.13	63.23	114.62	171.83	224.30	270.89	332.41	410.66	503.30	515.37	543.48	565.61	620.38	638.35
$H_2{}^{12}C^{18}O^{16}O^{17}\underline{O}$	-551.87	47.25	64.29	116.89	173.57	224.32	270.93	332.29	409.44	503.36	509.89	541.78	564.76	616.35	642.24
$H_2{}^{12}C^{18}O^{17}O^{16}\underline{O}$	-553.81	48.44	63.81	115.98	172.36	224.32	270.93	332.41	408.48	503.40	514.52	543.47	565.90	620.52	641.01
$H_2{}^{12}C^{17}O^{17}O^{17}\underline{O}$	-551.89	49.05	63.71	115.45	173.00	224.30	270.89	332.29	411.52	503.24	510.71	541.74	564.49	616.03	639.16
$H_2{}^{12}C^{18}O^{18}O^{18}\underline{O}$	-550.04	48.53	63.23	113.71	170.50	224.01	270.68	332.17	405.16	499.49	504.73	539.92	562.71	609.80	633.90
$H_2{}^{13}C^{17}O^{16}O^{16}\underline{O}$	-548.67	48.61	64.30	117.07	174.45	224.46	270.94	332.40	412.68	503.73	517.15	543.83	566.52	617.63	644.72
$H_2{}^{13}C^{16}O^{17}O^{16}\underline{O}$	-548.70	50.43	63.71	115.64	173.89	224.44	270.89	332.40	415.00	503.64	518.23	543.88	566.24	617.45	641.50
$H_2{}^{13}C^{16}O^{16}O^{17}\underline{O}$	-546.73	49.33	64.19	116.54	175.16	224.45	270.90	332.28	415.94	503.67	513.80	541.94	565.00	613.56	642.73
$H_2{}^{13}C^{17}O^{18}O^{18}\underline{O}$	-544.84	49.50	63.18	113.43	171.08	224.04	270.60	332.15	407.55	501.21	505.26	539.81	562.69	606.63	633.67
$H_2{}^{13}C^{18}O^{17}O^{18}\underline{O}$	-544.81	47.81	63.72	114.76	171.56	224.06	270.63	332.15	405.53	500.79	504.81	539.85	562.92	607.14	636.07
$H_2{}^{13}C^{18}O^{18}O^{17}\underline{O}$	-546.62	48.89	63.24	113.93	170.45	224.06	270.63	332.27	404.66	502.35	508.06	541.19	563.74	610.68	634.89
$H_2{}^{13}C^{16}O^{18}O^{18}\underline{O}$	-544.88	50.50	63.13	113.39	171.98	224.13	270.64	332.15	411.43	502.51	506.65	539.93	562.83	607.30	634.12
$H_2{}^{13}C^{18}O^{16}O^{18}\underline{O}$	-544.82	46.99	64.23	116.14	172.99	224.17	270.73	332.15	407.31	502.06	505.04	540.00	563.29	608.29	639.48
$H_2{}^{13}C^{18}O^{18}O^{16}\underline{O}$	-548.60	49.25	63.28	114.41	170.69	224.17	270.72	332.39	405.53	503.08	513.49	543.05	565.20	615.73	636.90
$H_2{}^{13}C^{18}O^{17}O^{17}\underline{O}$	-546.63	48.14	63.75	115.23	171.81	224.16	270.72	332.27	406.31	502.91	508.87	541.37	564.16	611.65	637.93
$H_2{}^{13}C^{17}O^{18}O^{17}\underline{O}$	-546.66	49.82	63.19	113.89	171.31	224.14	270.68	332.27	408.42	502.85	509.74	541.35	563.90	611.28	635.40
$H_2{}^{13}C^{17}O^{17}O^{18}\underline{O}$	-544.85	48.77	63.67	114.72	172.46	224.15	270.68	332.15	409.31	502.21	505.62	539.95	563.04	607.73	636.53
$H_2{}^{13}C^{16}O^{17}O^{17}\underline{O}$	-546.72	50.10	63.66	115.15	173.64	224.34	270.81	332.28	414.11	503.44	512.82	541.74	564.54	612.74	639.04
$H_2{}^{13}C^{17}O^{16}O^{17}\underline{O}$	-546.69	48.28	64.23	116.58	174.18	224.36	270.86	332.27	411.90	503.53	511.64	541.74	564.79	613.07	642.13
$H_2{}^{13}C^{17}O^{17}O^{16}\underline{O}$	-548.66	49.42	63.76	115.68	172.96	224.35	270.85	332.40	410.97	503.52	516.19	543.57	565.95	616.96	640.82
$H_2{}^{13}C^{16}O^{17}O^{18}\underline{O}$	-544.89	49.80	63.63	114.68	173.40	224.24	270.73	332.15	413.25	503.05	507.37	540.08	563.20	608.33	637.02
$H_2{}^{13}C^{16}O^{18}O^{17}\underline{O}$	-546.71	50.80	63.15	113.85	172.21	224.23	270.73	332.27	412.36	503.18	511.91	541.55	564.09	611.90	635.93
$H_2{}^{13}C^{17}O^{16}O^{18}\underline{O}$	-544.86	47.97	64.19	116.10	173.92	224.26	270.77	332.15	411.15	503.01	506.22	540.11	563.42	608.81	639.97
$H_2{}^{13}C^{17}O^{18}O^{16}\underline{O}$	-548.64	50.16	63.23	114.37	171.55	224.25	270.76	332.40	409.32	503.28	515.28	543.32	565.42	616.27	637.51
$H_2{}^{13}C^{18}O^{16}O^{17}\underline{O}$	-546.65	47.30	64.28	116.62	173.25	224.27	270.81	332.27	408.04	503.35	509.83	541.57	564.61	612.59	641.56
$H_2{}^{13}C^{18}O^{17}O^{16}\underline{O}$	-548.62	48.49	63.80	115.72	172.07	224.26	270.80	332.40	407.13	503.38	514.44	543.30	565.73	616.48	640.17
$H_2{}^{13}C^{17}O^{17}O^{17}\underline{O}$	-546.68	49.09	63.70	115.19	172.70	224.24	270.76	332.27	410.12	503.23	510.64	541.54	564.33	612.19	638.47
$H_2{}^{13}C^{18}O^{18}O^{18}\underline{O}$	-544.80	48.56	63.23	113.47	170.22	223.96	270.55	332.15	403.82	499.47	504.68	539.70	562.57	605.99	633.25

Sub-table (b)

Isotopologue[&]	ϖ_{16}	ϖ_{17}	ϖ_{18}	ϖ_{19}	ϖ_{20}	ϖ_{21}	ϖ_{22}	ϖ_{23}	ϖ_{24}	ϖ_{25}	ϖ_{26}	ϖ_{27}	ϖ_{28}	ϖ_{29}	ϖ_{30}
$H_2{}^{12}C^{16}O^{16}O\underline{^{16}O}$	739.40	820.93	912.60	1128.00	1279.44	1306.29	1533.53	1585.57	1650.24	1785.13	3047.93	3339.73	3579.72	3625.32	3648.52
$H_2{}^{13}C^{16}O^{16}O\underline{^{16}O}$	718.20	814.42	911.90	1127.83	1272.17	1302.18	1533.29	1585.56	1649.90	1735.88	3047.92	3339.65	3579.70	3625.32	3648.51
$H_2{}^{12}C^{18}O^{16}O\underline{^{16}O}$	735.51	813.85	911.92	1126.91	1263.27	1298.51	1533.50	1585.57	1650.16	1770.18	3047.93	3339.71	3579.71	3625.32	3648.51
$H_2{}^{12}C^{16}O^{18}O\underline{^{16}O}$	735.87	814.94	910.79	1118.34	1264.19	1302.09	1533.47	1585.56	1650.23	1774.68	3047.92	3339.69	3579.71	3625.32	3648.51
$H_2{}^{12}C^{16}O^{16}O\underline{^{18}O}$	737.55	818.48	909.67	1121.10	1277.82	1303.61	1533.16	1585.46	1647.49	1784.85	3047.91	3339.73	3568.12	3625.30	3648.51
$H_2{}^{13}C^{18}O^{16}O\underline{^{16}O}$	714.40	807.67	911.32	1126.66	1252.71	1297.21	1533.22	1585.55	1649.69	1720.61	3047.92	3339.62	3579.70	3625.32	3648.51
$H_2{}^{13}C^{16}O^{18}O\underline{^{16}O}$	714.78	808.68	910.31	1117.68	1254.62	1300.01	1533.20	1585.55	1649.83	1725.31	3047.92	3339.60	3579.70	3625.32	3648.51
$H_2{}^{13}C^{16}O^{16}O\underline{^{18}O}$	716.07	811.75	908.98	1120.98	1270.10	1299.86	1532.92	1585.44	1647.14	1735.61	3047.91	3339.65	3568.11	3625.30	3648.51
$H_2{}^{12}C^{17}O^{16}O\underline{^{16}O}$	737.34	817.26	912.23	1127.45	1272.00	1301.19	1533.51	1585.57	1650.20	1777.04	3047.93	3339.72	3579.72	3625.32	3648.51
$H_2{}^{12}C^{16}O^{17}O\underline{^{16}O}$	737.54	817.83	911.66	1123.21	1271.69	1303.54	1533.50	1585.57	1650.24	1779.46	3047.93	3339.71	3579.71	3625.32	3648.51
$H_2{}^{12}C^{16}O^{16}O\underline{^{17}O}$	738.41	819.62	911.04	1124.33	1278.58	1304.83	1533.34	1585.51	1648.77	1784.98	3047.92	3339.73	3573.56	3625.31	3648.51
$H_2{}^{12}C^{17}O^{18}O\underline{^{18}O}$	731.92	808.10	907.56	1111.67	1252.13	1297.38	1533.06	1585.44	1647.41	1765.68	3047.91	3339.68	3568.12	3625.30	3648.51
$H_2{}^{12}C^{18}O^{17}O\underline{^{18}O}$	731.75	807.62	908.11	1115.66	1251.19	1296.18	1533.08	1585.44	1647.37	1763.59	3047.91	3339.69	3568.12	3625.30	3648.51
$H_2{}^{12}C^{18}O^{18}O\underline{^{17}O}$	730.90	805.82	908.63	1113.64	1244.56	1296.82	1533.22	1585.49	1648.65	1758.43	3047.91	3339.67	3573.56	3625.31	3648.51
$H_2{}^{12}C^{16}O^{18}O\underline{^{18}O}$	734.01	812.12	907.88	1112.36	1261.46	1299.71	1533.09	1585.44	1647.47	1774.39	3047.91	3339.69	3568.12	3625.30	3648.51
$H_2{}^{12}C^{18}O^{16}O\underline{^{18}O}$	733.65	811.11	909.01	1120.22	1260.79	1296.56	1533.13	1585.45	1647.39	1769.86	3047.91	3339.71	3568.12	3625.30	3648.51
$H_2{}^{12}C^{18}O^{18}O\underline{^{16}O}$	731.90	807.50	910.16	1116.62	1246.45	1297.83	1533.42	1585.55	1650.13	1758.60	3047.92	3339.67	3579.71	3625.32	3648.51
$H_2{}^{12}C^{18}O^{17}O\underline{^{17}O}$	732.62	809.00	909.47	1118.56	1252.57	1297.05	1533.26	1585.50	1648.66	1763.74	3047.92	3339.69	3573.56	3625.31	3648.51
$H_2{}^{12}C^{17}O^{18}O\underline{^{17}O}$	732.78	809.49	908.91	1114.41	1253.60	1298.32	1533.24	1585.49	1648.70	1765.83	3047.91	3339.68	3573.56	3625.31	3648.51
$H_2{}^{12}C^{17}O^{17}O\underline{^{18}O}$	733.61	811.27	908.40	1116.21	1260.49	1297.92	1533.10	1585.44	1647.42	1770.75	3047.91	3339.70	3568.12	3625.30	3648.51
$H_2{}^{12}C^{16}O^{17}O\underline{^{17}O}$	736.55	816.43	910.11	1119.79	1270.52	1302.17	1533.30	1585.50	1648.76	1779.31	3047.92	3339.71	3573.56	3625.31	3648.51
$H_2{}^{12}C^{17}O^{16}O\underline{^{17}O}$	736.35	815.87	910.68	1123.84	1270.88	1299.96	1533.32	1585.51	1648.72	1776.88	3047.92	3339.72	3573.56	3625.31	3648.51
$H_2{}^{12}C^{17}O^{17}O\underline{^{16}O}$	735.47	814.07	911.31	1122.51	1263.15	1300.05	1533.47	1585.56	1650.19	1771.06	3047.93	3339.70	3579.71	3625.32	3648.51
$H_2{}^{12}C^{16}O^{17}O\underline{^{18}O}$	735.69	815.20	908.74	1116.77	1269.50	1301.03	1533.12	1585.45	1647.48	1779.18	3047.91	3339.71	3568.12	3625.30	3648.51
$H_2{}^{12}C^{16}O^{18}O\underline{^{17}O}$	734.88	813.44	909.24	1115.17	1262.73	1300.79	1533.27	1585.50	1648.76	1774.52	3047.91	3339.69	3573.56	3625.31	3648.51
$H_2{}^{12}C^{17}O^{16}O\underline{^{18}O}$	735.49	814.66	909.31	1120.65	1269.90	1298.93	1533.14	1585.45	1647.44	1776.74	3047.91	3339.72	3568.12	3625.30	3648.51
$H_2{}^{12}C^{17}O^{18}O\underline{^{16}O}$	733.78	811.08	910.45	1117.48	1255.30	1299.44	1533.44	1585.56	1650.18	1765.99	3047.92	3339.68	3579.71	3625.32	3648.51
$H_2{}^{12}C^{18}O^{16}O\underline{^{17}O}$	734.51	812.39	910.37	1123.37	1261.94	1297.45	1533.30	1585.50	1648.68	1770.01	3047.92	3339.71	3573.56	3625.31	3648.51
$H_2{}^{12}C^{18}O^{17}O\underline{^{16}O}$	733.61	810.57	911.01	1121.82	1254.19	1298.08	1533.45	1585.56	1650.14	1763.91	3047.93	3339.69	3579.71	3625.32	3648.51

Sub-table (b) Continued

Isotopologue[&]	ϖ_{16}	ϖ_{17}	ϖ_{18}	ϖ_{19}	ϖ_{20}	ϖ_{21}	ϖ_{22}	ϖ_{23}	ϖ_{24}	ϖ_{25}	ϖ_{26}	ϖ_{27}	ϖ_{28}	ϖ_{29}	ϖ_{30}
$H_2{}^{12}C^{17}O^{17}O^{\underline{17}}O$	734.47	812.58	909.77	1119.17	1261.72	1298.89	1533.28	1585.50	1648.71	1770.89	3047.92	3339.70	3573.56	3625.31	3648.51
$H_2{}^{12}C^{18}O^{18}O^{\underline{18}}O$	730.04	804.35	907.28	1110.98	1242.94	1295.97	1533.04	1585.44	1647.36	1758.27	3047.91	3339.67	3568.12	3625.30	3648.51
$H_2{}^{13}C^{17}O^{16}O^{\underline{16}}O$	716.19	810.92	911.59	1127.24	1262.65	1298.94	1533.25	1585.55	1649.80	1727.59	3047.92	3339.63	3579.70	3625.32	3648.51
$H_2{}^{13}C^{16}O^{17}O^{\underline{16}}O$	716.40	811.46	911.08	1122.84	1262.91	1300.77	1533.24	1585.55	1649.86	1730.14	3047.92	3339.62	3579.70	3625.32	3648.51
$H_2{}^{13}C^{16}O^{16}O^{\underline{17}}O$	717.06	813.00	910.35	1124.20	1271.07	1300.91	1533.09	1585.49	1648.42	1735.74	3047.92	3339.65	3573.55	3625.31	3648.51
$H_2{}^{13}C^{17}O^{18}O^{\underline{18}}O$	710.56	801.80	907.14	1111.08	1241.30	1296.25	1532.77	1585.42	1646.93	1716.05	3047.90	3339.59	3568.10	3625.30	3648.51
$H_2{}^{13}C^{18}O^{17}O^{\underline{18}}O$	710.39	801.36	907.64	1115.28	1240.00	1295.28	1532.79	1585.42	1646.85	1713.87	3047.90	3339.60	3568.11	3625.30	3648.51
$H_2{}^{13}C^{18}O^{18}O^{\underline{17}}O$	709.76	799.81	908.24	1112.86	1233.40	1295.98	1532.91	1585.47	1648.07	1708.63	3047.91	3339.58	3573.54	3625.31	3648.51
$H_2{}^{13}C^{16}O^{18}O^{\underline{18}}O$	712.61	805.63	907.41	1111.86	1251.41	1297.91	1532.82	1585.43	1647.08	1725.02	3047.90	3339.60	3568.11	3625.30	3648.51
$H_2{}^{13}C^{18}O^{16}O^{\underline{18}}O$	712.23	804.70	908.42	1120.06	1249.92	1295.43	1532.85	1585.43	1646.91	1720.28	3047.91	3339.62	3568.11	3625.30	3648.51
$H_2{}^{13}C^{18}O^{18}O^{\underline{16}}O$	710.95	801.61	909.77	1115.72	1235.51	1296.92	1533.10	1585.54	1649.55	1708.81	3047.92	3339.58	3579.70	3625.32	3648.51
$H_2{}^{13}C^{18}O^{17}O^{\underline{17}}O$	711.40	802.84	908.99	1118.12	1241.54	1296.08	1532.96	1585.48	1648.14	1714.03	3047.91	3339.60	3573.55	3625.31	3648.51
$H_2{}^{13}C^{17}O^{18}O^{\underline{17}}O$	711.58	803.30	908.49	1113.74	1242.95	1297.11	1532.95	1585.48	1648.22	1716.20	3047.91	3339.59	3573.55	3625.31	3648.51
$H_2{}^{13}C^{17}O^{17}O^{\underline{18}}O$	712.20	804.84	907.88	1115.89	1250.02	1296.51	1532.82	1585.43	1646.98	1721.19	3047.90	3339.61	3568.11	3625.30	3648.51
$H_2{}^{13}C^{16}O^{17}O^{\underline{17}}O$	715.24	809.93	909.53	1119.48	1261.49	1299.58	1533.04	1585.49	1648.39	1729.99	3047.91	3339.62	3573.55	3625.31	3648.51
$H_2{}^{13}C^{17}O^{16}O^{\underline{17}}O$	715.04	809.41	910.04	1123.68	1261.31	1297.86	1533.06	1585.49	1648.31	1727.43	3047.91	3339.63	3573.55	3625.31	3648.51
$H_2{}^{13}C^{17}O^{17}O^{\underline{16}}O$	714.38	807.87	910.78	1122.07	1253.07	1298.42	1533.20	1585.55	1649.74	1721.49	3047.92	3339.61	3579.70	3625.32	3648.51
$H_2{}^{13}C^{16}O^{17}O^{\underline{18}}O$	714.24	808.59	908.17	1116.50	1260.25	1298.58	1532.87	1585.43	1647.11	1729.85	3047.90	3339.62	3568.11	3625.30	3648.51
$H_2{}^{13}C^{16}O^{18}O^{\underline{17}}O$	713.62	807.06	908.77	1114.60	1252.90	1298.87	1533.00	1585.48	1648.36	1725.15	3047.91	3339.60	3573.55	3625.31	3648.51
$H_2{}^{13}C^{17}O^{16}O^{\underline{18}}O$	714.04	808.09	908.68	1120.51	1260.16	1296.96	1532.88	1585.43	1647.02	1727.29	3047.91	3339.63	3568.11	3625.30	3648.51
$H_2{}^{13}C^{17}O^{18}O^{\underline{16}}O$	712.75	805.02	910.02	1116.71	1244.88	1298.13	1533.15	1585.54	1649.69	1716.36	3047.92	3339.59	3579.70	3625.32	3648.51
$H_2{}^{13}C^{18}O^{16}O^{\underline{17}}O$	713.24	806.08	909.78	1123.16	1251.20	1296.24	1533.03	1585.48	1648.21	1720.43	3047.91	3339.62	3573.55	3625.31	3648.51
$H_2{}^{13}C^{18}O^{17}O^{\underline{16}}O$	712.58	804.54	910.53	1121.29	1243.35	1297.03	1533.16	1585.54	1649.62	1714.20	3047.92	3339.60	3579.70	3625.32	3648.51
$H_2{}^{13}C^{17}O^{17}O^{\underline{17}}O$	713.21	806.26	909.24	1118.80	1251.43	1297.38	1533.00	1585.48	1648.27	1721.33	3047.91	3339.61	3573.55	3625.31	3648.51
$H_2{}^{13}C^{18}O^{18}O^{\underline{18}}O$	708.74	798.23	906.90	1110.29	1231.61	1295.19	1532.73	1585.42	1646.78	1708.48	3047.90	3339.58	3568.10	3625.30	3648.51

[&] Oxygen atoms here are expressed in the order of atoms 1, 2, 3 as denoted in Fig. 4-2(b). The underlined oxygen atoms (atom 3) are the ones to be abstracted during HCO_3^- dehydration reaction.

Table 4-A3 Scaled vibration frequencies (unit: cm^{-1}) for all 54 isotopologues of our modeled reactant during HCO_3^- dehydroxylation reaction in aqueous solution (Fig. 4-2c; DFT-B3LYP/cc-pvtz(-f) with a frequency scaling factor of 0.9614; see sections 2.2 and 2.4 for details). The frequency set contains 9 modes of vibration frequencies for each isotopologue.

Isotopologue[&]	ϖ_1	ϖ_2	ϖ_3	ϖ_4	ϖ_5	ϖ_6	ϖ_7	ϖ_8	ϖ_9
$H^{12}C^{16}O^{16}O^{16}\underline{O}^-$	456.58	547.13	636.71	771.76	887.63	1170.90	1277.82	1637.48	3631.44
$H^{13}C^{16}O^{16}O^{16}\underline{O}^-$	456.58	545.12	635.56	747.69	875.89	1170.35	1257.23	1592.93	3631.42
$H^{12}C^{18}O^{16}O^{16}\underline{O}^-$	456.05	540.39	625.06	768.31	879.25	1163.14	1261.46	1626.75	3631.44
$H^{12}C^{16}O^{18}O^{16}\underline{O}^-$	453.87	538.65	623.04	769.92	870.39	1162.86	1277.66	1636.62	3619.92
$H^{12}C^{16}O^{16}O^{18}\underline{O}^-$	456.35	537.82	627.13	768.38	879.28	1169.80	1255.23	1626.72	3631.44
$H^{13}C^{18}O^{16}O^{16}\underline{O}^-$	456.04	538.50	623.79	744.13	868.66	1161.32	1240.75	1582.01	3631.42
$H^{13}C^{16}O^{18}O^{16}\underline{O}^-$	453.87	536.56	622.36	745.79	858.03	1162.43	1257.03	1592.02	3619.90
$H^{13}C^{16}O^{16}O^{18}\underline{O}^-$	456.35	535.96	625.87	744.20	868.71	1169.32	1233.12	1581.98	3631.42
$H^{12}C^{17}O^{16}O^{16}\underline{O}^-$	456.30	543.70	630.54	769.93	883.35	1167.11	1268.92	1631.63	3631.44
$H^{12}C^{16}O^{17}O^{16}\underline{O}^-$	455.15	542.70	629.78	770.78	878.37	1166.61	1277.73	1637.02	3625.33
$H^{12}C^{16}O^{16}O^{17}\underline{O}^-$	456.46	542.34	631.66	769.97	883.34	1170.38	1265.90	1631.61	3631.44
$H^{12}C^{17}O^{18}O^{18}\underline{O}^-$	453.36	525.93	607.70	764.68	856.57	1158.52	1246.45	1619.27	3619.91
$H^{12}C^{18}O^{17}O^{18}\underline{O}^-$	454.40	527.02	608.29	763.91	860.65	1158.59	1239.33	1614.30	3625.32
$H^{12}C^{18}O^{18}O^{17}\underline{O}^-$	453.23	527.07	606.73	764.64	856.74	1155.12	1249.52	1619.29	3619.91
$H^{12}C^{16}O^{18}O^{18}\underline{O}^-$	453.62	529.17	614.04	766.53	861.26	1161.86	1255.14	1625.77	3619.91
$H^{12}C^{18}O^{16}O^{18}\underline{O}^-$	455.83	531.68	614.66	764.90	870.50	1162.78	1239.52	1614.84	3631.43
$H^{12}C^{18}O^{18}O^{16}\underline{O}^-$	453.35	531.56	611.97	766.44	861.65	1155.29	1260.97	1625.84	3619.91
$H^{12}C^{18}O^{17}O^{17}\underline{O}^-$	454.51	531.29	613.07	765.51	865.10	1158.78	1249.70	1619.75	3625.32
$H^{12}C^{17}O^{18}O^{17}\underline{O}^-$	453.47	530.38	612.16	766.27	861.10	1158.85	1256.96	1624.49	3619.91
$H^{12}C^{17}O^{17}O^{18}\underline{O}^-$	454.64	530.11	614.04	765.55	865.03	1162.21	1246.54	1619.73	3625.32
$H^{12}C^{16}O^{17}O^{17}\underline{O}^-$	455.02	537.87	624.88	768.99	873.86	1166.11	1265.84	1631.12	3625.32
$H^{12}C^{17}O^{16}O^{17}\underline{O}^-$	456.18	539.08	625.27	768.13	878.95	1166.79	1257.19	1625.43	3631.44
$H^{12}C^{17}O^{17}O^{16}\underline{O}^-$	454.87	539.18	623.77	768.94	873.99	1162.86	1268.76	1631.16	3625.32
$H^{12}C^{16}O^{17}O^{18}\underline{O}^-$	454.91	533.30	620.50	767.40	869.61	1165.57	1255.18	1626.21	3625.32
$H^{12}C^{16}O^{18}O^{17}\underline{O}^-$	453.74	533.78	618.28	768.12	865.69	1162.38	1265.79	1630.70	3619.92
$H^{12}C^{17}O^{16}O^{18}\underline{O}^-$	456.08	534.70	620.54	766.53	874.79	1166.44	1246.64	1620.26	3631.44
$H^{12}C^{17}O^{18}O^{16}\underline{O}^-$	453.60	535.05	617.17	768.07	865.91	1159.15	1268.62	1630.74	3619.92
$H^{12}C^{18}O^{16}O^{17}\underline{O}^-$	455.93	535.92	619.58	766.50	874.76	1162.97	1249.92	1620.26	3631.43
$H^{12}C^{18}O^{17}O^{16}\underline{O}^-$	454.63	535.78	618.43	767.31	869.81	1158.95	1261.19	1626.26	3625.32
$H^{12}C^{17}O^{17}O^{17}\underline{O}^-$	454.75	534.53	618.63	767.14	869.38	1162.55	1257.07	1624.93	3625.32
$H^{12}C^{18}O^{18}O^{18}\underline{O}^-$	453.12	522.77	602.06	763.03	852.12	1154.94	1239.17	1613.82	3619.91
$H^{13}C^{17}O^{16}O^{16}\underline{O}^-$	456.30	541.75	629.33	745.81	872.20	1166.04	1248.15	1586.96	3631.42
$H^{13}C^{16}O^{17}O^{16}\underline{O}^-$	455.15	540.64	628.89	746.68	866.29	1166.12	1257.12	1592.44	3625.31
$H^{13}C^{16}O^{16}O^{17}\underline{O}^-$	456.46	540.41	630.44	745.84	872.21	1169.88	1244.53	1586.93	3631.42
$H^{13}C^{17}O^{18}O^{18}\underline{O}^-$	453.36	524.06	606.83	740.38	845.95	1157.83	1224.06	1574.26	3619.90
$H^{13}C^{18}O^{17}O^{18}\underline{O}^-$	454.40	525.26	607.14	739.59	850.89	1157.17	1216.98	1569.18	3625.30
$H^{13}C^{18}O^{18}O^{17}\underline{O}^-$	453.23	525.19	605.86	740.34	846.09	1153.75	1227.84	1574.29	3619.90
$H^{13}C^{16}O^{18}O^{18}\underline{O}^-$	453.62	527.24	613.25	742.30	850.05	1161.45	1233.06	1580.97	3619.90
$H^{13}C^{18}O^{16}O^{18}\underline{O}^-$	455.83	529.95	613.26	740.61	861.11	1161.17	1217.26	1569.76	3631.42

Table 4-A3 (Continued)

Isotopologue[&]	ϖ_1	ϖ_2	ϖ_3	ϖ_4	ϖ_5	ϖ_6	ϖ_7	ϖ_8	ϖ_9
$H^{13}C^{18}O^{18}O^{16}\underline{O}^-$	453.35	529.60	611.18	742.20	850.37	1153.84	1240.01	1581.05	3619.90
$H^{13}C^{18}O^{17}O^{17}\underline{O}^-$	454.50	529.45	611.99	741.24	854.77	1157.26	1228.11	1574.77	3625.30
$H^{13}C^{17}O^{18}O^{17}\underline{O}^-$	453.47	528.44	611.35	742.03	849.91	1158.09	1235.31	1579.59	3619.90
$H^{13}C^{17}O^{17}O^{18}\underline{O}^-$	454.64	528.28	612.96	741.28	854.71	1161.45	1224.16	1574.75	3625.31
$H^{13}C^{16}O^{17}O^{17}\underline{O}^-$	455.02	535.89	623.93	744.83	862.39	1165.66	1244.47	1586.42	3625.31
$H^{13}C^{17}O^{16}O^{17}\underline{O}^-$	456.18	537.21	623.98	743.95	868.43	1165.83	1235.62	1580.59	3631.42
$H^{13}C^{17}O^{17}O^{16}\underline{O}^-$	454.87	537.19	622.81	744.78	862.49	1161.92	1247.92	1586.46	3625.31
$H^{13}C^{16}O^{17}O^{18}\underline{O}^-$	454.91	531.40	619.50	743.19	858.70	1165.12	1233.09	1581.44	3625.31
$H^{13}C^{16}O^{18}O^{17}\underline{O}^-$	453.74	531.78	617.54	743.94	853.92	1161.97	1244.42	1585.97	3619.90
$H^{13}C^{17}O^{16}O^{18}\underline{O}^-$	456.08	532.91	619.20	742.30	864.84	1165.58	1224.28	1575.31	3631.42
$H^{13}C^{17}O^{18}O^{16}\underline{O}^-$	453.60	533.03	616.43	743.89	854.10	1158.31	1247.72	1586.02	3619.90
$H^{13}C^{18}O^{16}O^{17}\underline{O}^-$	455.93	534.12	618.23	742.27	864.79	1161.25	1228.45	1575.32	3631.42
$H^{13}C^{18}O^{17}O^{16}\underline{O}^-$	454.62	533.85	617.42	743.10	858.85	1157.34	1240.34	1581.49	3625.31
$H^{13}C^{17}O^{17}O^{17}\underline{O}^-$	454.75	532.62	617.60	742.93	858.49	1161.70	1235.45	1580.06	3625.31
$H^{13}C^{18}O^{18}O^{18}\underline{O}^-$	453.12	520.97	601.14	738.68	842.04	1153.66	1216.75	1568.68	3619.89

[&] Oxygen atoms here are expressed in the order of atoms 1, 2, 3 as denoted in Fig. 4-2c. The underlined oxygen atoms (atom 3) are the ones to be abstracted during HCO_3^- dehydroxylation reaction.

Table 4-A4 Scaled vibration frequencies (unit: cm^{-1}) for all 54 isotopologues of our modeled transition state during HCO_3^- dehydroxylation reaction in aqueous solution (Fig. 4-2d; DFT-B3LYP/cc-pvtz(-f) with a frequency scaling factor of 0.9614; see sections 2.2 and 2.4 for details). The frequency set contains 9 modes of vibration frequencies for each isotopologue.

Isotopologue[&]	ϖ_1	ϖ_2	ϖ_3	ϖ_4	ϖ_5	ϖ_6	ϖ_7	ϖ_8	ϖ_9
$H^{12}C^{16}O^{16}O^{16}\underline{O}^-$	-236.49	183.29	232.84	390.20	593.56	634.20	1300.65	2225.08	3593.01
$H^{13}C^{16}O^{16}O^{16}\underline{O}^-$	-233.16	183.33	232.36	389.76	584.06	615.95	1299.98	2161.68	3593.01
$H^{12}C^{18}O^{16}O^{16}\underline{O}^-$	-236.29	183.09	228.17	388.10	588.52	629.74	1263.61	2208.60	3593.01
$H^{12}C^{16}O^{18}O^{16}\underline{O}^-$	-231.58	178.82	229.91	381.54	592.45	634.19	1300.62	2225.07	3581.27
$H^{12}C^{16}O^{16}O^{18}\underline{O}^-$	-236.41	182.06	229.13	387.96	589.15	629.76	1263.76	2208.74	3593.01
$H^{13}C^{18}O^{16}O^{16}\underline{O}^-$	-232.99	183.12	227.74	387.57	579.02	611.36	1262.84	2144.75	3593.01
$H^{13}C^{16}O^{18}O^{16}\underline{O}^-$	-228.25	178.85	229.42	381.13	582.94	615.93	1299.95	2161.67	3581.27
$H^{13}C^{16}O^{16}O^{18}\underline{O}^-$	-233.10	182.09	228.67	387.45	579.67	611.38	1262.97	2144.90	3593.01
$H^{12}C^{17}O^{16}O^{16}\underline{O}^-$	-236.38	183.19	230.41	389.09	590.88	631.84	1281.34	2216.23	3593.01
$H^{12}C^{16}O^{17}O^{16}\underline{O}^-$	-233.93	180.93	231.29	385.65	592.97	634.20	1300.64	2225.07	3586.79
$H^{12}C^{16}O^{16}O^{17}\underline{O}^-$	-236.45	182.67	230.90	389.02	591.22	631.85	1281.41	2216.31	3593.01
$H^{12}C^{17}O^{18}O^{18}\underline{O}^-$	-231.34	177.54	223.75	378.04	585.31	627.36	1244.73	2199.31	3581.27
$H^{12}C^{18}O^{17}O^{18}\underline{O}^-$	-233.61	179.49	223.10	381.06	583.48	625.26	1227.30	2191.17	3586.79
$H^{12}C^{18}O^{18}O^{17}\underline{O}^-$	-231.27	178.04	223.28	378.06	585.04	627.36	1244.66	2199.24	3581.27

Table 4-A4 (Continued)

Isotopologue[&]	ϖ_1	ϖ_2	ϖ_3	ϖ_4	ϖ_5	ϖ_6	ϖ_7	ϖ_8	ϖ_9
$H^{12}C^{16}O^{18}O^{18}\underline{O}^-$	-231.47	177.65	226.07	379.31	588.01	629.74	1263.72	2208.73	3581.27
$H^{12}C^{18}O^{16}O^{18}\underline{O}^-$	-236.21	181.79	224.77	385.66	584.09	625.27	1227.31	2191.17	3593.01
$H^{12}C^{18}O^{18}O^{16}\underline{O}^-$	-231.33	178.66	225.13	379.36	587.41	629.73	1263.58	2208.59	3581.27
$H^{12}C^{18}O^{17}O^{17}\underline{O}^-$	-233.66	180.12	224.75	382.22	585.57	627.36	1244.67	2199.25	3586.79
$H^{12}C^{17}O^{18}O^{17}\underline{O}^-$	-231.39	178.14	225.51	379.15	587.40	629.46	1262.24	2207.15	3581.27
$H^{12}C^{17}O^{17}O^{18}\underline{O}^-$	-233.72	179.61	225.23	382.18	585.85	627.37	1244.75	2199.31	3586.79
$H^{12}C^{16}O^{17}O^{17}\underline{O}^-$	-233.88	180.33	229.32	384.47	590.62	631.84	1281.39	2216.30	3586.79
$H^{12}C^{17}O^{16}O^{17}\underline{O}^-$	-236.34	182.56	228.56	387.86	588.53	629.48	1262.27	2207.15	3593.01
$H^{12}C^{17}O^{17}O^{16}\underline{O}^-$	-233.82	180.85	228.84	384.53	590.29	631.83	1281.32	2216.23	3586.79
$H^{12}C^{16}O^{17}O^{18}\underline{O}^-$	-233.84	179.73	227.52	383.42	588.54	629.75	1263.74	2208.74	3586.79
$H^{12}C^{16}O^{18}O^{17}\underline{O}^-$	-231.52	178.23	227.90	380.36	590.09	631.83	1281.38	2216.30	3581.27
$H^{12}C^{17}O^{16}O^{18}\underline{O}^-$	-236.30	181.92	226.87	386.75	586.46	627.38	1244.77	2199.32	3593.01
$H^{12}C^{17}O^{18}O^{16}\underline{O}^-$	-231.45	178.74	227.43	380.39	589.77	631.83	1281.31	2216.22	3581.27
$H^{12}C^{18}O^{16}O^{17}\underline{O}^-$	-236.25	182.44	226.39	386.81	586.17	627.37	1244.69	2199.25	3593.01
$H^{12}C^{18}O^{17}O^{16}\underline{O}^-$	-233.71	180.76	226.57	383.51	587.93	629.73	1263.59	2208.59	3586.79
$H^{12}C^{17}O^{17}O^{17}\underline{O}^-$	-233.77	180.23	226.95	383.29	587.93	629.47	1262.25	2207.15	3586.79
$H^{12}C^{18}O^{18}O^{18}\underline{O}^-$	-231.22	177.42	221.60	376.91	582.94	625.25	1227.28	2191.16	3581.27
$H^{13}C^{17}O^{16}O^{16}\underline{O}^-$	-233.07	183.23	229.96	388.61	581.38	613.52	1280.63	2152.58	3593.01
$H^{13}C^{16}O^{17}O^{16}\underline{O}^-$	-230.61	180.97	230.81	385.23	583.47	615.94	1299.97	2161.68	3586.78
$H^{13}C^{16}O^{16}O^{17}\underline{O}^-$	-233.13	182.71	230.43	388.54	581.73	613.53	1280.70	2152.66	3593.01
$H^{13}C^{17}O^{18}O^{18}\underline{O}^-$	-228.06	177.57	223.31	377.52	575.81	608.90	1243.99	2135.15	3581.27
$H^{13}C^{18}O^{17}O^{18}\underline{O}^-$	-230.35	179.51	222.68	380.47	573.99	606.74	1226.56	2126.75	3586.78
$H^{13}C^{18}O^{18}O^{17}\underline{O}^-$	-228.00	178.07	222.86	377.53	575.53	608.90	1243.93	2135.08	3581.27
$H^{13}C^{16}O^{18}O^{18}\underline{O}^-$	-228.17	177.68	225.60	378.83	578.51	611.35	1262.93	2144.90	3581.27
$H^{13}C^{18}O^{16}O^{18}\underline{O}^-$	-232.94	181.81	224.36	385.04	574.61	606.75	1226.58	2126.75	3593.01
$H^{13}C^{18}O^{18}O^{16}\underline{O}^-$	-228.04	178.69	224.70	378.87	577.89	611.33	1262.81	2144.74	3581.27
$H^{13}C^{18}O^{17}O^{17}\underline{O}^-$	-230.38	180.15	224.33	381.67	576.07	608.91	1243.94	2135.08	3586.78
$H^{13}C^{17}O^{18}O^{17}\underline{O}^-$	-228.10	178.17	225.06	378.66	577.89	611.06	1261.54	2143.22	3581.27
$H^{13}C^{17}O^{17}O^{18}\underline{O}^-$	-230.44	179.64	224.79	381.64	576.36	608.92	1244.01	2135.16	3586.78
$H^{13}C^{16}O^{17}O^{17}\underline{O}^-$	-230.57	180.37	228.85	384.01	581.12	613.52	1280.68	2152.66	3586.78
$H^{13}C^{17}O^{16}O^{17}\underline{O}^-$	-233.04	182.59	228.12	387.33	579.04	611.09	1261.57	2143.22	3593.01
$H^{13}C^{17}O^{17}O^{16}\underline{O}^-$	-230.51	180.88	228.39	384.06	580.78	613.51	1280.62	2152.58	3586.78
$H^{13}C^{16}O^{17}O^{18}\underline{O}^-$	-230.54	179.77	227.05	382.92	579.06	611.36	1262.95	2144.90	3586.78
$H^{13}C^{16}O^{18}O^{17}\underline{O}^-$	-228.21	178.27	227.42	379.92	580.59	613.50	1280.67	2152.66	3581.27
$H^{13}C^{17}O^{16}O^{18}\underline{O}^-$	-233.02	181.96	226.43	386.19	576.98	608.93	1244.03	2135.16	3593.01
$H^{13}C^{17}O^{18}O^{16}\underline{O}^-$	-228.14	178.77	226.97	379.94	580.25	613.50	1280.60	2152.57	3581.27
$H^{13}C^{18}O^{16}O^{17}\underline{O}^-$	-232.97	182.47	225.97	386.24	576.68	608.92	1243.96	2135.09	3593.01
$H^{13}C^{18}O^{17}O^{16}\underline{O}^-$	-230.42	180.79	226.14	383.00	578.42	611.35	1262.82	2144.74	3586.78
$H^{13}C^{17}O^{17}O^{17}\underline{O}^-$	-230.47	180.26	226.51	382.78	578.43	611.08	1261.55	2143.22	3586.78
$H^{13}C^{18}O^{18}O^{18}\underline{O}^-$	-227.96	177.45	221.18	376.34	573.45	606.73	1226.55	2126.75	3581.27

[&] Oxygen atoms here are expressed in the order of atoms 1, 2, 3 as denoted in Fig. 4-2(d). The underlined oxygen atoms (atom 3) are the ones to be abstracted during HCO_3^- dehydration reaction.

Table 4-A5 Model predicted kinetic isotope fractionations (unit: ‰) for all isotopologues during HCO_3^- dehydration reaction in aqueous solution at 25°C. For isotopologues comprising more than one isotopomers, 'Average' denotes the average isotopic fractionation of its all comprising isotopomers.

Temperature (°C)	**0**	**5**	**15**	**25**	**35**	**45**	**55**	**65**	**75**	**85**	**95**	**100**
$H_2{}^{12}C^{16}O^{16}O^{16}O$												
$H_2{}^{13}C^{16}O^{16}O^{16}O$	-32.5	-31.9	-30.8	-29.7	-28.7	-27.7	-26.8	-26.0	-25.2	-24.5	-23.8	-23.5
$H_2{}^{12}C^{18}O^{16}O^{16}O$	-5.3	-5.2	-4.9	-4.7	-4.5	-4.3	-4.1	-4.0	-3.8	-3.6	-3.5	-3.4
$H_2{}^{12}C^{16}O^{18}O^{16}O$	-10.3	-10.1	-9.7	-9.3	-8.9	-8.5	-8.2	-7.9	-7.6	-7.4	-7.1	-7.0
$H_2{}^{12}C^{16}O^{16}O^{18}O$	-13.8	-13.7	-13.4	-13.1	-12.9	-12.6	-12.4	-12.1	-11.9	-11.7	-11.5	-11.4
Average	-9.8	-9.7	-9.3	-9.0	-8.7	-8.5	-8.2	-8.0	-7.8	-7.6	-7.4	-7.3
$H_2{}^{13}C^{18}O^{16}O^{16}O$	-37.9	-37.2	-35.8	-34.4	-33.2	-32.1	-31.0	-30.0	-29.1	-28.2	-27.4	-27.0
$H_2{}^{13}C^{16}O^{18}O^{16}O$	-42.6	-41.8	-40.2	-38.7	-37.3	-36.0	-34.8	-33.7	-32.7	-31.7	-30.8	-30.3
$H_2{}^{13}C^{16}O^{16}O^{18}O$	-46.8	-46.0	-44.5	-43.1	-41.8	-40.6	-39.5	-38.4	-37.4	-36.5	-35.6	-35.2
Average	-42.4	-41.6	-40.1	-38.8	-37.5	-36.2	-35.1	-34.0	-33.1	-32.1	-31.2	-30.8
$H_2{}^{12}C^{17}O^{16}O^{16}O$	-2.8	-2.7	-2.6	-2.5	-2.4	-2.3	-2.2	-2.1	-2.0	-1.9	-1.8	-1.8
$H_2{}^{12}C^{16}O^{17}O^{16}O$	-5.5	-5.4	-5.2	-4.9	-4.7	-4.5	-4.4	-4.2	-4.1	-3.9	-3.8	-3.7
$H_2{}^{12}C^{16}O^{16}O^{17}O$	-7.3	-7.2	-7.0	-6.9	-6.7	-6.6	-6.5	-6.4	-6.2	-6.1	-6.0	-6.0
Average	-5.2	-5.1	-4.9	-4.8	-4.6	-4.5	-4.3	-4.2	-4.1	-4.0	-3.9	-3.8
$H_2{}^{12}C^{17}O^{18}O^{18}O$	-27.0	-26.5	-25.7	-24.9	-24.1	-23.4	-22.8	-22.1	-21.5	-21.0	-20.5	-20.2
$H_2{}^{12}C^{18}O^{17}O^{18}O$	-24.7	-24.3	-23.5	-22.8	-22.1	-21.5	-20.9	-20.3	-19.8	-19.3	-18.8	-18.6
$H_2{}^{12}C^{18}O^{18}O^{17}O$	-22.9	-22.4	-21.6	-20.8	-20.1	-19.4	-18.8	-18.2	-17.6	-17.1	-16.6	-16.4
Average	-24.8	-24.4	-23.6	-22.8	-22.1	-21.4	-20.8	-20.2	-19.7	-19.1	-18.6	-18.4
$H_2{}^{12}C^{16}O^{18}O^{18}O$	-24.2	-23.8	-23.1	-22.4	-21.8	-21.2	-20.6	-20.1	-19.6	-19.1	-18.6	-18.4
$H_2{}^{12}C^{18}O^{16}O^{18}O$	-19.2	-18.9	-18.4	-17.9	-17.4	-16.9	-16.5	-16.1	-15.7	-15.4	-15.0	-14.9
$H_2{}^{12}C^{18}O^{18}O^{16}O$	-15.6	-15.2	-14.5	-13.9	-13.3	-12.8	-12.3	-11.8	-11.4	-11.0	-10.6	-10.4
Average	-19.7	-19.3	-18.7	-18.1	-17.5	-17.0	-16.5	-16.0	-15.6	-15.1	-14.7	-14.6
$H_2{}^{12}C^{18}O^{17}O^{17}O$	-18.1	-17.7	-17.1	-16.5	-16.0	-15.5	-15.0	-14.5	-14.1	-13.7	-13.3	-13.1
$H_2{}^{12}C^{17}O^{18}O^{17}O$	-20.4	-20.0	-19.3	-18.6	-18.0	-17.4	-16.9	-16.3	-15.9	-15.4	-15.0	-14.8
$H_2{}^{12}C^{17}O^{17}O^{18}O$	-22.2	-21.8	-21.2	-20.6	-20.0	-19.4	-18.9	-18.4	-18.0	-17.6	-17.2	-17.0
Average	-20.2	-19.9	-19.2	-18.6	-18.0	-17.4	-16.9	-16.4	-16.0	-15.6	-15.2	-15.0
$H_2{}^{12}C^{16}O^{17}O^{17}O$	-12.8	-12.6	-12.2	-11.8	-11.5	-11.2	-10.9	-10.6	-10.3	-10.1	-9.8	-9.7
$H_2{}^{12}C^{17}O^{16}O^{17}O$	-10.1	-9.9	-9.6	-9.4	-9.1	-8.9	-8.7	-8.5	-8.3	-8.1	-7.9	-7.8
$H_2{}^{12}C^{17}O^{17}O^{16}O$	-8.3	-8.1	-7.7	-7.4	-7.1	-6.8	-6.5	-6.3	-6.1	-5.8	-5.6	-5.5
Average	-10.4	-10.2	-9.9	-9.5	-9.2	-9.0	-8.7	-8.4	-8.2	-8.0	-7.8	-7.7
$H_2{}^{12}C^{16}O^{17}O^{18}O$	-19.4	-19.1	-18.6	-18.1	-17.6	-17.2	-16.7	-16.4	-16.0	-15.6	-15.3	-15.1
$H_2{}^{12}C^{16}O^{18}O^{17}O$	-17.6	-17.3	-16.7	-16.1	-15.6	-15.1	-14.7	-14.3	-13.9	-13.5	-13.2	-13.0
$H_2{}^{12}C^{17}O^{16}O^{18}O$	-16.7	-16.4	-16.0	-15.6	-15.2	-14.9	-14.6	-14.2	-13.9	-13.6	-13.4	-13.2
$H_2{}^{12}C^{17}O^{18}O^{16}O$	-13.1	-12.8	-12.2	-11.7	-11.2	-10.8	-10.4	-10.0	-9.6	-9.3	-9.0	-8.8
$H_2{}^{12}C^{18}O^{16}O^{17}O$	-12.6	-12.4	-12.0	-11.6	-11.3	-10.9	-10.6	-10.3	-10.1	-9.8	-9.5	-9.4
$H_2{}^{12}C^{18}O^{17}O^{16}O$	-10.8	-10.5	-10.0	-9.6	-9.2	-8.8	-8.5	-8.1	-7.8	-7.6	-7.3	-7.2
Average	-15.0	-14.8	-14.3	-13.8	-13.4	-13.0	-12.6	-12.2	-11.9	-11.6	-11.3	-11.1
$H_2{}^{12}C^{17}O^{17}O^{17}O$	-15.6	-15.3	-14.8	-14.3	-13.8	-13.4	-13.0	-12.7	-12.3	-12.0	-11.7	-11.5
$H_2{}^{12}C^{18}O^{18}O^{18}O$	-29.5	-29.0	-28.0	-27.1	-26.2	-25.4	-24.7	-24.0	-23.3	-22.7	-22.1	-21.8

Table 4-A5 (Continued)

Temperature (°C)	**0**	**5**	**15**	**25**	**35**	**45**	**55**	**65**	**75**	**85**	**95**	**100**
$H_2{}^{13}C^{17}O^{16}O\underline{^{16}O}$	-35.4	-34.7	-33.4	-32.2	-31.1	-30.0	-29.0	-28.1	-27.3	-26.4	-25.7	-25.3
$H_2{}^{13}C^{16}O^{17}O\underline{^{16}O}$	-37.9	-37.2	-35.8	-34.5	-33.3	-32.1	-31.1	-30.1	-29.2	-28.3	-27.5	-27.1
$H_2{}^{13}C^{16}O^{16}O\underline{^{17}O}$	-40.0	-39.3	-38.0	-36.7	-35.6	-34.5	-33.5	-32.5	-31.6	-30.8	-30.0	-29.6
Average	-37.8	-37.1	-35.7	-34.5	-33.3	-32.2	-31.2	-30.2	-29.4	-28.5	-27.7	-27.4
$H_2{}^{13}C^{17}O^{18}O\underline{^{18}O}$	-59.7	-58.6	-56.6	-54.7	-52.9	-51.3	-49.7	-48.3	-46.9	-45.6	-44.4	-43.8
$H_2{}^{13}C^{18}O^{17}O\underline{^{18}O}$	-57.5	-56.5	-54.6	-52.7	-51.0	-49.4	-47.9	-46.5	-45.2	-44.0	-42.8	-42.3
$H_2{}^{13}C^{18}O^{18}O\underline{^{17}O}$	-55.4	-54.3	-52.3	-50.5	-48.8	-47.1	-45.6	-44.2	-42.9	-41.6	-40.5	-39.9
Average	-57.5	-56.5	-54.5	-52.6	-50.9	-49.3	-47.8	-46.3	-45.0	-43.7	-42.6	-42.0
$H_2{}^{13}C^{16}O^{18}O\underline{^{18}O}$	-56.8	-55.8	-53.9	-52.2	-50.5	-49.0	-47.5	-46.1	-44.9	-43.7	-42.5	-42.0
$H_2{}^{13}C^{18}O^{16}O\underline{^{18}O}$	-52.2	-51.3	-49.6	-47.9	-46.4	-45.0	-43.7	-42.5	-41.3	-40.2	-39.1	-38.7
$H_2{}^{13}C^{18}O^{18}O\underline{^{16}O}$	-47.9	-46.9	-45.1	-43.4	-41.8	-40.3	-39.0	-37.7	-36.5	-35.3	-34.3	-33.8
Average	-52.3	-51.4	-49.5	-47.8	-46.3	-44.8	-43.4	-42.1	-40.9	-39.7	-38.7	-38.1
$H_2{}^{13}C^{18}O^{17}O\underline{^{17}O}$	-50.7	-49.8	-48.0	-46.3	-44.7	-43.3	-41.9	-40.6	-39.4	-38.3	-37.2	-36.7
$H_2{}^{13}C^{17}O^{18}O\underline{^{17}O}$	-52.9	-51.9	-50.0	-48.2	-46.6	-45.1	-43.7	-42.3	-41.1	-39.9	-38.8	-38.3
$H_2{}^{13}C^{17}O^{17}O\underline{^{18}O}$	-55.0	-54.0	-52.2	-50.5	-48.9	-47.4	-46.0	-44.7	-43.4	-42.3	-41.2	-40.6
Average	-52.9	-51.9	-50.1	-48.3	-46.7	-45.2	-43.8	-42.5	-41.3	-40.2	-39.1	-38.5
$H_2{}^{13}C^{16}O^{17}O\underline{^{17}O}$	-45.4	-44.6	-43.0	-41.5	-40.2	-38.9	-37.7	-36.6	-35.6	-34.6	-33.7	-33.3
$H_2{}^{13}C^{17}O^{16}O\underline{^{17}O}$	-47.8	-46.9	-45.2	-43.6	-42.2	-40.8	-39.5	-38.2	-37.1	-36.0	-35.0	-34.5
$H_2{}^{13}C^{17}O^{17}O\underline{^{16}O}$	-35.7	-35.1	-33.8	-32.6	-31.5	-30.5	-29.5	-28.6	-27.8	-27.0	-26.2	-25.9
Average	-43.0	-42.2	-40.7	-39.3	-37.9	-36.7	-35.6	-34.5	-33.5	-32.5	-31.6	-31.2
$H_2{}^{13}C^{16}O^{17}O\underline{^{18}O}$	-52.1	-51.2	-49.5	-48.0	-46.5	-45.1	-43.8	-42.5	-41.4	-40.3	-39.3	-38.8
$H_2{}^{13}C^{16}O^{18}O\underline{^{17}O}$	-50.1	-49.1	-47.4	-45.8	-44.2	-42.8	-41.5	-40.2	-39.1	-38.0	-36.9	-36.4
$H_2{}^{13}C^{17}O^{16}O\underline{^{18}O}$	-49.6	-48.8	-47.2	-45.7	-44.3	-43.0	-41.7	-40.6	-39.5	-38.4	-37.5	-37.0
$H_2{}^{13}C^{17}O^{18}O\underline{^{16}O}$	-45.4	-44.5	-42.8	-41.2	-39.7	-38.3	-37.0	-35.8	-34.7	-33.6	-32.6	-32.1
$H_2{}^{13}C^{18}O^{16}O\underline{^{17}O}$	-45.4	-44.6	-43.0	-41.5	-40.1	-38.9	-37.7	-36.5	-35.5	-34.5	-33.5	-33.1
$H_2{}^{13}C^{18}O^{17}O\underline{^{16}O}$	-43.2	-42.4	-40.7	-39.2	-37.8	-36.5	-35.2	-34.1	-33.0	-32.0	-31.1	-30.6
Average	-44.7	-43.8	-42.2	-40.6	-39.2	-37.9	-36.6	-35.5	-34.4	-33.4	-32.4	-31.9
$H_2{}^{13}C^{17}O^{17}O\underline{^{17}O}$	-48.2	-47.3	-45.6	-44.1	-42.6	-41.2	-39.9	-38.7	-37.6	-36.6	-35.6	-35.1
$H_2{}^{13}C^{18}O^{18}O\underline{^{18}O}$	-62.2	-61.1	-58.9	-56.9	-55.0	-53.3	-51.7	-50.1	-48.7	-47.3	-46.1	-45.5

Table 4-A6 Model predicted kinetic isotope fractionations (unit: ‰) for all isotopologues during HCO_3^- dehydroxylation reaction in aqueous solution at 25°C. For isotopologues comprising more than one isotopomers, 'Average' denotes the average isotopic fractionation of its all comprising isotopomers.

Temperature (°C)	**0**	**5**	**15**	**25**	**35**	**45**	**55**	**65**	**75**	**85**	**95**	**100**
$H^{12}C^{16}O^{16}O^{16}O^-$												
$H^{13}C^{16}O^{16}O^{16}O^-$	-25.3	-24.7	-23.5	-22.5	-21.5	-20.5	-19.7	-18.9	-18.2	-17.5	-16.9	-16.6
$H^{12}C^{18}O^{16}O^{16}O^-$	13.5	13.3	13.0	12.7	12.4	12.1	11.8	11.5	11.2	10.9	10.6	10.5
$H^{12}C^{16}O^{18}O^{16}O^-$	-83.2	-81.5	-78.2	-75.2	-72.3	-69.7	-67.3	-65.1	-63.0	-61.0	-59.2	-58.3
$H^{12}C^{16}O^{16}O^{18}O^-$	13.2	13.1	12.8	12.5	12.2	11.9	11.6	11.4	11.1	10.8	10.6	10.5
Average	-18.8	-18.4	-17.5	-16.7	-15.9	-15.3	-14.6	-14.1	-13.6	-13.1	-12.7	-12.4
$H^{13}C^{18}O^{16}O^{16}O^-$	-11.4	-10.9	-10.1	-9.4	-8.7	-8.1	-7.6	-7.1	-6.6	-6.3	-5.9	-5.8
$H^{13}C^{16}O^{18}O^{16}O^-$	-109.1	-106.7	-102.2	-98.1	-94.2	-90.7	-87.4	-84.4	-81.6	-78.9	-76.5	-75.3
$H^{13}C^{16}O^{16}O^{18}O^-$	-11.7	-11.3	-10.4	-9.6	-8.9	-8.3	-7.7	-7.2	-6.8	-6.4	-6.0	-5.9
Average	-44.1	-43.0	-40.9	-39.0	-37.3	-35.7	-34.2	-32.9	-31.7	-30.5	-29.5	-29.0
$H^{12}C^{17}O^{16}O^{16}O^-$	7.1	7.0	6.8	6.7	6.5	6.3	6.2	6.0	5.9	5.7	5.6	5.5
$H^{12}C^{16}O^{17}O^{16}O^-$	-43.8	-42.9	-41.1	-39.5	-38.0	-36.7	-35.4	-34.2	-33.1	-32.1	-31.1	-30.6
$H^{12}C^{16}O^{16}O^{17}O^-$	6.9	6.9	6.7	6.5	6.4	6.3	6.1	6.0	5.8	5.7	5.6	5.5
Average	-9.9	-9.7	-9.2	-8.8	-8.4	-8.0	-7.7	-7.4	-7.1	-6.9	-6.6	-6.5
$H^{12}C^{17}O^{18}O^{18}O^-$	-63.2	-61.7	-58.9	-56.3	-53.9	-51.8	-49.8	-47.9	-46.3	-44.7	-43.3	-42.6
$H^{12}C^{18}O^{17}O^{18}O^-$	-17.1	-16.5	-15.4	-14.5	-13.6	-12.8	-12.1	-11.5	-10.9	-10.4	-10.0	-9.8
$H^{12}C^{18}O^{18}O^{17}O^-$	-63.1	-61.6	-58.8	-56.2	-53.9	-51.7	-49.7	-47.9	-46.3	-44.7	-43.3	-42.6
Average	-47.8	-46.6	-44.4	-42.3	-40.5	-38.8	-37.2	-35.8	-34.5	-33.3	-32.2	-31.7
$H^{12}C^{16}O^{18}O^{18}O^-$	-70.3	-68.7	-65.7	-62.9	-60.4	-58.0	-55.9	-53.9	-52.1	-50.3	-48.8	-48.0
$H^{12}C^{18}O^{16}O^{18}O^-$	26.9	26.6	26.0	25.3	24.7	24.1	23.5	22.9	22.4	21.8	21.3	21.1
$H^{12}C^{18}O^{18}O^{16}O^-$	-70.0	-68.5	-65.5	-62.8	-60.3	-58.0	-55.8	-53.9	-52.0	-50.4	-48.8	-48.1
Average	-37.8	-36.8	-35.1	-33.4	-32.0	-30.6	-29.4	-28.3	-27.2	-26.3	-25.4	-25.0
$H^{12}C^{18}O^{17}O^{17}O^-$	-23.4	-22.8	-21.5	-20.4	-19.4	-18.5	-17.6	-16.9	-16.2	-15.6	-15.0	-14.7
$H^{12}C^{17}O^{18}O^{17}O^-$	-69.4	-67.9	-64.9	-62.2	-59.7	-57.4	-55.2	-53.3	-51.5	-49.8	-48.2	-47.5
$H^{12}C^{17}O^{17}O^{18}O^-$	-23.6	-22.9	-21.6	-20.5	-19.5	-18.5	-17.7	-16.9	-16.2	-15.6	-15.0	-14.7
Average	-38.8	-37.8	-36.0	-34.3	-32.8	-31.4	-30.2	-29.0	-28.0	-27.0	-26.1	-25.7
$H^{12}C^{16}O^{17}O^{17}O^-$	-36.9	-36.1	-34.5	-33.0	-31.7	-30.5	-29.3	-28.3	-27.3	-26.4	-25.6	-25.2
$H^{12}C^{17}O^{16}O^{17}O^-$	14.1	13.9	13.6	13.3	12.9	12.6	12.3	12.0	11.7	11.5	11.2	11.1
$H^{12}C^{17}O^{17}O^{16}O^-$	-36.8	-35.9	-34.4	-32.9	-31.6	-30.4	-29.3	-28.2	-27.3	-26.4	-25.6	-25.2
Average	-19.9	-19.4	-18.4	-17.6	-16.8	-16.1	-15.4	-14.8	-14.3	-13.8	-13.3	-13.1
$H^{12}C^{16}O^{17}O^{18}O^-$	-30.7	-29.9	-28.5	-27.2	-26.0	-24.9	-23.8	-22.9	-22.1	-21.3	-20.6	-20.2
$H^{12}C^{16}O^{18}O^{17}O^-$	-76.4	-74.8	-71.6	-68.7	-66.1	-63.6	-61.3	-59.2	-57.2	-55.4	-53.7	-52.9
$H^{12}C^{17}O^{16}O^{18}O^-$	20.4	20.2	19.7	19.2	18.8	18.3	17.9	17.5	17.0	16.6	16.2	16.0
$H^{12}C^{17}O^{18}O^{16}O^-$	-76.3	-74.6	-71.5	-68.6	-66.0	-63.5	-61.3	-59.2	-57.2	-55.4	-53.7	-52.9
$H^{12}C^{18}O^{16}O^{17}O^-$	20.6	20.3	19.8	19.3	18.8	18.4	17.9	17.5	17.1	16.7	16.3	16.1
$H^{12}C^{18}O^{17}O^{16}O^-$	-30.4	-29.7	-28.3	-27.0	-25.8	-24.7	-23.8	-22.9	-22.0	-21.3	-20.6	-20.2
Average	-28.8	-28.1	-26.7	-25.5	-24.4	-23.3	-22.4	-21.5	-20.7	-20.0	-19.4	-19.0
$H^{12}C^{17}O^{17}O^{17}O^-$	-29.8	-29.1	-27.7	-26.4	-25.2	-24.2	-23.2	-22.3	-21.5	-20.7	-20.0	-19.7
$H^{12}C^{18}O^{18}O^{18}O^-$	-56.9	-55.4	-52.8	-50.3	-48.1	-46.1	-44.3	-42.6	-41.0	-39.6	-38.3	-37.7

Table 4-A6 (Continued)

Temperature (°C)	**0**	**5**	**15**	**25**	**35**	**45**	**55**	**65**	**75**	**85**	**95**	**100**
$H^{13}C^{17}O^{16}O\underline{^{16}O}^{-}$	-18.0	-17.5	-16.5	-15.6	-14.8	-14.0	-13.3	-12.7	-12.1	-11.6	-11.1	-10.9
$H^{13}C^{16}O^{17}O\underline{^{16}O}^{-}$	-69.4	-67.8	-64.9	-62.2	-59.7	-57.4	-55.3	-53.3	-51.5	-49.8	-48.2	-47.4
$H^{13}C^{16}O^{16}O\underline{^{17}O}^{-}$	-18.2	-17.6	-16.6	-15.7	-14.9	-14.1	-13.4	-12.8	-12.2	-11.7	-11.2	-11.0
Average	-35.2	-34.3	-32.7	-31.2	-29.8	-28.5	-27.3	-26.3	-25.3	-24.3	-23.5	-23.1
$H^{13}C^{17}O^{18}O\underline{^{18}O}^{-}$	-88.4	-86.3	-82.3	-78.6	-75.3	-72.2	-69.3	-66.7	-64.3	-62.1	-60.1	-59.1
$H^{13}C^{18}O^{17}O\underline{^{18}O}^{-}$	-41.9	-40.7	-38.4	-36.4	-34.5	-32.8	-31.3	-29.9	-28.6	-27.5	-26.4	-26.0
$H^{13}C^{18}O^{18}O\underline{^{17}O}^{-}$	-88.3	-86.2	-82.2	-78.5	-75.2	-72.1	-69.3	-66.7	-64.3	-62.1	-60.1	-59.1
Average	-72.9	-71.1	-67.6	-64.5	-61.7	-59.0	-56.6	-54.4	-52.4	-50.6	-48.8	-48.0
$H^{13}C^{16}O^{18}O\underline{^{18}O}^{-}$	-95.7	-93.5	-89.3	-85.4	-81.9	-78.6	-75.6	-72.9	-70.3	-67.9	-65.7	-64.7
$H^{13}C^{18}O^{16}O\underline{^{18}O}^{-}$	2.4	2.7	3.2	3.6	4.0	4.3	4.5	4.7	4.9	5.0	5.0	5.1
$H^{13}C^{18}O^{18}O\underline{^{16}O}^{-}$	-95.4	-93.2	-89.1	-85.3	-81.8	-78.5	-75.5	-72.8	-70.3	-67.9	-65.7	-64.7
Average	-62.9	-61.3	-58.4	-55.7	-53.2	-51.0	-48.9	-47.0	-45.2	-43.6	-42.1	-41.5
$H^{13}C^{18}O^{17}O\underline{^{17}O}^{-}$	-48.4	-47.1	-44.7	-42.5	-40.5	-38.7	-37.0	-35.5	-34.1	-32.8	-31.6	-31.1
$H^{13}C^{17}O^{18}O\underline{^{17}O}^{-}$	-94.8	-92.6	-88.5	-84.7	-81.2	-77.9	-75.0	-72.2	-69.7	-67.3	-65.2	-64.1
$H^{13}C^{17}O^{17}O\underline{^{18}O}^{-}$	-48.5	-47.2	-44.8	-42.6	-40.6	-38.7	-37.1	-35.5	-34.1	-32.8	-31.6	-31.1
Average	-63.9	-62.3	-59.3	-56.6	-54.1	-51.8	-49.7	-47.7	-45.9	-44.3	-42.8	-42.1
$H^{13}C^{16}O^{17}O\underline{^{17}O}^{-}$	-62.3	-60.8	-58.1	-55.5	-53.2	-51.0	-49.1	-47.2	-45.5	-44.0	-42.5	-41.8
$H^{13}C^{17}O^{16}O\underline{^{17}O}^{-}$	-10.8	-10.4	-9.6	-8.8	-8.1	-7.5	-7.0	-6.5	-6.1	-5.7	-5.4	-5.2
$H^{13}C^{17}O^{17}O\underline{^{16}O}^{-}$	-62.1	-60.7	-57.9	-55.4	-53.1	-51.0	-49.0	-47.2	-45.5	-43.9	-42.5	-41.8
Average	-45.1	-44.0	-41.8	-39.9	-38.1	-36.5	-35.0	-33.6	-32.4	-31.2	-30.1	-29.6
$H^{13}C^{16}O^{17}O\underline{^{18}O}^{-}$	-55.9	-54.5	-51.9	-49.5	-47.3	-45.3	-43.4	-41.7	-40.2	-38.7	-37.4	-36.8
$H^{13}C^{16}O^{18}O\underline{^{17}O}^{-}$	-102.0	-99.7	-95.4	-91.4	-87.8	-84.4	-81.2	-78.3	-75.6	-73.2	-70.8	-69.7
$H^{13}C^{17}O^{16}O\underline{^{18}O}^{-}$	-4.3	-3.9	-3.3	-2.7	-2.2	-1.7	-1.3	-1.0	-0.7	-0.4	-0.2	-0.1
$H^{13}C^{17}O^{18}O\underline{^{16}O}^{-}$	-101.9	-99.6	-95.3	-91.3	-87.7	-84.3	-81.2	-78.3	-75.6	-73.1	-70.8	-69.7
$H^{13}C^{18}O^{16}O\underline{^{17}O}^{-}$	-4.2	-3.8	-3.1	-2.6	-2.1	-1.6	-1.2	-0.9	-0.6	-0.4	-0.2	-0.1
$H^{13}C^{18}O^{17}O\underline{^{16}O}^{-}$	-55.6	-54.2	-51.6	-49.3	-47.1	-45.1	-43.3	-41.6	-40.1	-38.6	-37.3	-36.7
Average	-54.0	-52.6	-50.1	-47.8	-45.7	-43.7	-41.9	-40.3	-38.8	-37.4	-36.1	-35.5
$H^{13}C^{17}O^{17}O\underline{^{17}O}^{-}$	-55.0	-53.6	-51.0	-48.7	-46.5	-44.5	-42.7	-41.0	-39.5	-38.1	-36.8	-36.2
$H^{13}C^{18}O^{18}O\underline{^{18}O}^{-}$	-81.9	-79.8	-76.0	-72.5	-69.3	-66.3	-63.7	-61.2	-58.9	-56.8	-54.9	-54.0